UNIVERSITÀ DEGLI STUDI DELLA TUSCIA

DEIM Dipartimento di Economia, Ingegneria, Società e Impresa

UNIVERSITÀ DEGLI STUDI DELLA TUSCIA DI VITERBO

DIPARTIMENTO DI ECONOMIA, INGEGNERIA, SOCIETA E IMPRESA (DEIM)

Corso di Dottorato di Ricerca in

Engineering for Energy and Environment – XXXII Ciclo

TITOLO TESI DI DOTTORATO DI RICERCA

INNOVATIVE NON-INVASIVE TECHNIQUES FOR INTEGRATED IMAGING DIAGNOSTICS OF PAINTINGS AND DATA ANALYSIS

(S.S.D. CHIM/01, ING/22)

Tesi di dottorato di:

Dott.ssa Claudia Colantonio

Claudia Colantonio

Coordinatore del corso

Prof. Danilo Monarca

Firma

Tutor

Prof. Giuseppe Calabro

Firma

Co-tutor

Dott.ssa Claudia Pelosi

Firma

Data della discussione
24/06/2020

Ai miei genitori.
La mia direzione, il mio polo nord.

INDEX

1. INTRODUCTION

The use of non-invasive and non-destructive methods is highly relevant for cultural heritage objects, due to their uniqueness, fragility and conservative needs that often restrict or even exclude the possibility to run in-depth scientific investigations that involve micro-sampling [1]. Furthermore, analytic semi- or micro-destructive methods for material characterization are mostly punctual analyses that could not be representative of the state of conservation of the whole investigated artwork in terms of its surface and volume. Another aspect to considerate is that, beyond sample observation by traditional optical microscopy (OM) and scanning electronic microscopy (SEM), a limited number of analytic characterization tests are possible on the same samples because of the usually small amount of the available material and the partial or complete destruction and loss of the sample imposed by many of these techniques for microanalysis as Gas Chromatography coupled with Mass Spectrometry (GC-MS) and High-Performance Liquid Chromatography (HPLC), X-ray diffraction (XRD), Laser Induced Breakdown Spectroscopy (LIBS), Atomic Absorption (AAS) and Atomic Emission (AES) spectroscopies, ^{14}C radiocarbon dating and other laboratory methods for material characterization.

In this scenario, non-destructive techniques have become widely applied in conservation science and art restoration as they provide the possibility to use complementary methods and obtain more information from the same sample. Some of them are portable and allow *in situ* analysis while protecting the integrity of ancient artworks, as for instance Fibre Optic Reflectance Spectroscopy (FORS), X-rays Fluorescence Spectrometry (XRF), portable Nuclear Magnetic Resonance in the configuration called "mobile universal surface explorer" (NMR-MOUSE), Fourier Transform Infrared Spectroscopy (FTIR) and portable Raman Spectroscopy [2].
Although these methods are commonly used for scientific art investigation as well as for some other applications, there is still a need for new, non-invasive techniques that could extend the amount of information obtained from a first diagnostic investigation of the artwork analysed and limit the number of eventual invasive testing required.

To gain more information about materials distribution, manufacturing techniques, provenance of the artworks and their current conservative conditions, imaging methods and non-destructive testing (NDT) techniques have been assuming an increasing importance. Current digital imaging technologies may significantly assist in documental study and scientific investigation of cultural heritage supporting complicate matters as dating and authentication issues. As non-contact methods using restrained energy to collect information about features of interest in art objects (e.g. pigments, varnishes, erased text, degradation factors, defects in the support), this kind of non-invasive techniques can integrate punctual analyses from traditional chemical-physical methods.[3]
The application of imaging methods regularly used also in the cultural heritage field can often supply a complete knowledge of investigated artworks [4], starting from the

wide range of scientific photography -Ultraviolet Reflected (UVR) photography, Ultraviolet-induced visible Fluorescence (UVF), Infrared False Color (IRFC), Raking Light (RAK), Infrared (IR) and Infrared Fluorescence (IRF) photography-, to get to several physical methods as X-ray Radiography (XRR), Infrared Reflectography (IRR) and macroscopic X-ray Fluorescence (MA-XRF) scanning, Infrared Thermography (IRT), Terahertz (THz) imaging and Optical Coherence Tomography (OCT). However, there are numerous cases where these methods cannot be fully exploited, especially when a bad state of conservation of an artwork or its intrinsic fragility makes impossible its handlings towards a specialized laboratory.
Here, technological advancement in the sensitivity and miniaturization of sensors, as well as existing complementarity of different imaging and traditional physical methods [5,6], can provide new insights into the investigated artwork, allowing to correlate data to gain hidden information as overpainted pictures and underdrawings or support a deepened inspection of material characterization and inner layers of the object in a complete non-invasive way.

Modern multispectral and hyperspectral imaging (MSI and HSI) systems enable objects investigation with both high spatial and spectral precision. The acquisition of spatial data is possible with resolutions of a few hundredths of a millimeter using active projection-based camera systems, while spectral data can be obtained using filter-based multispectral camera systems that can capture surface spectral reflectance with high spatial resolution.
Human eye is only sensitive to a limited part of light spectrum and can distinguish between objects based on their different spectral responses in that narrow spectral range. However, multispectral imaging sensors can acquire in an extended portion of electromagnetic spectrum from ultraviolet (UV) to near infrared (NIR) range. This allows material identification because of their unique spectral signature in a wide spectral range. Multispectral imaging exploits the property that each material has its own unique spectral signatures and associating a spectral response to each pixel it provides information about surface properties and material characterization.

MSI technology is being used for environment and land observation remote sensing in satellite and airborne systems since late 1960s [7]. Multispectral imaging systems acquire data in a small number of spectral bands (generally from three to six, from visible to infrared range) by using parallel sensor arrays. However, such low number of spectral bands is the limiting factor for discrimination of various materials. Nonetheless, recent developments in digital image processing (DIP) algorithms development during the past two decades has made it possible to acquire more and more significant information from the spectral bands between ultraviolet (UV) and near- infrared (NIR) range and to reduce times of acquisition.
Contrary to MSI, hyperspectral imaging uses several well-defined optical bands in broad spectral range. Originally implemented on satellite and airborne platforms for remote sensing applications, during last two decades it has been applied to numerous applications including agricultural and water resources control, military defence, art

conservation and archaeology, medical diagnosis, analyses of crime scene details, document imaging, forensic medicine, food quality control and mineralogical mapping of earth surface [8]. The main advantages of MSI techniques in art examination consist of mapping and identifying pigments, binders, restored areas and zones of retouching on the entire surface of the investigated artwork in a non-invasive modality [9–12]. The diagnostic potentialities of MSI can be improved by implementing data processing algorithms for digital images, supporting various aspects of conservation, allowing to observe materials below the surface and, through the combination of different spectral range imaging, to gain latent information on painting technique and old restorations as well as to support artwork authentication [13,14].

Non-invasive mapping using several mathematical and statistical tools have been proposed in MSI applications to fully exploit the multispectral set of data and extract relevant information to present a diagnostic evaluation in a visually meaningful way. Moreover, multispectral imaging allows the generation of useful hybrid mapping products for quantitative and qualitative analysis: rectified images and orthoimages for visual interpretation (in true or false color), 3D textured models from images acquired at different regions of the spectrum and clusters of materials comparable over time in order to address monitoring processes. All of them may act as input data in the application of different strategies of multispectral classification and dimensional analysis, in order to differentiate constitutive materials and monitor possible degradation factors.

Multispectral imaging techniques play a key role since they allow the integration of data acquired by different non-destructive technologies proving to be a powerful tool to analyse cultural heritage objects. Data integration is provided by digital image processing (DIP) algorithms and statistic tools that can align imaging output from different analysis and correlate them in dedicated software to enhance hidden information [15]. Diagnostic imaging native datum is furthermore enriched when associated to metadata coming from traditional analytic methods, as chemical characterization of art materials, detailed restoration reports properly filled out, dating of organic materials, identification of degradation products and related cause of origin.

This doctoral research was focused on the application of innovative imaging technologies for non-invasive investigation of artworks putting successfully together different scientific competences and skills in a multidisciplinary approach for a novel integrated diagnostic strategy for heritage study and conservation.

Such a goal was achieved thanks to the knowledge and expertise acquired in five years of academic education in Conservation Science and the enhancement of specific scientific and engineering competences grew during the last three years of doctoral research. In this path, fundamental steps were done through worthy collaborations both with public research institutions and private business companies that led to important scientific results, illustrated in this doctoral thesis and scientific peer-reviewed publications.

A cooperation agreement made with Profilocolore® Srl, Italian company developer of a refined multispectral analysis technique called Hypercolorimetric Multispectral Imaging (HMI), was focused on the training for acquisition of multispectral images of painted surfaces and enhancement of knowledge in theorical basis of scientific imaging as radiometry, colorimetry, optics and sensors, digital image processing, remote sensing, deep learning.
The fruitful collaboration continued through an intense and shared applied research focused in testing and validating HMI technique on real artworks of different nature, from Baroque's paintings on copper foil to Italian Renaissance wood panel paintings, ancient detached wall paintings and Islamic manuscript's pages from Louvre Museum in Paris. This last research activity was possible through a four-months Erasmus+ traineeship scholarship at Imaging Laboratory of the Centre de Recherche et Restauration des Musées de France (C2RMF) in Paris where, under the supervision of Dr. Clotilde Boust, Head of Scientific Imaging research group, it was possible to use HMI to study new kind of artworks not investigated before with the technique, to perform HMI system through C2RMF high-resolution Hasselblad 4HD digital camera and to integrate multispectral images with MA-XRF scans in HMI image processing software obtaining new useful mapping for materials characterization.
Most interesting results of integration of diagnostic imaging data was reached through the collaboration of Tuscia University and Profilocolore® with engineering experts in non-destructive techniques for material testing from NDT laboratory of Terni (University of Perugia) and Engineering Department of University of Calabria, who developed an innovative setup to perform thermography on paintings. This technique, known as Pulse-Compression Thermography (PuCT), for the first time considered for Cultural Heritage analysis in collaboration with Engineering Department of L'Aquila University in 2017, enables completely non-invasive investigation of artworks through the use of led source and coded modulated heating stimuli and to highlight defects inside material, understanding their extension and position through the existing correlation of thermal diffusivity -"spread" in time thanks to pulse compression algorithms- with the different inner layers making up the art object, discernible in different imaging thermograms.

In this doctoral thesis are reported the interesting results obtained thanks to the use of HMI and PuCT for the first time applied in an integrated approach for the diagnostic non-invasive investigation of ancient artworks. Analyses were done in both scientific laboratories and museums (without transportation of the artwork), in a completely contactless and rapid way. Conservation science competences acquired in the academic career and enhanced in this three-years doctoral research under the priceless supervision of Prof. Giuseppe Calabrò and Prof. Claudia Pelosi -respectively Head of Engineering School and main expert in scientific diagnostics for cultural heritage of Tuscia University- allowed an optimal programming of diagnostic campaigns and a correct interpretation of imaging data for the evaluation of the state

of conservation of the artworks and identification of artists materials and painting technique.

2. STATE OF THE ART

The purpose of this doctoral research is the application of new non-invasive techniques to safely investigate an artwork for its study and conservation. In cultural heritage safeguard, knowledge and conservation come together in a symbiotic development, because it is not possible to protect what is unknown. Most ancient art masterpieces that survived to our times have experienced a troubled preservative past, frequently marked by changes of location, collections and collectors, intended use and other historical occurrences that unavoidably caused damages or engaged indirect degradation processes, prejudicing their conservation state. During their lifetime, ancient artworks have usually been subjected to restorations that are not completely documented or -more often- not documented at all, resulting in aggregated stratifications of original materials, later additions, restoration contributions and degradation products that are hard to differentiate and characterize in the perspective of an adequate conservation plan.

Heritage diagnostics is pushing towards a deeper and inner knowledge of artists materials and executive techniques, supported by scientific documentation of restoration operations and materials, aiming to understand the causes of degradation afflicting artworks and how to intervene in a complex and dynamic chemical-physical but also semantic equilibrium between original materials, original artistic will, intentional modifications happened through the centuries, restoration interventions and current physical conservation issues.

Restoration is like performing a medical operation: accurate observation and well-aimed analysis of materials and techniques are essential to plan an intervention with a satisfactory equilibrium between invasiveness and effectiveness, firstly approaching the patient with non-invasive screening methods to later address focused analyses to define the clinical picture and the therapy protocol, any eventual interventions and the related follow-up.
In art conservation studies, this means choosing the investigation technique according to diagnostic question and the object state of conservation, interpret imaging and analytical data with the support of restorers, art historians, technicians and experts and choosing the right materials and procedures to restore the art object, ensuring it a proper and safe exposition setting and supporting monitoring planning.

The application of electromagnetic radiation extended beyond the limits of eyesight to investigate artworks may be traced to 1895 when Roentgen made his first X-ray shadowgraphs (one of which was done on a painted surface), but it was not until the 1930s, when X-radiography first entered into museums, that a new art history formed around scientific imaging and the ability to assess style and attribution of an artwork

from material and physical aspects of the painted surface not visible to the naked eye [16].
This new open sea of possibility to go "inside" an artwork continued to be explored with other wavelengths of the electromagnetic domain. Specifically, UV-induced visible fluorescence helped reveal areas of loss/repair and provided a general sense of chemical composition and infrared reflectography (IRR) became the standard analysis to reveal hidden underdrawings and preparatory design in paintings. In the late 1960s, more specialized techniques, such as autoradiography achieved by neutron activation [17] of artworks, introduced the fascinating opportunity to combine elemental composition together with imaging for the first time —a technique that several decades later inspired further developments in X-ray fluorescence imaging [18]. By the 1980s, new three-dimensional (3D) acquisition techniques were being explored for the 3D documentation and display of cultural objects, which remain relevant subjects of investigation in the development of cutting-edge technologies for diagnostics to this day.
The recent outburst in cultural heritage imaging has grown mainly out of the fields of remote sensing and color science, with excellent success for hyperspectral and multispectral imaging instruments for pixelwise material characterization, mapping and investigation of pictorial layers in painted surfaces. A parallel development has been the use of synchrotron-based X-ray fluorescence and diffraction imaging that has grown in conjunction with the diversification of users of these large-scale facilities from all research disciplines, which nonetheless remain hardly accessible for minor conservation centers and museums. In the same period, computational illumination techniques were developed to dynamically analyze artworks in post-processing, as for the digitalization of existing X-radiographs, enabling recent advances in image processing algorithms to be applied to these historical works.
The proliferation of affordable digital sensors has been allowing museums to capture large amounts of high-resolution photographs in multiple modalities that were then computationally put together to provide new imaging documentation with unprecedented detail. Optical coherence tomography (OCT) [19] and THz imaging [20] provide *in situ* 3D reconstructions of microscopically thin layers of paint comprising pictures and drawings. Moving to imaging investigations on macro-scale, the popularity of techniques extensively used in geographic information systems (GIS) and remote sensing as light detection and ranging (LiDAR) [21] and photogrammetric methods as structure-from-motion (SfM) [22] have allowed to discover and investigate vast architectures and entire ancient cities, as well as to document the historic landscapes of modern ones.

In the last two decades, computational imaging of cultural heritage is offering many new perspectives for investigating the technical art history of objects and to assess the condition of artworks to best approach and plan their long-term preservation. Several areas of computational imaging that have not been thoroughly explored on cultural heritage objects. Also compressive sensing and sparse imaging could

significantly improve sensitivities especially for conditions where low light is necessary for light-sensitive materials and when increased imaging speeds are necessary for experiments that cannot be conducted in the public spaces of museums over days (as in MA-XRF scanning). Improved material databases could lead to advances in reconstruction algorithms that produce more accurate image archives and renderings. Scalability is another principal obstacle. For example, a comprehensive measurement of the chemical composition and spatial structure of layers of paint in an entire work of art could provide new and valuable tools for art historians and conservators. Another important direction is the dissemination, visualization, and display of the great body of visual information now being captured by museums and galleries around the world. For instance, augmented reality is projected to strongly impact the museum visitor's experience in coming decades. Finally, for the computational imaging field, it is important to note that artworks provide inestimable test scenes that can inspire researchers to push the envelope by providing new imaging and display techniques that can probe the complex light-material interactions inherent in so many works of art. In this regard, it is the hope that cultural heritage can serve as a catalyst for novel research in computational imaging [23].

3. APPLIED METHODOLOGY

The purpose of this doctoral research was focused on the application of new non-destructive techniques and the development of an innovative integrated approach for non-invasive diagnostics of artworks.
Considering a wide set of imaging technologies available in national research institutes and on the international commercial market, two innovative imaging techniques were chosen, one developed by Italian SME Profilocolore®, expert in optics and engineering for image analysis, and the other one developed by Engineering departments of University of Perugia and University of Calabria.
The two imaging techniques are respectively Hypercolorimetric Multispectral Imaging (HMI) and Pulse-Compression Thermography (PuCT), which were tested and applied on different kind of real artworks (panel paintings, oil paintings on canvas, oil paintings on copper, wall paintings and illuminated manuscripts).
Both techniques were chosen for their advantages in terms of leading criteria in the applied diagnostics for Cultural Heritage:

- non-invasiveness, a primary concern when approaching fragile and unique artworks whose conservation state is uncertain at the beginning of a restoration campaign;
- portability, allowing *in situ* analysis which means to avoid exposing the artwork to the risks (mechanical damages, harsh micro-climatic changes, etc.) connected to movement towards specialized laboratories and to guarantee the fruition of the artwork all the while, as the compact dimensions and needing

of no special conditions (specific power supply, protections for radiations, more operators) allow to investigate the object in its ordinary exposition space.
- low time of analysis, considering two hours for both imaging acquisition and the possibility to immediately examine the imaging data;
- affordable costs

3.1 Hypercolorimetric Multispectral Imaging (HMI)

Considering human eye sensitivity to light and color, it is not able to resolve the spectrum of the received radiation with great detail, rather it makes a coarse sampling weighed through the sensitivity curves of the cones of the retina, transforming the received radiation into three nervous stimula: blue, green and red, composing the visible light spectrum from 380 to 700 nm [24].
Since 1931 the CIE (Commission Internationale de l'Eclairage), on the basis of human eye's physiology, established three weighting functions, known as Color Matching Functions (CMF), to convert sensory spectral sensitivity curves into a set of XYZ numerical values (Fig. 1(a)). The represented values are the so-called XYZ colorimetric coordinates of a spectrum of radiation in the visible range. In the space of the XYZ coordinates, a spectrum of radiation will then be represented by a point $Q_{(XYZ)}$. The vector OQ intersects a plane passing through (001, 010, 100) at a point q of normalized coordinates $x = X / (X + Y + Z)$, $y = Y / (X + Y + Z)$ $z = Z / (X + Y + Z)$. The figures x, y and z are called chromaticity coordinates. By varying the wavelength of a monochromatic source from the far red to the extreme visible blue, its chromaticity coordinates would draw a counterclockwise arc inside the triangle (001, 010, 100). Connecting the ends of the arc with a segment on the XY plane we obtain the Chromaticity Diagram (Fig.1(b)).
The reconstruction of a continuous spectrum with only three input values, from the information theory point of view, means a loss of the original data. In fact, it is common that more spectra origin the same colorimetric output, a phenomenon known as metamerism. In the human eye's physiology based on tristimulus values, metamerism occurs because each type of cone responds to the cumulative energy from a broad range of wavelengths, so that different combinations of light across all the visible (VIS) spectrum can produce an equivalent receptor response and the same set of tristimulus values or color sensation.

In fact, the CIE CMF curves for a standard observer do not minimize the metamerism and fail to properly represent a source at maximum saturation (monochrome) except in some areas of the XY plane. An ideal set of CMFs should have a linear behavior and a triangular shape. Company producing imaging sensors and digital cameras tend to approximate the ideal curves with the spectral sensitivity of the Sensor/Bayer matrix pair.

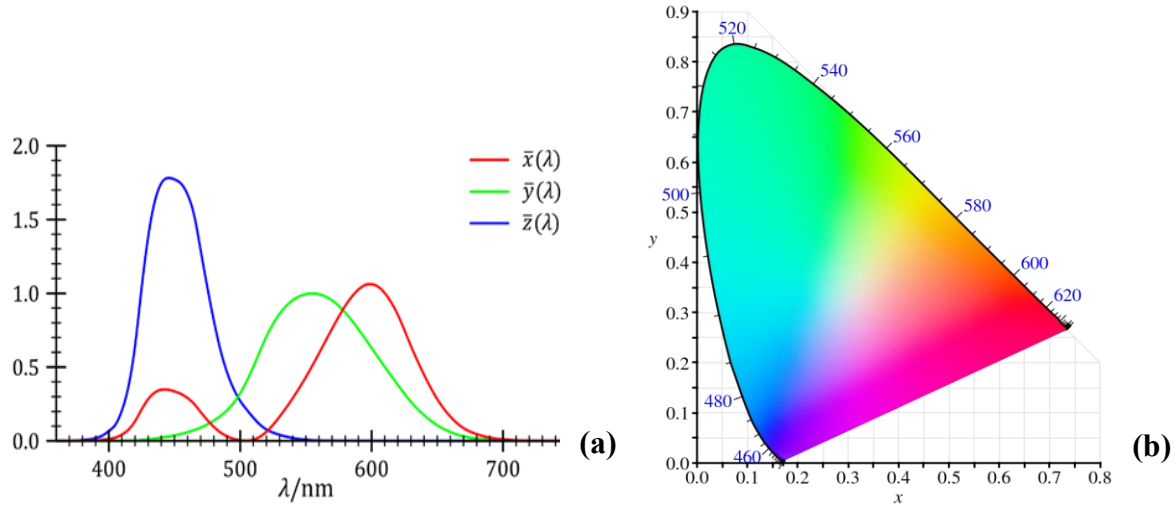

Figure. (a) The CIE XYZ standard observer color matching functions; (b) the CIE 1931 color space chromaticity diagram. The outer curved boundary is the spectral (or monochromatic) locus, with wavelengths shown in nanometers.

In fact, digital cameras spectral sensitivity curves are the output of the combination of the silicon sensor's sensitivity and the spectral transmittance of the so-called Bayer matrix.

Commercial digital cameras are indeed provided with CMOS silicon image sensors, which are active-pixel sensors (meaning that each pixel-sensor unit cell is associated to a photodetector and one or more active transistors) that uses the Bayer sensor (from his developer Bryce E. Bayer, Kodak patent) to reconstruct the image from the RAW image file of reflex digital cameras. The density of pixels on a sensor is responsible of the megapixel value of a digital camera.

Briefly, a Bayer sensor is based on a matrix of several millions of pixel, each being a receptor of photons; the quantity of photons hitting the sensor is calculated by a processor which traduce it in a value of intensity (or bit depth), e.g. between 0 and 255 in an 8-bit sensor. To produce a color (RGB) image, each photosensor/pixel is covered with a red, green or blue Bayer filter, where the number of green filters is double respect to red and blue ones, in a proportion of 50% green, 25% red and 25% blue filters (Fig. 2(a)), in order to reflect the actual major sensitivity of human retina to green light in daytime vision. The output is a matrix of filters (also known as Color Filter Array, CFA) made up of two columns (R+G) and (G+B) filters that is called Bayer matrix (Fig. 2(b)).

Because the sensors are placed side by side and not superimposed, it is necessary to integrate the information in the regions where no sensor is present through an interpolation operation known as demosaicing process, which uses various algorithms to understand the full color values of each pixel. The simplest demosaicing algorithms average the input of nearby pixels to obtain a full-fledged color data for the image.

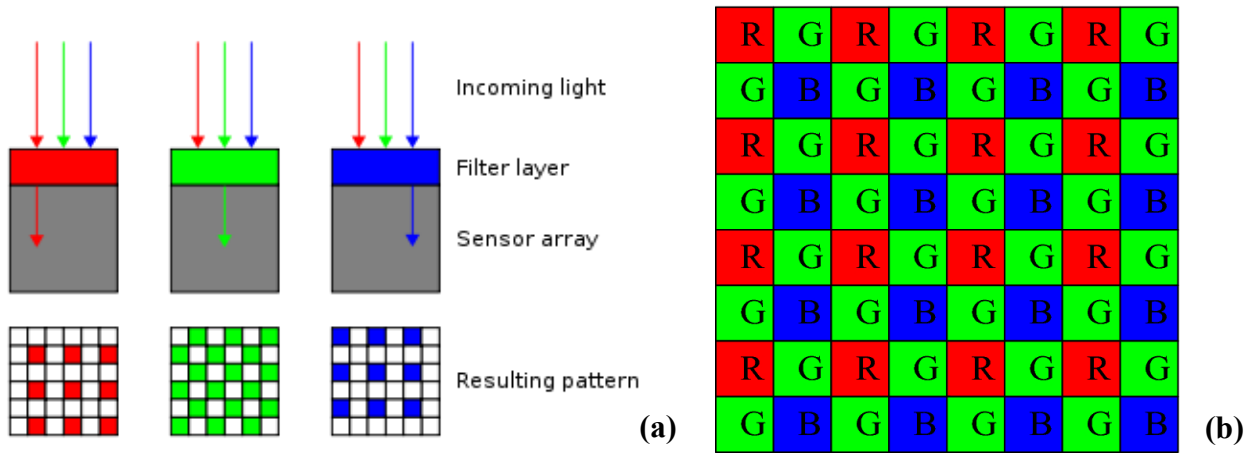

Figure 2. R, G, B color filters (a) making up the Bayer matrix (b).

Each digital camera owns its spectral sensitivity curves. A commercial digital camera can be used as an accurate radiometric and colorimetric measurement instrument if its CMFs are as much as possible similar to the standard observer's ones. The easiest way to reduce the deviation between the standard observer's and the camera's CMFs is to apply the Ordinary Least Squares (OLS) method to define an esteem of the CMFs through the linear combination of the three camera's spectral sensitivity curves (1) where M is the matrix of transformation of the curves.

$$\begin{aligned} x_s(\lambda) &= M_{rx}\, r_{RAW}(\lambda) + M_{gx}\, g_{RAW}(\lambda) + M_{bx}\, b_{RAW}(\lambda) \\ y_s(\lambda) &= M_{ry}\, r_{RAW}(\lambda) + M_{gy}\, g_{RAW}(\lambda) + M_{by}\, b_{RAW}(\lambda) \\ z_s(\lambda) &= M_{rz}\, r_{RAW}(\lambda) + M_{gz}\, g_{RAW}(\lambda) + M_{bz}\, b_{RAW}(\lambda) \end{aligned} \qquad (1)$$

The camera's CMF obtained using OLS method do not perfectly match the CMFs of CIE 1931 standard observer, as shown in Fig. 3(a). The Italian company Profilocolore Srl, expert in digital image analysis, developed a set of genetic algorithms that allowed to successfully optimize a digital single-lens reflex (DSLR) camera's colorimetric functions (Fig.3(b)) through the use of stochastic and not-deterministic operators for an esteem of a best solution in a group of optimum solutions, in a heuristic approach [24].

Applying Profilocolore® genetic algorithm, a set of lookup tables (LUT) are produced together with an array (tables) of numeric factors to apply for a linear combination of the genetically synthesized LUT. In (2) the tables of numeric factors are indicated with K, while F are the non-linear functions representing the LUTs.

$$\begin{aligned} x_s(\lambda) &= K_{rx}\, F_{rx}(r_{RAW}(\lambda)) + K_{gx}\, F_{gx}(g_{RAW}(\lambda)) + K_{bx}\, F_{bx}(b_{RAW}(\lambda)) \\ y_s(\lambda) &= K_{ry}\, F_{ry}(r_{RAW}(\lambda)) + K_{gy}\, F_{gy}(g_{RAW}(\lambda)) + K_{by}\, F_{by}(b_{RAW}(\lambda)) \\ z_s(\lambda) &= K_{rz}\, F_{rz}(r_{RAW}(\lambda)) + K_{gz}\, F_{gz}(g_{RAW}(\lambda)) + K_{bz}\, F_{bz}(b_{RAW}(\lambda)) \end{aligned} \qquad (2)$$

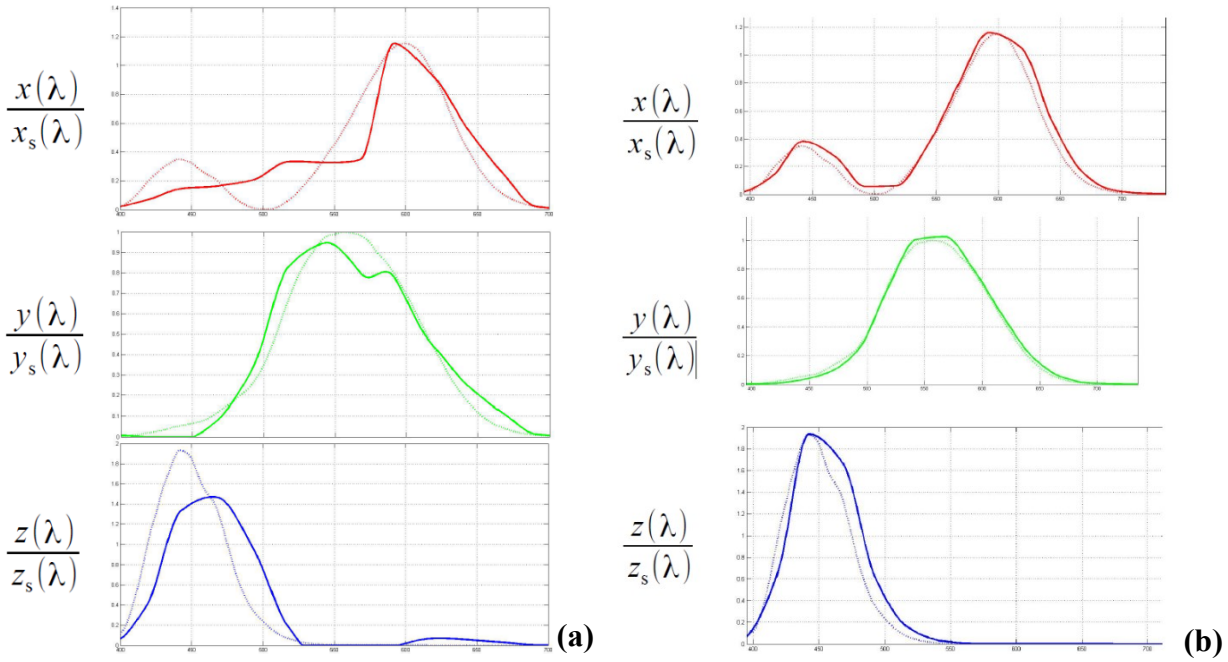

Figure 3. (a) Color matching functions of a DSLR camera gained through the linear combination of fundamental spectral sensitivities (continue lines) compared with CMFs of CIE 1931 standard observer (dotted lines); (b) CMFs of a digital DSLR camera obtained by Profilocolore® LUTs, compared with CMFs of CIE 1931 standard observer [16].

As already stated above, each digital camera owns its spectral sensitivity curves, e.g. CMFs of a Nikon D800 -used in this research work- are represented in Fig.4.(a); furthermore, ideal CMFs should have a linear behaviour, be equally energetic and equally spaced, in order to allow the reconstruction of a spectrum with minimal errors and a maximum differentiation between spectra, overcoming metamerism (Fig. 4(b)). Hypercolorimetric Multispectral Imaging (HMI) system developed by Profilocolore® is based on an extended colorimetry, applied through simultaneous exploitation of the electromagnetic spectrum from the ultraviolet (UV) to the near infrared (NIR) region of the electromagnetic spectrum [25].

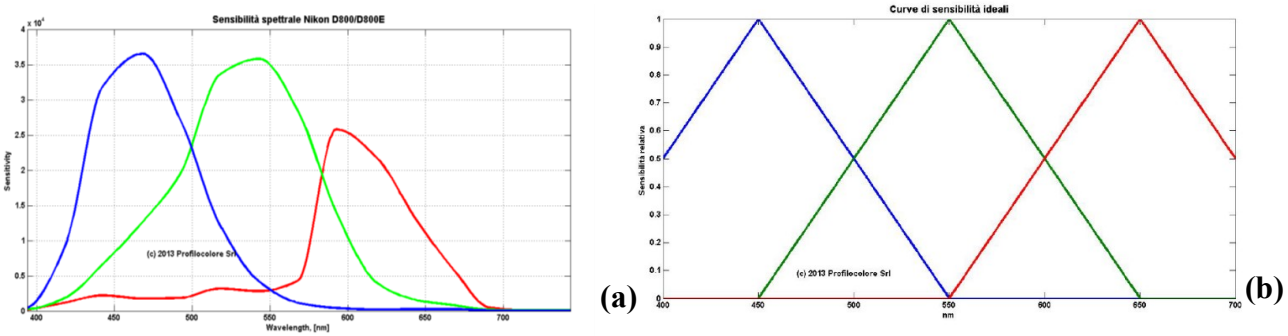

Figure 4. Nikon D800's spectral sensitivity curves (a) and ideal color matching functions.

The acquisitions, made under a standard metric, allow to characterize the investigated surfaces in a more detailed way than the standard colorimetry. In fact, the classical colorimetry is substituted with a new and wider one resulting in a seven-bands colorimetry with CMFs centered at 350, 450, 550, 650, 750, 850and 950 nm (Fig.5). HMI system (illustrated in Fig.6) transforms any spectrum in the range 300–1000 nm into sevenfold hypercolorimetric coordinates applying genetic artificial intelligence (AI)-based algorithms developed by Profilocolore® and defended by patent protection.
To obtain the calibrated multispectral images, the acquisition is done through a Nikon D800FR (Full Range) camera, a 36megapixel reflex camera modified under a Nikon/ Profilocolore® common project to achieve an extended 300-1000 nm range sensitivity, with the use of portable camera flashes also modified in full-range. The accurate calibration of the system is done through a color checker made of 36 color patches from NCS (Natural Colour System® catalogue) standard catalogue and the use of white reference patches with 98% of spectral reflectance. Color checker and white references spectral reflectance was measured through a laboratory spectroradiometer (Instrument System Spectroradiometer CAS 140 CT) in the range 220-1050 nm with 0.7 nm accuracy in a dark room in Profilocolore® laboratory.
Thanks to the refined research at the foundation of the process explained above, a modified commercial digital camera can turn into a completely trustworthy instrument of measurement, with high-precision, accuracy and repeatability

Image acquisition in the UV-NIR range is done through the use of two bandpass filters called A (whose spectral transmittance include UV and VIS range) and B (including VIS and NIR band until 1000 nm) designed by Profilocolore®; a third UV-IR cut filter is used coupled with filter A to restore the natural sensitivity in the visible band, in order to make UV-induced fluorescence images [25, 26] using a UV light source, which could be obtained using an external UV narrow band source (with emission cut before 395 nm, ensuring no emission in the blue portion of the visible) or putting a UV band-pass filter on the portable flash units. In the doctoral research described in this thesis, both UV light setting were used, choosing Madatec® high-power portable UV lamps, with narrow peak of emission between 365-370 nm.

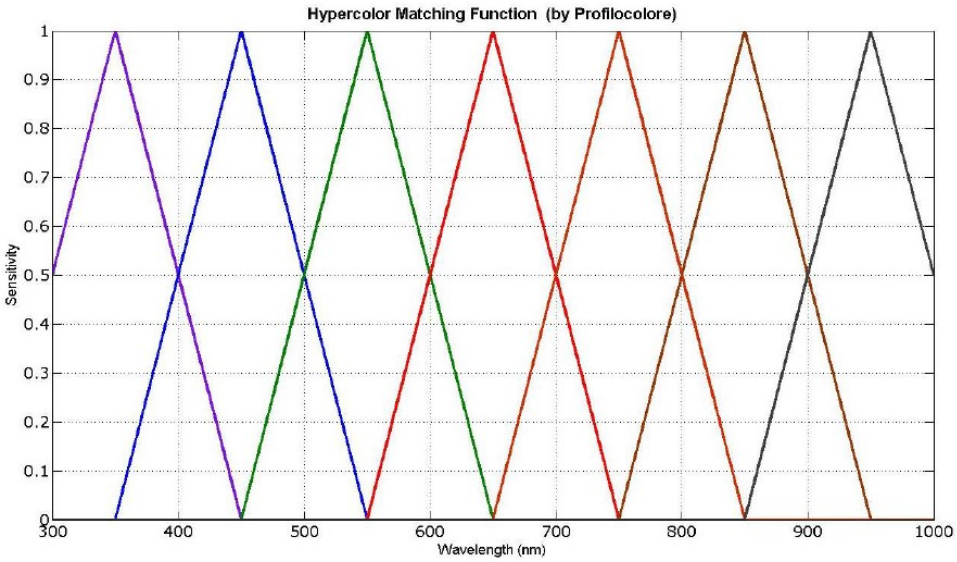

Figure 5. Ideal CMF in extended Profilocolore® HMI colorimetry.

The obtained reflectance values are weighed with the Hypercolor Matching Functions and transformed into 7 hypercolorimetric coordinates. The same target is acquired in imaging mode through the camera in RAW format, which represent the not-processed native image, as it was captured by the sensor. This allows to collect and keep the original numerical datum related to an image without any compression. A RAW imaging file stores the unrefined monochromatic data related to the intensity of incident light on each single R, G, B photodiode in a Bayer CFA.

Normally, RAW image file is larger than other formats as tiff. e jpg. Because, together with the digital information on pixels, it records also the file format code, that is the data responsible for its identification (header) and its readability. In the RAW/tiff transformation, lens chromatic, spherical geometric and vignetting aberrations and distortions are corrected. The hypercolor profile itself consists of a 7 input/7 output non-linear conversion function automatically synthesized by Profilocolore® proprietary genetic algorithm that provides a very high radiometric (better than 95%) and colorimetric precision (better than $\Delta E = 2$) to the entire system.

The hypercolorimetric coordinates coincide with the continuous spectral reflectance sampled at 350,450, 550, 650, 750, 850 and 950 nm. The achieved result has a great value as it shows how it is possible to obtain a pixelwise (i.e. pixel by pixel) sampled spectral reflectance in imaging mode and how this is equivalent to an instrumental local measurement. Moreover, further relevant information that is not visible to the naked eye can be obtained from digital image processing (DIP) tools [25]. In fact, most interesting findings can be observed by combining different spectral acquisitions and advanced image processing algorithms such as principal component analysis (PCA), pattern recognition, edge detection and cluster analysis.

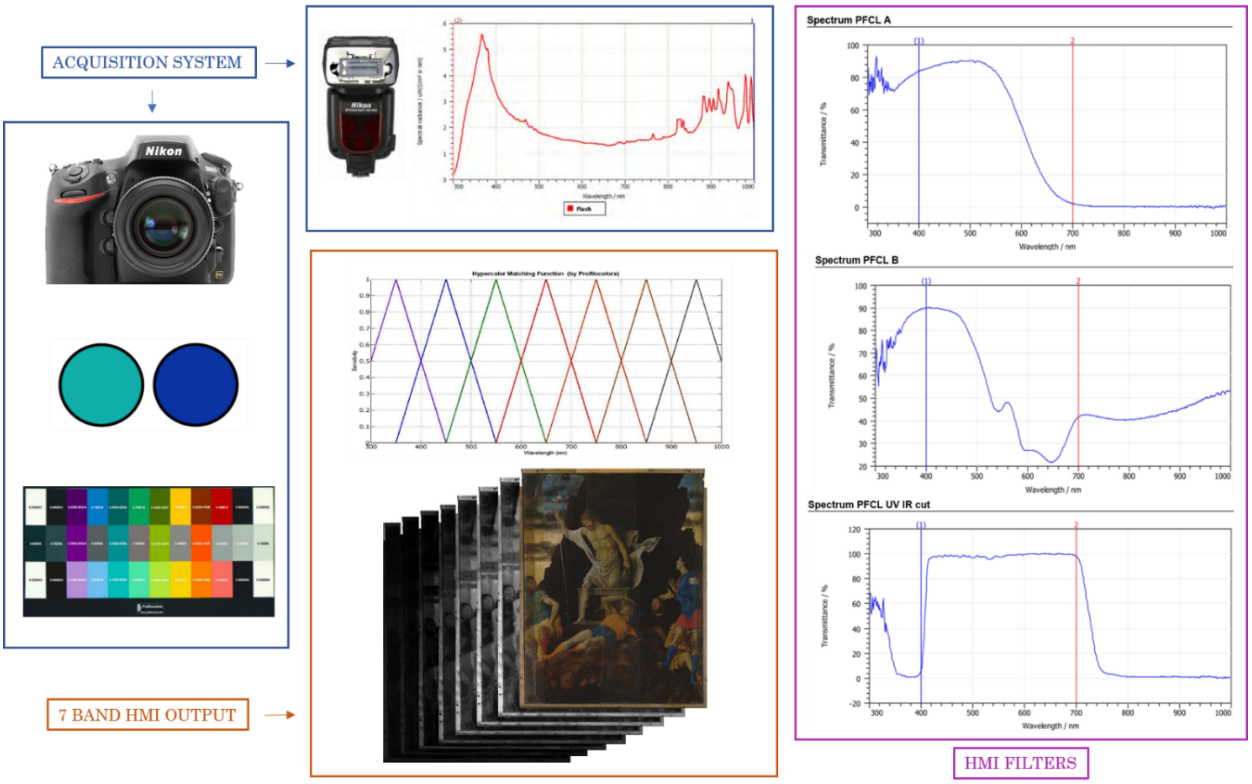

Figure 6. Scheme of HMI acquisition system and imaging output. The multispectral images are acquired through two FR camera shots with two band-pass filters (A and B), registering entirely from 300 to 1000 nm. Flash units are modified for an extensive emission from UV to NIR and covered with UV-bandpass filter for UVF photography, done using filter A coupled with UV-IR cut filter on the camera. Final HMI calibrated seven spectral images are obtained in the HMI software through native Profilocolore® AI-based algorithms.

Considering well-established multispectral methods, HMI allows the multispectral channels to be effectively combined due to the calibrated data obtained after the acquisition through a modified camera. Indeed, it has been shown in that the possibility of combining the multispectral channels after calibration provides great advantages in terms of information amount that can be extracted from the acquired data. Another great advantage of HMI is the short time needed for the acquisition – only three shots are needed – without the necessity of any power supply, thus providing great advantages in artworks examination, especially during *in situ* investigations, in order to:

- investigate the general conservation status of an artwork in order to support restoration and conservation actions;
- acquire UVF images (to map restorations, identify different varnishes and other organic materials) and run UV and IR false-color images to distinguish materials that are not discernible in the visible light;

- detect details in the painting layers, areas of ancient retouching and re-paintings, preparatory drawings;
- compare spectral reflectance curve and colorimetry (L,a,b values) of two points in the scene;
- query a database to hypothesize pigments attribution;
- map pigments/materials on the base of their spectral similarity, as well as areas of degradation, loss of pictorial layer, etc.;
- add and integrate any other imaging data (fluorescence, X-ray, thermal, terahertz etc.);
- run PCA, cluster analysis and contrast enhancement through normalized difference index (NDI) on different spectral bands to highlight hidden details, as covered signatures or *pentimenti* (changes in the artist's mind during the painting process);
- build new databases, e.g. specific of an artist or used in a certain historical period, differentiating between ancient and contemporary materials.

3.2 Pulse-Compression thermography (PuCT)

Among the most valuable NDT methods for inspecting cultural heritage objects, IRT currently holds an important place of prominence. InfraRed (IR) and thermal methods are based on the principle that the heat flowing into a Sample Under Test (SUT) is perturbed by the presence of anomalies, such as splitting, voids, etc. These changes in the heat flow cause localized temperature differences detectable onto the material's surface. The imaging or visualization of such thermal imprints by means of a thermal camera, i.e., a camera sensitive to IR radiation, is known as IRT [27, 28].

The method allows fast inspections and real-time measurements to be carried out over a given detection area by using suitable lenses. IRT's popularity has grown in recent years due to improvements of thermal cameras that became cheaper, lighter and more accurate. IRT can be applied both with and without the use of a con-trolled heat source; the former case is called active IRT, whilst the latter is referred as passive IRT. In passive IRT, the thermal excitation is provided by the environmental conditions (e.g. sun exposure). However, the thermal contrast between defective and non-defective areas is in general low, thus leading to poor Signal-to-Noise Ratio (SNR). In addition, experiments cannot be easily reproduced. To improve the sensitivity of passive IRT, advanced image processing techniques were developed, even for the inspection of cultural heritage structures [29,30].
Nonetheless, the use of an external controlled heat source is in general beneficial to further improve IRT performances, leading to the active IRT. In active IRT, the SUT is assumed being at thermal equilibrium [31], and a heat excitation is applied to reach the desired thermal contrast. The most used active IRT scheme is called Pulsed-Thermography (PT) and it is exploited in a wide range of non-destructive technique applications. PT makes use of high-power flash head lamps (some kJ of energy) for

lighting the SUT surface. The same surface is usually monitored by an IR camera. The flash induces a change of the surface temperature causing heat diffusion towards the inner part of the SUT to retrieve thermal equilibrium.

An important characteristic of PT is that the flash duration is significantly shorter than the typical heat diffusion time duration within the samples, so that the heating is quasi-instantaneous while the cooling is regulated by the thermal characteristics of the SUT, i.e., specific heat, density and thermal conductivity. The IR camera collects a sequence of thermograms during the cooling process and information concerning the outer and inner part of the SUT can be inferred from the analysis of the cooling trends of each pixel. Precisely, a cooling trend is associated to any pixel of the IR image, which depends on the pixel emissivity but also on the characteristics of the SUT interior structure.
If a thermal anomaly is present, a change in the related pixels' temperature decay curves can be observed. From a system theory perspective, neglecting lateral diffusion [32,33] and non-linear phenomena, the cooling curve $h_{jx,jy}(t)$ of the (jx,jy) pixel can be considered as its thermal one-dimensional (1D) impulse response where the flash excitation plays the role of the impulsive Dirac delta excitation $\delta(t)$. This assumption has important consequences, since a 1D linear system – as the pixel is assumed to be – is completely described by its impulse response. PT thus provides a powerful tool to inspect painting allowing: the analysis of the conservation status of paintings [34]; a preliminary characterization of constitutive materials and painting technique [35]; the comparison with additional imaging data [36].

Further, it is possible to distinguish between different SUT depths by analyzing thermograms related to different times of the cooling process. This is possible since layers corresponding to different depths in the SUT will affect the thermal impulse responses at different time instants due to the finite time needed for the heat flow to diffuse from the excited surface towards the interior. The major potential drawback in applying PT to paintings diagnostic is the risk of provoking thermochromism on the painting surface, as well as the deposition of too high thermal stresses, which may occur if very powerful flashes are used [37]. However, a certain amount of thermal energy must be delivered to the sample to achieve an SNR level that assures the needed sensitivity to detect defects or anomalies.
As a consequence, the main challenge in the application of active IRT to cultural heritage is to reduce the power of the heating system without losing neither the capability of penetration inside the sample nor the sensitivity.

This result was successfully achieved by the research group of Professor Pietro Burrascano of NDT laboratory of the Engineering department in Terni (University of Perugia) and Professor Marco Ricci of the Department of Informatics, Modeling, Electronics and System Engineering (DIMES) of University of Calabria, who developed an innovative SUT to apply PT not only to investigate industrial and aerospace materials -which is the main focus of their engineering research-, but also

for the investigation of materials that are characteristic of heritage objects, in collaboration Prof. Stefano Sfarra of L'Aquila University's Engineering department who applied thermography and image segmentation for the investigation of heritage materials from central Italy [35].
In 2019, both Engineering research groups of University of Perugia and University of Calabria signed a cooperation agreement with DEIM department of Tuscia University to test PuCT on real ancient paintings.
To manage this delicate process in complete safety for artworks, a crucial element was the knowledge and expertise acquired in the five years of academic education in Heritage Conservation and enhanced in the three years of doctoral research here presented, under the supervision of Dr. Claudia Pelosi, main Tuscia University's scientific expert in diagnostics for cultural heritage and Prof. Giuseppe Calabrò, head of the Engineering School of Tuscia University.

The use of coded modulated heating stimuli in combination with pulse-compression, hereafter referred as Pulse-compression Thermography (PuCT) [38] provides a valid aid in this direction. This is because PuCT allows the impulse responses of the pixels to be retrieved even when using long low-power excitations, if some spectral characteristics of the coded signals are assured. Silipigni *et al.* proposed a PuCT scheme based on coded LED excitation capable of optimizing the estimation of the impulse responses compared to the state-of-the-art PuCT literature [39]. The entire procedure was tested by NDT group of Terni, DIMES department of University Calabria and Engineering department of L'Aquila University on mockups realized on both wooden panel and canvas reproducing a realistic painting containing artificially fabricated defects [38].
It must be noted that the commonly used approach of lowering the heat power while increasing the excitation time is not the optimal one. In fact, the single pixel signal would be no longer a good approximation of the impulse/response if the excitation pulse is too long. Such incorrect procedure makes difficult to interpret data, even if it increases the SNR for some defects [39]. The physical reason underlying this aspect is that by extending the pulse duration, the frequency content of the excitation signal is compressed to low frequencies, thus reducing the information content of the thermograms sequence. This is a crucial point and it is worth giving more insight. Suppose that a heat source is modulated by a sinusoidal signal at frequency f [Hz].
The extended engineering research group approach investigate the limit of penetration/inspection within the sample with such excitation and the spatial resolution achievable.
The theory behind both these issues is provided by the definition of the thermal diffusion length μ, which is the characteristic distance from the SUT surface at which the heat flow amplitude is decreased by a factor $e \approx 2.71$ with respect to its initial amplitude. Further, the parameter μ is also related to the depth resolution achievable at a given inspection frequency. The quantity μ depends on the sample physical characteristics and on the modulation frequency, according to expression (3):

$$\mu = \sqrt{\frac{\alpha}{\pi f}}\,[\mathrm{m}] \tag{3}$$

where $\alpha = \frac{k}{c\rho}\left[\frac{\mathrm{m}^2}{\mathrm{s}}\right]$ is the thermal diffusivity. Here c $\left[\frac{\mathrm{J}}{\mathrm{kg\cdot K}}\right]$ is the specific heat, ρ $\left[\frac{\mathrm{kg}}{\mathrm{m}^3}\right]$ is the density, and k $\left[\frac{\mathrm{W}}{\mathrm{m\cdot K}}\right]$ is the thermal conductivity.

The higher is *f*, the smaller is the inspection depth achievable, but the higher is the depth resolution. A range of frequencies/thermal diffusion lengths must be therefore excited contextually to assure both a good sensitivity of inspection for all the layers of interest in a painting (varnish, paint, drawing, canvas or wooden support, etc.), and a spatial resolution capable of separating thinner surface layers from thicker inner ones. In addition, a certain SNR value – which is also frequency dependent – must be achieved for all the inspection depth/frequency range. PT accomplishes this goal by using a very short excitation pulse that excites a wide range of frequencies but, if the peak power of the pulse is reduced, the delivered energy is too small to assure a good SNR, especially at low frequencies/high inspection depths. PuCT instead modulates a low-power heat source by means of a coded waveform, which can be designed to cope with a wanted excitation spectrum. As a result, the energy is delivered to the SUT spread both in time and in frequency, assuring a great flexibility in the measurement procedure and making possible the use of low power sources. To better understand the proposed approach, it is useful to compare graphically the PT and the PuCT techniques, as shown in Fig. 7. [39].
In PT (Fig. 7(a)), the excitation is considered instantaneous and the sample impulse thermal response is measured for a time Th, which is the expected duration of the impulse response of interest, i.e. the time necessary for the heat diffusion and to retrieving a new thermal equilibrium. In PuCT (Fig. 7(b)), the sample is excited with a coded excitation of duration *T*, while the thermograms are collected for a time ($T + T_h$) [40,41]. By applying the Pulse Compression (PuC) algorithm, an estimated impulse thermal response of duration Th can be retrieved. A thorough description of the PuC theory lies beyond the scope of this thesis and the reader is referred to the literature on the topic, see for instance [39,43–49].

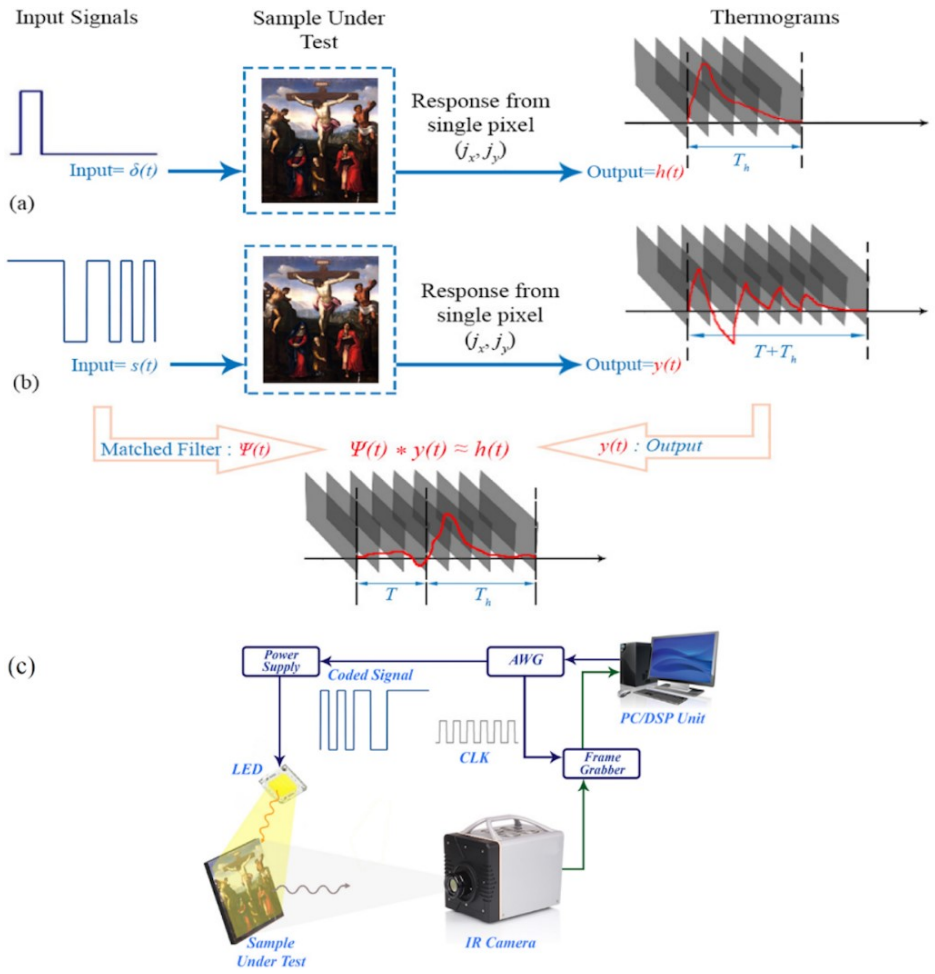

Figure 7. (a) Pulsed Thermography (PT) measurement scheme; (b) Pulse-Compression Thermography (PuCT) measurement scheme; (c) sketch of the PuCT experimental setup. The AWG board provided a clock signal for the frame grabber at which the Xenics Onca-MWIR-InSb IR camera is connected, and it provide also the input signal for the LED power supply. The LED driving current waveform is therefore synchronized with the camera frame grabber. (Image realized by Dr. Stefano Laureti of NDT laboratory of Terni, Engineering Dept., University of Perugia).

Here, only the main steps of the PuCT are summarized and illustrated in Fig. 7(b). A coded excitation $s(t)$ is provided along with the so-called matched filter (t) such that their convolution, here represented by the symbol "*", approximates the Dirac's Delta function: $(t) * \Psi(t) \approx \delta(t)$ excites the SUT that outputs the signal $y(t) = h(t) * s(t)$. By exploiting the properties of linear systems, an estimate of $h(t)$ is retrieved by convolving the system output $y(t)$ with $\Psi(t)$:

$$y(t) * \Psi(t) = \big(h(t) * s(t)\big) * \Psi(t) = h(t) * (s(t) * \Psi(t)) \approx h(t) * \delta(t) \approx h(t) \qquad (4)$$

Many possible choices of the pair $\{s(t), \Psi(t)\}$ were proposed in literature and applied also to PuCT (Barker codes [36-37], linear and non-linear chirp signals [40-45]).
In all the cases, $\Psi(t) = s(-t)$maximizes the SNR but could not be optimal in term of fidelity in the reconstruction of the $h(t)'s,$ which is very important in paintings inspection because of the complexity of the SUT. Moreover, after the application of PuC, some further processing must be implemented, such as the selection of the time interval of interest by removing the first T seconds of the PuC output, as shown in Fig. 7(b). However, beside these technical considerations, here it is worth to highlight two physical aspects that differentiate PuCT from other PuC applications: (i) the difficulty in realizing a bipolar heat source and (ii) the need to distribute, in a reasonable measurement time, the excitation energy in a frequency band wide enough for ensuring contextually both sensitivity to hidden defects and high time-resolution in the $h(t)$ estimation. The first issue was successfully tackled in [37] where it was shown how to optimally apply PuC while using unipolar heat sources. To solve the second point, in this research activity a pseudo-noise (PN) Legendre code was used as $s(t)$[46] and the PuC scheme described in [47-48] was adopted.

PN codes are sequences of 1's and 0's with randomness properties that make them appear noise-like even if generated by deterministic algorithms. Legendre's sequences are a family of PN constructed from Legendre symbol (x/p), which is a short-hand notation for expressing whether "x" is a quadratic residue modulo p or not, where p must be intended as a prime number. With respect to Barker and chirp based PuCT protocols, the present one relying on Legendre sequences provides a better estimation of the $h(t)'s$, allowing the full exploitation of the PT powerful analysis. The experimental setup used to implement the PuCT procedure is the same used in [38-40, 43] and illustrated in Fig. 7(c).
In particular, the signal generation/acquisition was managed by LabviewTM software. Thermograms were collected through a Xenics Onca-MWIR (3.6–4.9 µm)-InSb camera placed in reflection mode, having a resolution of 320×240 pixels, connected to a NI-1433 Camera Link Frame Grabber. The distance between the painting and the camera was between 50 and 100 cm. Eight LED chips emitting in the visible spectrum were used as heat source with an operating total power of ~110 W. The coded excitation driving the LEDs was provided by a TDK Lambda GEN 750W power supply. The frame grabber and the power supply were synchronously driven by the signals provided by a National Instrument PCI-6711 Arbitrary Waveform Generation (AWG) board. Both the AWG board and the grabber were connected to a central PC/DSP Unit.

Before applying PuCT to the paintings, some tests were performed on ad-hoc realized samples to evaluate painting materials stability for the employed heating scheme. In order to ensure the non-invasiveness of PuCT techniques on cultural heritage materials, three small samples of oil painting on panel were realized in the Laboratory of Diagnostics and Materials Science of Tuscia University using art materials (pigments, binders and support preparation for panel painting) coherent

with traditional recipes used in the 16th century panel painting as Giorgio Vasari [50] and Cennino Cennini [51] renowned technical literature.
As a variety of conditions can influence the stability of traditional inorganic and organic ancient pigments [52], the experimental tests led on these samples aimed to esteem a possible colour degradation of pigments under the thermal impulse used in PuCT.
Two sample paintings on wood (10x10x2 cm) were realized and covered with a traditional ground layer made of gypsum and animal glue. After the ground was completely dried, on Sample 1 (Fig. 8(a)) four different ochre pigments were applied in few drops of walnut oil (a suitable quantity to fluidly slather the colours with a paint brush): goethite, green earth, litharge and vermilion. Sample 2 (Fig. 8(b)) was painted with ultramarine blue, azurite, indigo and madder lake. Zecchi (Florence) supplied all pigments.
The choice of the pigments to test was addressed by previous XRF analysis done on the Crucifixion panel painting, which detected elements associated to pigments typically used in Renaissance panel paintings.
A third sample (Fig. 9) was chosen from the archive of the Laboratory of Diagnostics and Materials Science "Michele Cordaro" of Tuscia University's DEIM department. It was prepared with traditional *imprimitura*, that is a preparatory layer suitable for receiving oil painting and described by Vasari [50]. After the complete drying of the *imprimitura* layer, ten mixtures of lead-tin-yellow with nine different growing concentrations from 10% to 90% of *verdigris* (basic copper acetate) were applied on the surface (Fig. 10) [53].

To verify unwanted colour changes due to PuCT pulsed heating excitation, colorimetric measurements [54,55] were performed on Samples 1-3 before and after thermographic investigations. Samples 1 and 3 were irradiated with PuCT emissions of 110W for 90 seconds. Sample 2 was investigated when 140W of power was used to heat it for 90 seconds.
Colorimetric measurements were performed through a reflectance spectrophotometer operating in the visible range between 400 and 700 nm, X-Rite model CA22. The characteristics of the measuring instrument are: geometry 45°/0°; 4 mm diameter measuring area; CIE standard illuminant D65; standard observer 10°; CIELAB 1976 colour space where L* represents the lightness and a* and b* represent the green–red and blue–yellow colour components, respectively. Each colour was measured in five points with three repetition of the measure so that to gather 15 values for each pigment. Average values were then calculated.

To evaluate colour changes, the following equation was used:

$$\Delta E^* = \sqrt{\{(\Delta L^*)^2 + (\Delta a^*)^2 + (\Delta b^*)^2\}}$$

where the value ΔE^* is the distance between two points in the CIELAB colorimetric space. It is generally accepted that for values of ΔE^* under 1.0 no color change is perceptible for the human eye and it is acceptable under a value of 3.0.
In all painting samples, the calculated values of $\Delta E^*$are under 4.0, meaning that no significant colour change was noticeable after PuCT experimental tests. Results reported in Table 1, show how the maximum value ΔE^* was 2.74 in azurite. It must be considered that the values used for testing the PuCT analysis are much higher than those used for the Crucifixion painting so that to be sure of avoiding pigment changes.

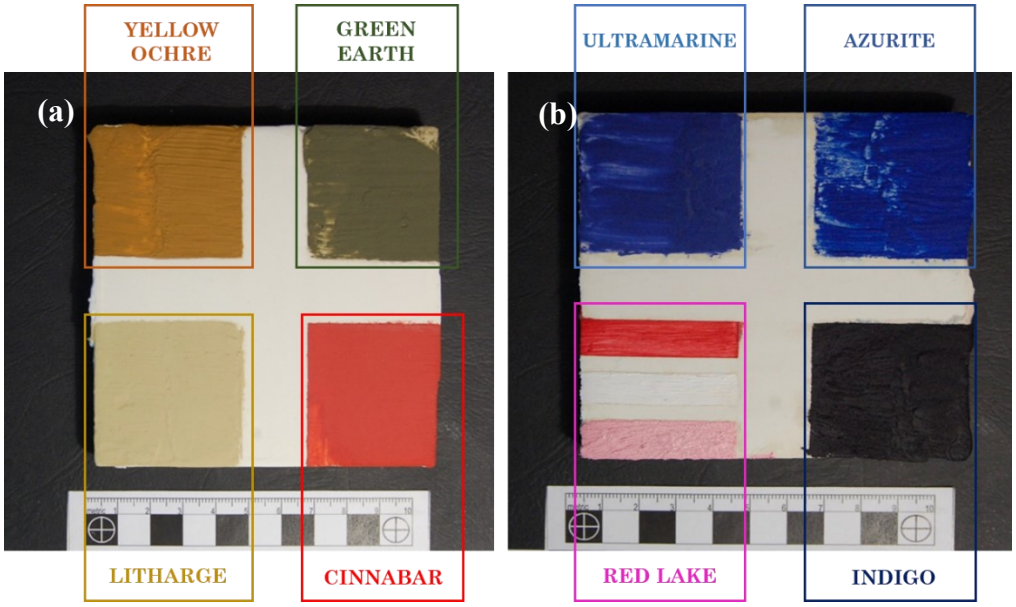

Figure 8. Sample 1 (a) and Sample 2 (b) of ancient pigments in oil binder over a gypsum and glue preparation on wooden support.

V1 Y = 90% + V= 10%	**V2** Y = 80% + V= 20%	**V3** Y = 70% + V= 30%	**V4** Y = 60% + V= 40%	**V5** Y = 50% + V= 50%
Y= 100%	**V9** Y = 10% + V= 90%	**V8** Y = 20% + V= 80%	**V7** Y = 30% + V= 70%	**V6** Y = 40% + V= 60%
V= 100%				

Figure 9. Sample 3, oil painting on panel with *imprimitura* (left) and schematic representation of painting (right) with mixtures of lead-tin- yellow (Y) and verdigris (V).

Sample 1	**Measurements**	**L***	**a***	**b***	**ΔE^***
Yellow Ochre	Before PuCT	50.1	15.9	37.4	**0.443**
	After PuCT	50.5	15.9	37.2	
Green Earth	Before PuCT	40.3	-0.439	13.9	**1.20**
	After PuCT	39.2	-0.366	13.7	
Litharge	Before PuCT	73.2	-0.974	31.4	**0.726**
	After PuCT	72.7	-1.18	30.9	
Cinnabar	Before PuCT	45.2	39.2	21.8	**0.943**
	After PuCT	44.3	38.9	21.7	

Sample 2	**Measurement**	**L***	**a***	**b***	**ΔE^***
Ultramarine	Before PuCT	32.3	2.02	-29.5	**1.00**
	After PuCT	31.8	1.90	-28.6	
Azurite	Before PuCT	28.0	7.91	-37.3	**2.74**
	After PuCT	27.5	6.19	-35.1	
Red lake	Before PuCT	49.1	52.7	20.0	**1.36**
	After PuCT	48.6	51.6	19.4	
Indigo	Before PuCT	19.1	0.461	-1.61	**2.06**
	After PuCT	17.0	0.484	-1.78	

Sample 3	Measurement	L*	a*	b*	ΔE^*
Verdigris (V)	Before PuCT	41.7	-31.5	-3.83	**0.506**
	After PuCT	41.5	-31.1	-3.91	
Lead-tin-yellow (Y)	Before PuCT	80.6	4.40	35.2	**0.275**
	After PuCT	80.8	4.23	35.1	
V1	Before PuCT	74.1	-3.84	26.5	**0.251**
	After PuCT	74.4	-3.79	26.5	
V2	Before PuCT	71.1	-14.6	20.3	**0.0990**
	After PuCT	71.0	-14.5	20.3	
V3	Before PuCT	68.0	-17.9	16.6	**0.419**
	After PuCT	68.4	-18.0	16.7	
V4	Before PuCT	66.6	-17.8	15.4	**1.19**
	After PuCT	65.5	-17.5	14.9	
V5	Before PuCT	64.1	-18.3	13.3	**0.400**
	After PuCT	64.5	-18.3	13.2	
V6	Before PuCT	60.9	-18.8	11.5	**1.92**
	After PuCT	62.8	-19.2	11.6	
V7	Before PuCT	56.6	-21.3	8.22	**0.332**
	After PuCT	56.3	-21.1	8.14	
V8	Before PuCT	51.2	-24.8	3.13	**0.444**
	After PuCT	51.6	-25.0	3.10	
V9	Before PuCT	46.6	-26.3	0.627	**0.376**
	After PuCT	46.3	-26.1	0.561	

Table 1. Results of colorimetric tests on painted samples to evaluate PuCT non-invasiveness.

4. RESEARCH

In this chapter the applications of the innovative integrated diagnostics on real artworks are illustrated. A first case study was the testing of multispectral analysis during the restoration of two ancient copper paintings. To my research group's knowledge, it was the first application of HMI technique for analysis of painted copper surfaces.

4.1 "Hypercolorimetric Multispectral Imaging (HMI) system for cultural heritage diagnostics: an innovative study for copper painting examination"

Published in: ***Eur. Phys. J. Plus (2018) 133: 526. DOI 10.1140/epjp/i2018-12370-9***

The practice of painting on metal surfaces to produce art objects has been engaged since ancient times and their popularity increasingly grew in Europe, especially in the Netherlands and in Italy, during 15th and 16th century [56-57]. It is foreseeable that the development of rolling machines and techniques as etching and engraving during the 15th century, as well as the growth of enameling on copper, contributed to the usage and availability of metals for artistic purpose.
Painting on copper supports has been attractive to artists for a variety of reasons of both practical and aesthetic nature: they are expected to be more durable than paintings on canvas or wood, due to the support being rigid (thus, not being susceptible to tearing or cracking), and due to being made from metal, which does not suffer from biological attack nor does it exhibit a strong response to fluctuations of temperature and relative humidity, but only from minor dimensional changes due to temperature in normal indoor conditions. Such features account for the surprisingly good state of preservation that some paintings exhibit still today. In addition, the rigidity of the support, added to their usually small format, contributed greatly to their portability [58].

Copper supports are non-absorbent [59], can preserve rich and highly saturated colors, even if applied in very thin layers/glazes, due to the oil binder not being absorbed to a great extent. This, in combination with the above-mentioned smoothness and the metal substrate providing a reflective support, resulted in paintings with a real unique, translucent and luminous aspect often described as 'jewel-like' [60], which can contribute to explain copper oil paintings popularity.
A wide range of factors influence the durability, adhesion, uniformity and protective performance of the copper substrate as a support for oil paint: metal purity, alloying, crystallographic structure and surface inhomogeneities bear on the initiation and speed of copper corrosion processes. These characteristics are themselves affected by the production and manufacturing methods, due to residual stresses left by deformation [61].
In order to investigate and restore such complex and unique artefacts, an increasing need for efficient, portable and cost-effective, non-invasive methods for diagnostics is required. Such techniques can extend the amount of information obtained from the artwork analyses with traditional methods and limit the number of invasive testing required [62-64].

In recent years multispectral imaging technique has undergone significant development by virtue of an increasing amount of camera technologies that are rapidly finding applications in different fields, including pharmaceuticals, agriculture and food quality control, as well as cultural heritage diagnostics and in particular for paintings conservation [65-72]. Main advantages of MSI technique are material identification and mapping of artistic materials, to reveal retouching and restored areas in the painting, to differentiate degradation patterns and collect data with the purpose of authentication [73-75]. It is also recognized that full diagnostic potential of MSI may be improved by implementation of robust data processing algorithms for digital images, supporting various aspects of conservation, allowing to observe materials below the surface and, through the combination of different spectral range imaging, to gain latent information on executive painting technique and ancient restorations, as well as for evaluating artwork's authenticity.

One important aspect of spectral imaging is that it generates a large amount of data, which may be difficult to interpret; in this perspective post-processing methods are needed in order to fully exploit the information contained in the image cube. The main achievement of MSI data processing is to distinguish and identify materials from their spectral signatures and to spatially group pixels with similar characteristics.
A large variety of methods are available to perform this task, primarily based on spectral transform and multivariate statistic techniques such as Principal Component Analysis (PCA), spatial domain filtering and neural networks tools [76].
PCA has been widely used for art conservation applications, either as a stand-alone technique or to reduce the dimensionality of datasets using linear algebra techniques prior to another classification algorithm [73, 77-78] whereby multiple variables are analyzed to evaluate the contribution of each variable to an observed result. Clustering techniques can classify data based on a comparison of the spectral character of each point in the image with the spectral character of every other point; this permits patterns or clusters to emerge from within the data, indicating areas of compositional similarity and returning a spatial distribution of components [76].

To the authors' knowledge, this work presents the first ever application of a MSI system of very high radiometric precision, named Hypercolorimetric Multispectral Imaging (HMI), extended in seven spectral bands from 300 to 1000 nm and high spatial resolution digital images for copper painting analysis.

The investigated objects are two 17th century oil paintings on copper plate, one representing a *Virgin of the Immaculate Conception* ("painting A", 14.5 x 19.5 cm) and the other a *Praying Virgin with Sleeping Child* ("painting B", 15.3 x 20 cm) (Fig. 10). The two small copper plates were originally positioned on the external surface of the two shutters pertaining to a wooden chest drawer from the S. Giuliano monastery in L'Aquila (Italy). Both copper plates were altered from previous restorations actions, specifically surface treatments, also interested by conservative problems typical of copper support.
Before restoration, the copper paintings were indeed affected by mechanical deformations of the thin and well-polished metallic support and they both showed significant chromatic alteration of the upper finishing layer (with a probable original finishing still present), consisting of the browning of shellac coats also used for the

maintenance of the wooden shutters and carbonaceous deposits due to the prolonged indoor use of candles.

A further relevant conservative issue was the extended presence of detached areas and losses in the painting layer, which is made up of an overlapping of several thin oil glazing; the presence of an underlying oil preparation layer seems to be probable, also according to specific literature.
Horovitz [56] and Stock [75] both mention a specific practice for the copper plate preparation, which is to apply a layer of linseed oil. They note that this could be done in order to clean the surface from any residues of substances used to roughen the plate, being a practice borrowed from etchers; or as Stock [75] notes, for practical purposes, as its presence is thought to facilitate the subsequent application of the preparation layers. Stock also links, though with reservations, the presence of this oil layer to the etchers' practice of applying a special ground, known as a 'hard ground', consisting of linseed oil and colophony, prior to etching.

In copper painting restoration a great attention is required in the cleaning operation; due to the non-absorbance of the metallic surface, the chosen cleaning agent is not able to homogeneously spread through the support, but it tends to linger on the surface or to be stagnant in the interface between copper and the painting layers, persisting its action on oil binders with an increasing risk of softening and losing of pictorial material. In addition, it is recommended not to use cleaning aqueous systems in order to avoid the start of corrosive reactions [74].

For this reason, some preliminary tests were performed, as usual in restoration works, through the application of organic solvent mixtures. These tests were not effective in removing the surface altered layer.
So, a further test was tried using an aqueous system containing a weak chelating agent (1% of tri-ammonium citrate) alternated with methyl-ethyl ketone. In order to avoid the diffusion of the aqueous solution into the painting layers and the copper support, a hydrophobic compound was applied before cleaning. Specifically, cyclometicone D5 was used as silicone-based gel able to prevent the interaction of the aqueous solution with artwork layers. This new approach seemed to effectively remove the altered finishing layer by means of a weak chelating agent.
Velvesil Plus, a commercial gel made of reticulated siloxane polymers, was also used in correspondence of higher thickness of the altered layer.
The tested systems seemed to be effective in making a highly controlled cleaning of the surfaces avoiding a vertical diffusion of the aqueous solution through the pictorial layer that could affect the painting layers and above all the copper support.

The two copper paintings were investigated with the HMI technique during the cleaning of the altered finishing varnish which entirely covered the original painting layer. The whole acquisition process, including the UV-induced fluorescence image, required only a few minutes and, after calibration, it provided spectral reflectance and colorimetry.

Figure 10. *Virgin of the Immaculate Conception* (painting A) and *Praying Virgin with Sleeping Child* (painting B) before starting the cleaning operation.

The potentiality of the technique can be seen in Figure 11, representing the visible image of painting B during the initial phase of restoration, where the cleaning operation was started on the left vertical half of the painting and the right part was still covered by the altered varnish (Fig. 11(a)). Here Normalized Difference Index (NDI), a common mathematical tool used in digital image processing to enhance contrasts and improve visibility of details [79] was applied using UV band (that is the UV reflected band calibrated and centered at 350 nm) and the IR2 band, image processing (spectral similarity and edge detection) are shown, immediately highlighting some losses of pictorial materials.

Here the most relevant results are reported and discussed in terms of relevance for the conservative aspects of the restoration work. The criterion for choosing the combination of different images was related to the information that conservators expected from the elaboration. The conservation status and the cleaning result were the main interesting aspects for the restoration work: for this reason, UV reflectance and fluorescence images were selected for processing.

In painting A, contrast enhancement operations performed on the combined UV reflectance and the induced fluorescence images have highlighted all the punctual discontinuities in the painted layer, which are mostly concentrated along the edges of the small copper board, where the original frame was before restoration procedures began (Fig. 12(a)). Other contrast enhancement algorithms were applied on the second principal component from PCA performed on the UV-induced fluorescence image combined with the colorimetric blue component of the VIS image (normalized difference: [A − B]/[A + B]). This elaboration allowed to clearly distinguish areas where the altered varnish was completely removed, from areas still covered by residuals of the varnish (Fig. 12(b)).


(a)
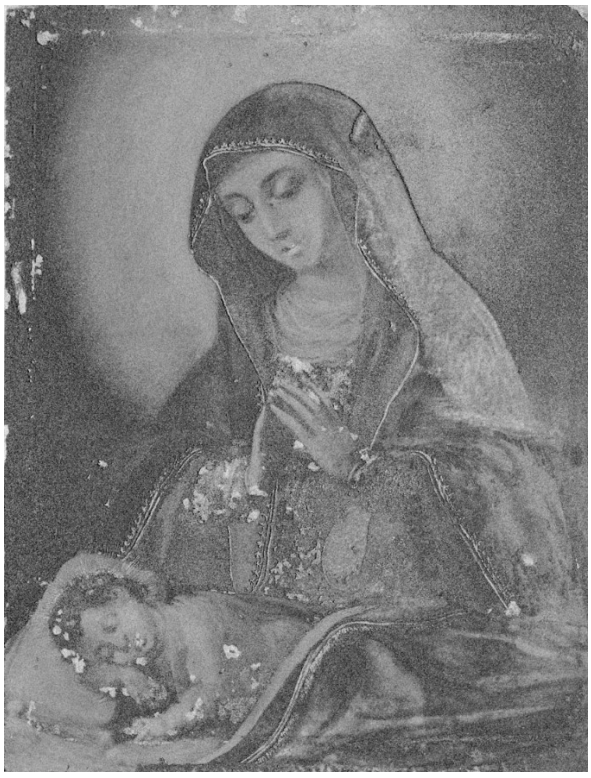
(b)

Figure 11. Painting B: (a) during restoration, with right half still covered by the altered varnish; (b) result of image processing applying NDI on UV and IR2 bands and edge detection tool to highlight the losses of pictorial materials enhanced as white irregular areas.

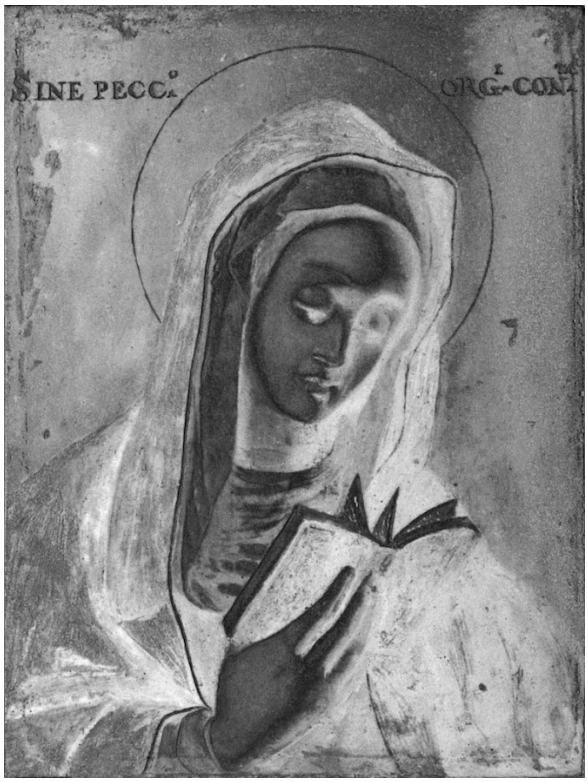

(a)

(b)

Figure 12. Painting A: (a) result of NDI algorithm using UV band (UV reflected at 350 nm) and the UVF images. Punctual discontinuities in the pictorial layer are highlighted. (b) imaging output of second PC from PCA applied on UV-induced fluorescence image and colorimetric blue component of VIS image.

The still uncleaned areas are well visible on the upper part of the Virgin veil and on some letters in the left upper corner of the painting, appearing lighter in respect to the rest of the digital elaborated image. Because these uncleaned areas were both not valuable in the VIS image, the conservators were able to completely remove the altered varnish.
In the HMI investigation of painting B, principal components from PCA run on the induced-fluorescence image were processed with the IR2 image (i.e., the band centered at 850 nm) and the radiometric blue component of the VIS image in order to highlight detachment spots and small mechanical hollows in the metallic foil (Fig. 13a). These are particularly visible in the left part of the painting background (which, at the moment of multispectral acquisition, had been cleaned from the overlaid altered varnish) and in correspondence of the foil's borders originally covered by the ancient frame.
A further contrast enhancement operation, processing the first three components of PCA performed on the UV-induced fluorescence and the RGB image in the UV band, permitted to better investigate the right part of the copper painting, highlighting alteration (probably in the ground layer or in the metallic support) on the top right part of the Virgin's veil (Fig. 13b).

Figure 13. Painting B: (a) result of PCA applied on the induced-fluorescence image processed with IR2 (centered at 850nm) image and the radiometric blue component of the VIS image. (b) image resulting from contrast enhancement, processing the first three PCs applied on UV-induced fluorescence and the RGB image in the UV spectral band.

Thanks to the possibility of having highly reliable spectral reflectance measurement for each pixel of the image, after identifying a little area where the painting layer is missing, pixels of spectral similarity within a given threshold were identified on the whole painting (Fig. 14(a)). Edge detection output on the resulting map has been extracted and over-imposed to the original VIS image, allowing to highlight all the areas where the original pictorial material was missing (*lacuna*), including the ones not

clearly discernible to the naked eye, because of the adjoining painting spots presenting the same color (Fig. 14(b)).
Considering the high resolution and radiometric precision of the HMI imaging technique and the small dimensions of the copper painting, these acquisitions and damage mappings are extremely precious for studying the state of conservation of the painting during the restoration intervention, allowing to clearly distinguish original and restoration materials, alteration products and deformations in the metal support. These results helped to complete a noteworthy restoration project and to preserve an accurate calibrated and high-resolution digital documentation for future conservation and monitoring actions [80,81].

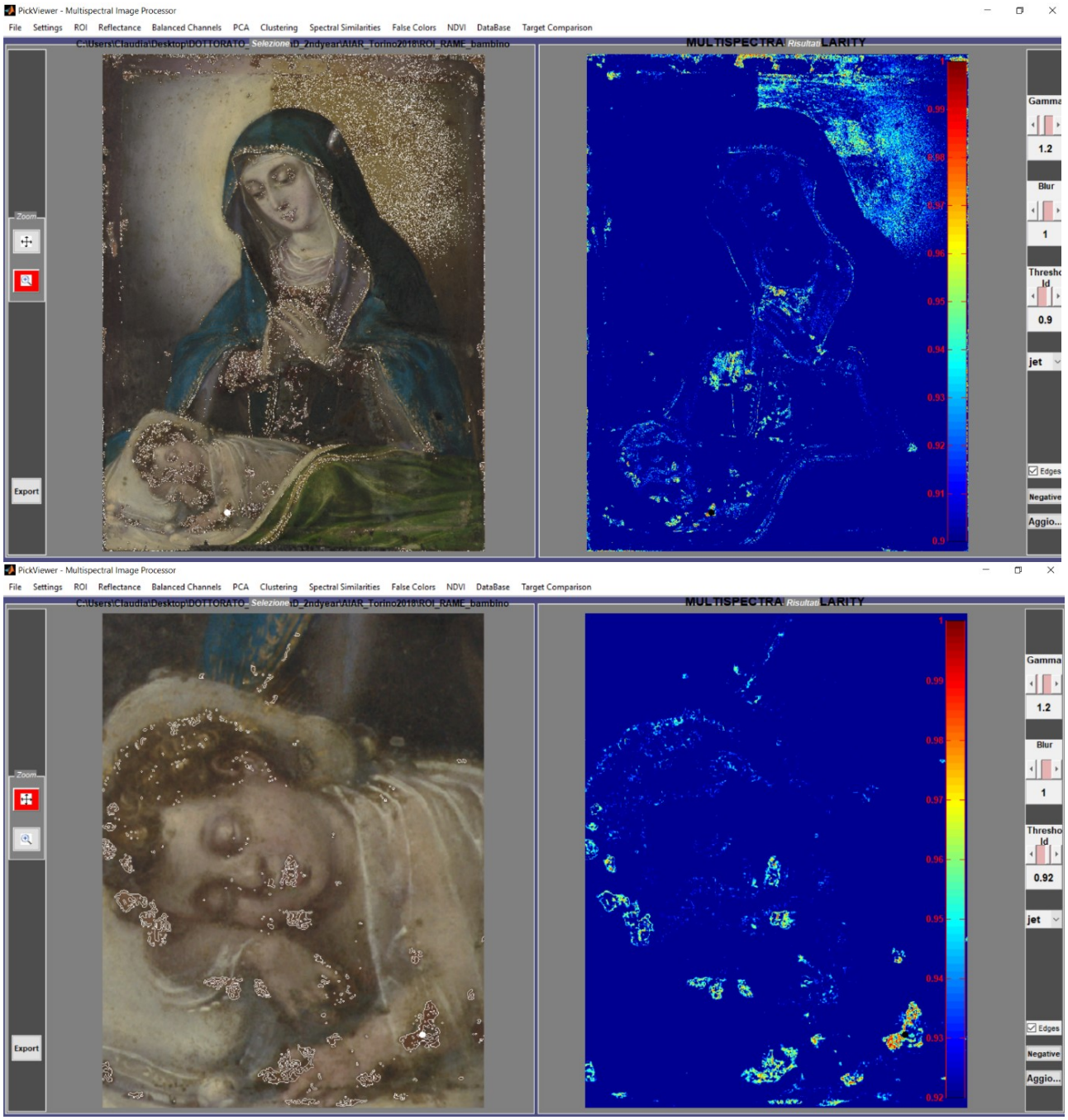

Figure 14. Painting B: (a) multispectral similarity of copper support to map areas of detachments; (b) *lacunae* in the painting layer in the detail of the Child.

In this study, HMI systems provided a powerful tool for non-invasive identification and characterization of pigments, substrates and conservative treatments of cultural heritage objects, allowing non-destructive analyses for paintings restoration and for conservation and documentation purposes.
Residuals of the altered shellac finishing layer, as highlighted in the UVF image, were removed by restorers, thanks to the HMI analysis that detected them by means of spectral and spatial HMI resolution and allowed to address and complete the cleaning process. The HMI system can be considered as a valuable support to evaluate the state of conservation of painting through the identification and mapping of damages and discontinuities in the painting layers and copper support in order to support restorers and monitoring process before, during and after restoration.

4.2 Development of integrated innovative techniques for paintings examination: The case studies of The Resurrection of Christ attributed to Andrea Mantegna and the Crucifixion of Viterbo attributed to Michelangelo's workshop

Published in: ***J. Cult. Herit. (2019) 40, 1–11. DOI 10.1016/j.culher.2019.05.005***

In this second work, the two imaging techniques tested in this doctoral research were applied on two Italian Renaissance panel paintings having not only great historical and artistic values, but also peculiar stories. The first artwork tested was a 16th century oil on panel painting representing a *Crucifixion* attributed to Michelangelo's workshop and currently on display in the Museum of Colle del Duomo in Viterbo, Italy (Fig.15(a)). Previous investigations, based on traditional photographic and spectroscopic techniques, highlighted interesting details in the Crucifixion painting that deserved further deepening, such as the technique used to draw the St. John face [82]. The face, in fact, changes its traits when observed under UV fluorescence assuming a more masculine appearance.
This hypothesis was made after the discovery of a will, dated 1725, reporting that a crucifixion by Michelangelo was donated to the Jesuits of Viterbo by Paolo Brunamonti [83]. Even though this document alone does not prove the attribution of the "Viterbo Crucifixion" painting to Michelangelo, there are some elements, such as the presence of Buonarroti in Tuscia and his relationship with Vittoria Colonna and with the reform movement known as Spirituali (or *Ecclesia Viterbiensis*), that suggest that an artwork of the Master should be present in Viterbo [83–89]. The deep friendship between Michelangelo and Vittoria Colonna, well-documented by their extensive epistolary relationship, had probably a role in the spiritual nearness of Michelangelo with the *Ecclesia Viterbensis* and influenced Michelangelo's artistic thought and production, as reported in various relevant studies [86–91]. Some interesting elements of the "Viterbo Crucifixion" painting support the proposed attribution hypothesis. One is the unusual landscape at the back of the cross: a view on a towered town, which recalls the present Porta Faul in Viterbo, while the ruins in the background evoke the Bacucco thermal baths [90].
A second interesting element of the painting concerns a garment detail, the perizoma of Christ that exhibits a quite anomalous pink hue. Indeed, in liturgical terms this is usually referred to Easter, and not to Crucifixion.
According to Elisabetta Gnignera [90], the use of this unusual color should be associated to the peculiar thinking expressed both by the Spirituali and by Vittoria Colonna (in

two of her spiritual sonnets) that considers the death of Saviour as a joyful event because of man's salvation in Christ. Indeed, the anomalies and variants in the *Crucifixion* of Colle del Duomo (in comparison, for example, with later replicas by painter Marcello Venusti) strengthen the hypothesis of a link between this artwork and the religious debate that originated immediately after the publication in 1543 of the book *Beneficio di Cristo* (The Benefit of Christ's Death), which reflects the radical thinking of the Spirituali [91].
Another interesting detail concerns the face of Christ that appears dark and seems re-painted from the rest of the figure. Lastly, the Magdalene at the foot of the cross seems to be added subsequently both to the Virgin and the cross, leading to the hypothesis that it was added subsequently to the other parts of the painting. Art historians hypothesized that the change in Christ face and the probable addition of Magdalene could be linked to the 1556 Catholic reforming decree of the Pope Paul IV (born Gian Pietro Carafa), that established some dictates in religious painting representations such as that forbidding to depict the crucified Christ alive [91].
The second artwork inspected was *The Resurrection of Christ*, a late 15th century (about 1492) tempera on panel painting owned by the Accademia Carrara, Bergamo, Italy (Fig.15(b)). In May 2018, this painting was re-attributed to Italian Renaissance's master Andrea Mantegna by Dr. Giovanni Valagussa, who identified it as the upper half of a unique composition, whose lower part is the Descent into Limbo painting [92]. The dismembering of famous paintings was a well-known and frequent practice since the Renaissance, with the purpose to gain more in a sale but also to adapt the artworks to customer's demands [93].

Figure 15. (a) *Crucifixion*, oil on panel painting, Museo del Colle del Duomo, Viterbo (Italy), attributed to the Michelangelo's workshop; (b) *The Resurrection of Christ* during restoration at the time of the measurements, tempera on panel, Accademia Carrara, Bergamo (Italy), attributed to Andrea Mantegna, ca. 1492.

Beyond the main lengthwise cut, *The Resurrection* underwent other further modifications as the added of a 2-cm-wide board of walnut wood on the left edge of the panel in a restoration of late 16th – early 17th century. In this new appearance, the painting was bought by Guglielmo Lochis in 1846 before entering the Accademia Carrara collection in 1866, where -probably after some bad restorations suffered in those 20 years- it was at that time downgraded as a copy of Andrea Mantegna, maybe made by his son Francesco Mantegna [94]. At the time of the experimental activities reported here, *The Resurrection of Christ* was being restored at the Accademia Carrara by Ms. Delfina Fagnani Sesti.
The main aims for applying the two techniques on the panel paintings can be summarize as follows: i) to investigate the general conservation status of both artworks in order to support the restoration work, underway in the case of *The Resurrection of Christ*, and to be carried out in the near future in the case of the *Crucifixion*; ii) to detect details of the painting layers, of the ground and of the wood support such as areas of ancient retouching and re-paintings, grouting, preparatory drawing, wood defects, nails, cracks, etc.; iii) to make hypothesis about pigment composition; iv) to reveal details in the paintings' construction that could help to support the artworks attribution. In fact, especially for the Crucifixion panel painting, the attribution to Michelangelo Buonarroti workshop is still under discussion between art historians and the information derived from the present investigation can be particularly useful for the discussion.

The PuCT output consists in a time- sequence of images where the time evolution of the (j_x, j_y) pixel intensity is nothing but its thermal impulse response $h_{jx,jy}(t)$. By analyzing images at different cooling times, it is possible to clearly appreciate the upper painting layer and the wood inner structure of the support in the same acquisition, permitting a non-invasive stratigraphic analysis of the painting. This is illustrated in Fig.16 for the *Crucifixion*, wherein acquisitions were made on the whole figure and zooming then onto the Christ's figure.

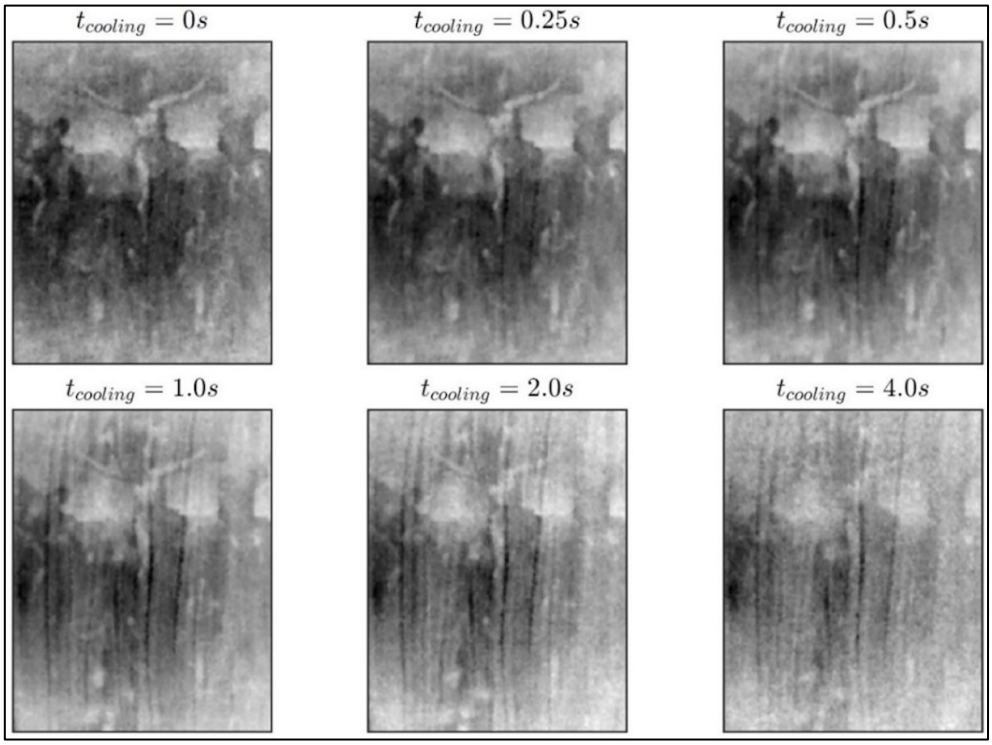

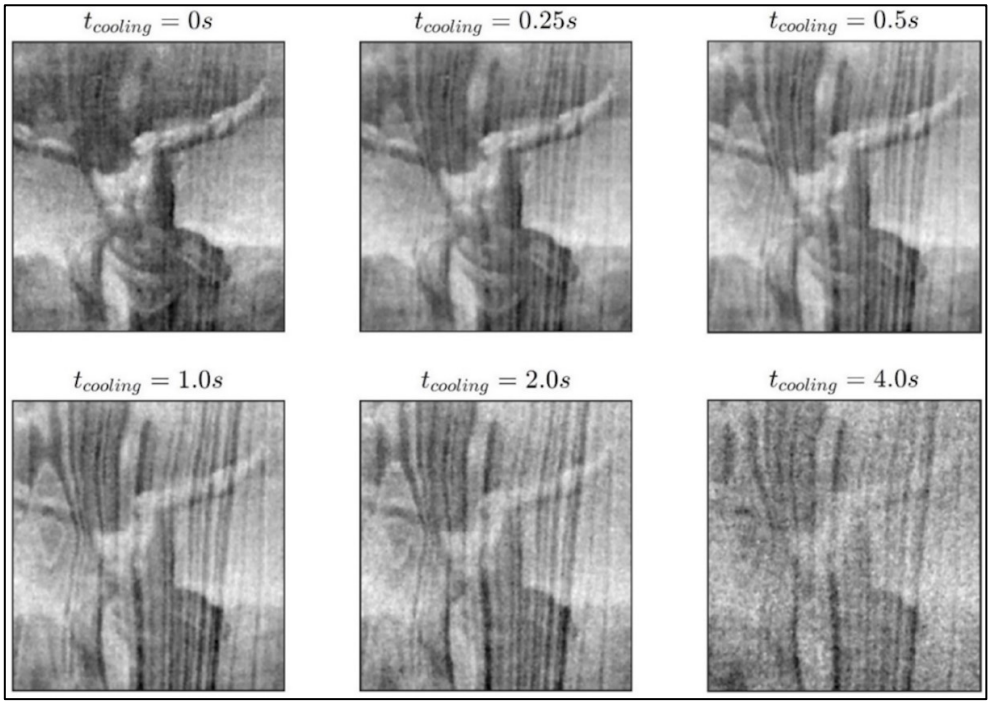

Figure 16. (a) *Crucifixion*, images of thermographic emissivity retrieved after PuCT at different cooling times; (b) zoom on the Christ's figure. The details of wood panel become clearly visible after 1 s of cooling while the influence of the paint texture becomes negligible after 2 s of cooling.

At the beginning ($t_{cooling} \leq 0.5$ s) only the paint layer affects the surface emissivity, so the thermal image is strictly correlated with the visible one (lighter colors appear colder than darker ones). As the cooling proceeds, the surface emissivity is affected also by the wood grain of the underlying panel. After few seconds ($t_{cooling} \geq 4$ s), the contribute of the paint layer to the thermal image is almost null while the deep structure of the wood panel is visualized.

The same analysis was also executed on Mantegna's painting *The Resurrection of Christ* and results are depicted in Fig. 17, showing both Christ's figure and the top-right part of the painting. Even in this case, only the paint layer affects the surface emissivity at the beginning of the cooling stage. However, the surface emissivity starts to be affected also by the wood grain of the underlying panel as time elapses, i.e. as the cooling takes place. In addition, quite regular horizontal lines are visible for $0.25s \leq t_{cooling} \geq 0.5s$, especially on the top-right part, which should be located just underneath the paint layer and over the wooden support.

The horizontal lines are very regular - they have the same height and are equidistant. This led the authors to suppose that the horizontal lines might be related to the application of the gypsum and glue preparatory layer in coatings, as described by the Medieval artist Cennino Cennini in his technical essay [51], where he recommended to finish the preparatory layer with up to eight thin gypsum coatings, alternating vertical and horizontal brushstrokes. It's worth noting that only few frames are shown here, but any other time interval of the sequence can be willfully chosen, enabling the examination of a high and changeable number of investigated layers: this is a significant advantage when inspecting complex objects like those of cultural heritage. To the best of the authors' knowledge, such results are not achievable with other diagnostic imaging techniques, but only when combining different methods from different sources, though no real imaging integration is often possible. Further, in this case at different times

correspond different thermal images, which can be correlated to different depths within the SUT.

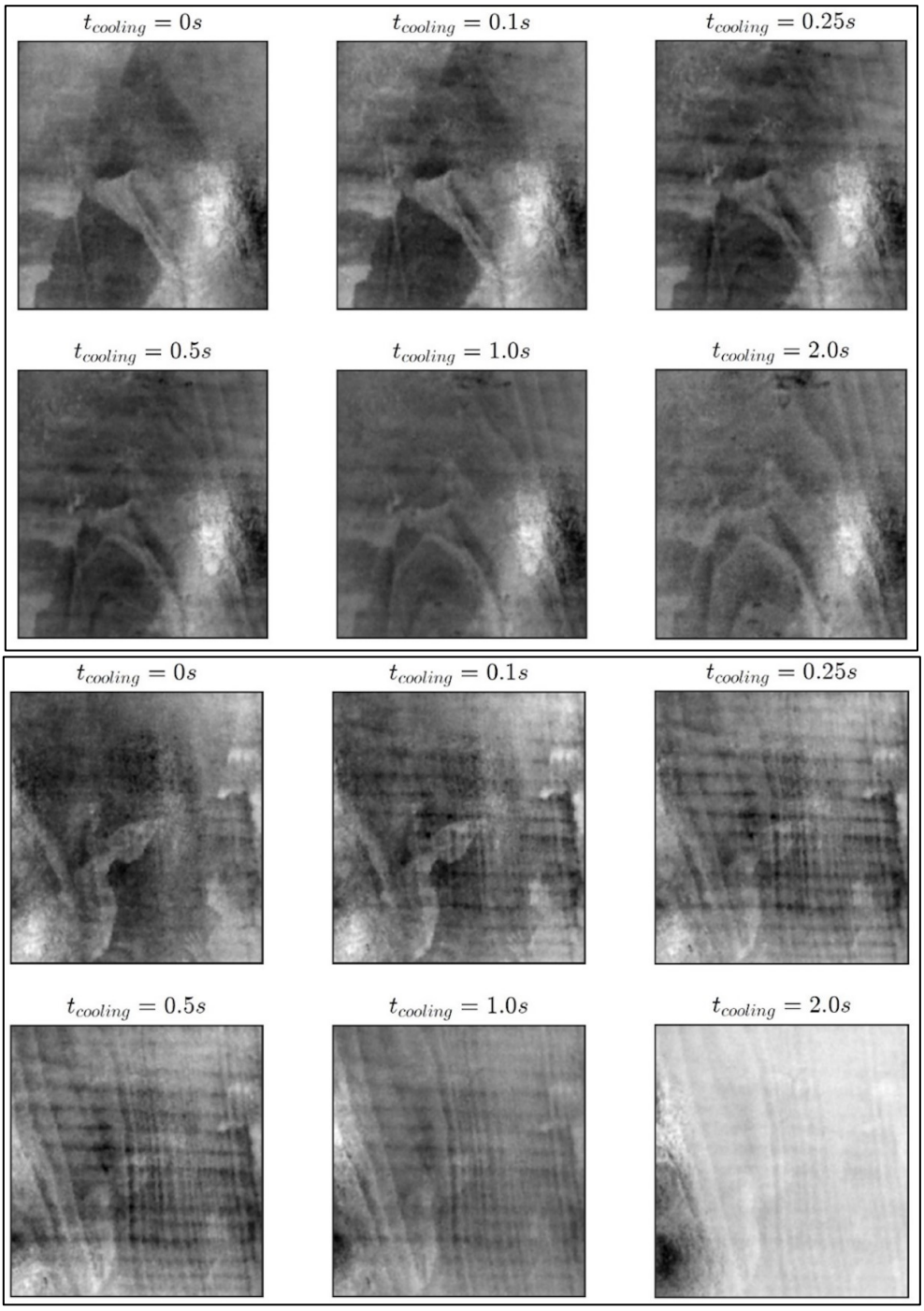

Figure 17. *The Resurrection of Christ*, images of thermographic emissivity retrieved after PuCT at different cooling times. The details of wood panel become clearly visible after1 s of cooling while the influence of the paint texture become negligible after 2 s of cooling for: (A) Christ's figure and (B) Christ's body.

In addition, PuCT analysis can also consider different features than just emissivity for imaging purposes. For instance, time-phase was introduced in [43-49] in combination with PuCT. Time-phase is a feature extracted from pixel impulse response and it is expected to be almost independent from the pixel emissivity, hence from the color. Fig.18 shows the images of four areas of *The Resurrection of Christ* obtained by

visualizing both emissivity (left) and time-phase (right) features at $t_{cooling}$ = 0 s. Time-phase allows a direct visualization of the wood grain of the panel and in general of the structure behind the paint layer. Besides these imaging capabilities, the analysis of PuCT images also confirmed some facts or hypotheses on specific details of both paintings. In fact, PuCT confirmed alterations in Christ's face in the *Crucifixion*, since the pictorial layer presents significant differences in the thermographic response (shown in grayscale in terms of thermal emissivity as a darker area) in comparison to the body. In *The Resurrection of Christ*, PuCT images reported in Fig. 19, bottom-left quadrant, highlight the presence of two nails and the related grouting.

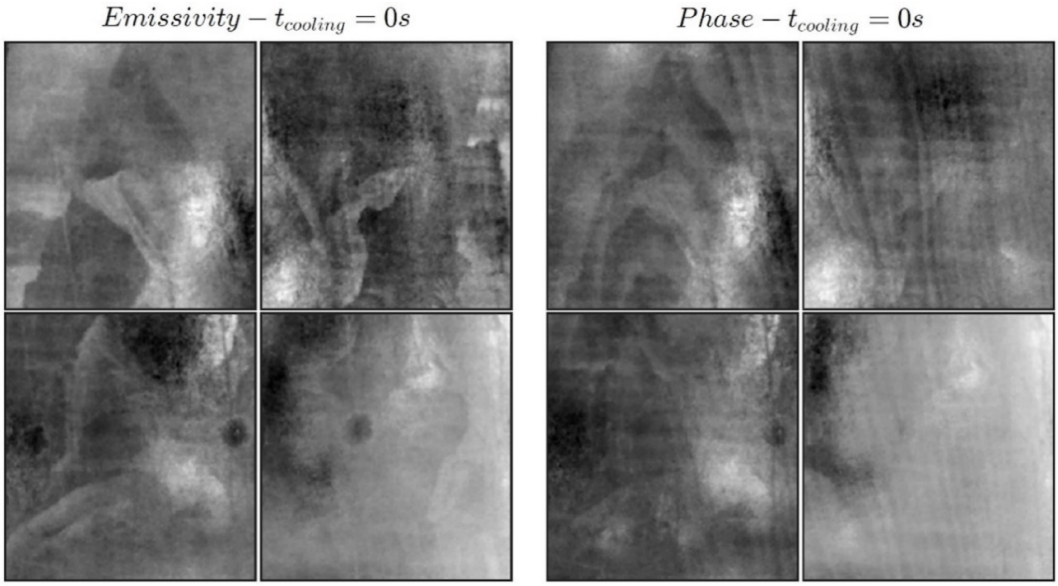

Figure 18. *The Resurrection of Christ*, comparison between PuCT images of the thermographic emissivity (left) and time-phase (right) features in partially overlapping painting areas.

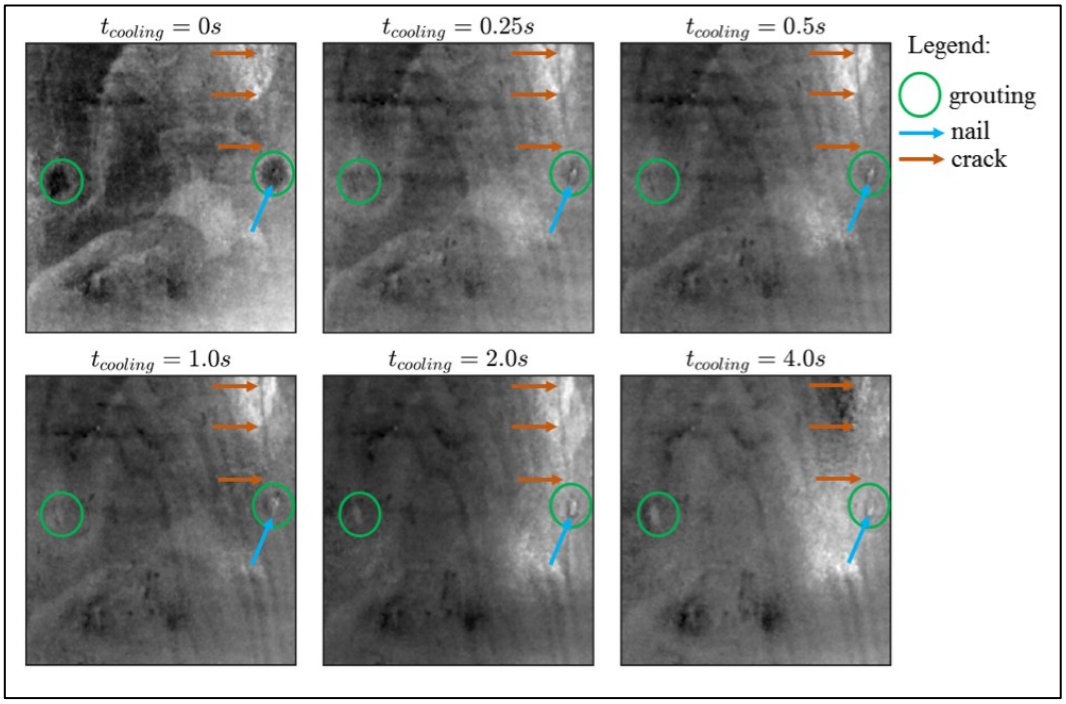

Figure 19. *The Resurrection of Christ*, comparison among PuCT images of the bottom-left-quadrant corresponding to different cooling times, showing the grouting, nails and cracks. (image realized by NDT laboratory of Engineering department of Terni, University of Perugia).

A long crack is also visible in correspondence of one nail underneath the lying down figure. To better highlight these details, Fig. 19 reports a sequence of images of the bottom-left-quadrant corresponding to different cooling times that illustrate how, in the case of the nails, firstly is detected the grouting as a hot spot. Then, the section of the nails appears as a cold spot as time elapses, due to the higher thermal conductivity of metal with respect to the background. Regarding the crack, the authors assume this is the case since the wood grain pattern, which is well visible, has a different direction around the crack.
As a curiosity, by comparing emissivity and time-phase images reported in Fig. 18, it is possible to notice that the mountain shape on the background of the Christ figure follows the pattern of the wood grains underneath.
Starting from these results, many image and signal processing techniques could be applied to the thermal images. As a starting point, in this work the PuCT results are integrated with those from HMI, as explained in the next subsection.
As explained in the previous chapter of this thesis, HMI allows several image processing possibilities that can be performed on the calibrated multispectral images. In the present discussion, the most relevant images and their combinations will be shown. The UVF image obtained through HMI (Fig. 20(a)) clearly shows the conservation condition of the entire painting surface of the two paintings examined, highlighting areas repaired (dark color) and abrasions.

Figure 20. *Crucifixion* panel painting: HMI UVF image (a) and results of HMI processing output of contrast enhancement (NDVI) on IR3 and first PC of PCA on UVF of the Crucifixion showing the fractures and the restored areas (b).

In the (Fig. 20(a)) UVF highlighted three main vertical cracks in the painting layers in correspondence of ancient repairs of the wooden support. Some areas seem to exhibit bright red fluorescence (Christ's perizoma and St. John's garment), suggesting the possible presence of organic lakes. UVF image also reveals a detail (Fig. 21(b)) of St. John's face appearing different from what is seen in the visible (Fig. 21(a)).

In particular, it assumes more masculine traits and a hollowed aspect, the neck appears slim and the hair hung loose on the shoulder respect to its aspect, more graceful, round and feminine in the visible radiation. The singularity of this difference is that it is present only in the face of St. John and so it appears intentional, as previously discussed also in relation to the historical background [82-83].

Figure 21. Comparison of the detail and detail of St. John's face in the Crucifixion in HMI VIS (a) and HMI UVF image (b).

The hypothesis of art historians is that the painting should be observed with glass, lamp and mirror in order to see the changes in Saint John face, according to the letter "*del lume*" (of the lamp) that Vittoria Colonna wrote to Michelangelo about a Crucifixion. The possible relation of the letter to the Crucifixion is reported by Antonio Rocca, an art historian of Egidio17, in his book [91, pag. 53].
The friendship of Michelangelo with Vittoria Colonna, and consequently with the *Ecclesia Viterbensis* is well-documented in literature and most certainly influenced his artistic thought and production, as reported in the literature [83-85].

Other worth-mentioning DIP outputs were obtained applying contrast enhancement on IR3 and the first principal component resulting from PCA run on the UVF image of the *Crucifixion* (Fig. 15(b)). This processing highlighted general structural damages and discontinuities especially in the left part of the painting. Three main vertical cracks in the painting layers are visible in correspondence of ancient repairs of the wood support. The area corresponding to the vertical crack is darker with respect to the background, suggesting that it was filled by stucco, during the previous mentioned restoration, and retouched. The garment of Magdalene at the foot of the cross overlays with the Virgin's mantle, as confirmed by previous investigation by 3D video microscopy HR HIROX 2000 under the supervision of Dr. Claudia Pelosi and Dr. Giorgia Agresti, that revealed a thickening of ~380μm in the pictorial layer in the area where the two garments meet (Fig. 22(a)). Furthermore, the use of two different blue pigments for the vests of the Virgin and the Magdalene's one was highlighted by HIROX macro images (Fig. 22(b)). The possibility of using this high-resolution 3D microscope was due to SIMITECNO Srl Society and to its responsible Dr. Marco Brecciaroli who performed the acquisitions in the Museum of Colle del Duomo on the panel painting.
This data supported art historian studies according to which the Magdalene is a later addition, due to the garment typology that can be dated back to the '60s of the 16th century (private communication made by Dr. Elisabetta Gnignera, art historian and specialist of Renaissance costume). The same analysis was performed on the detail of the Christ's face, darkened and of a different material consistence respect to the body

as highlighted by HMI and PuCT, confirming a lowering in the pictorial layer of ~100µm as it was abraded and retouched (Fig.23).

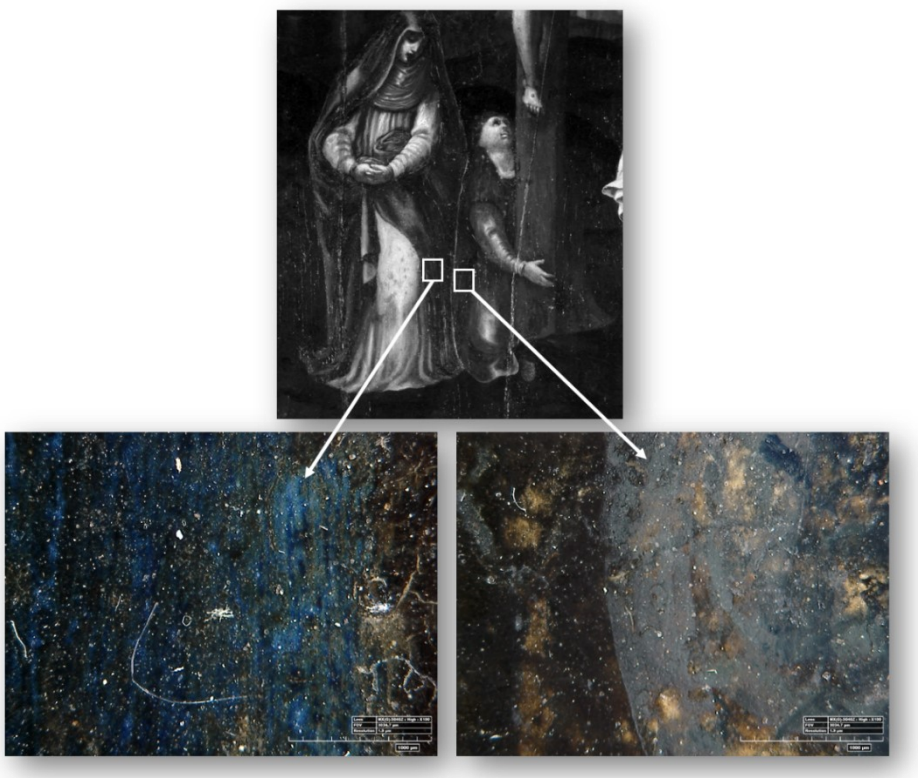

Figure 22(a). Detail of HMI IR image enhancing the overlaying of the Magdalene vest over the Virgins garment and HIROX macro details of two different blue pigments.

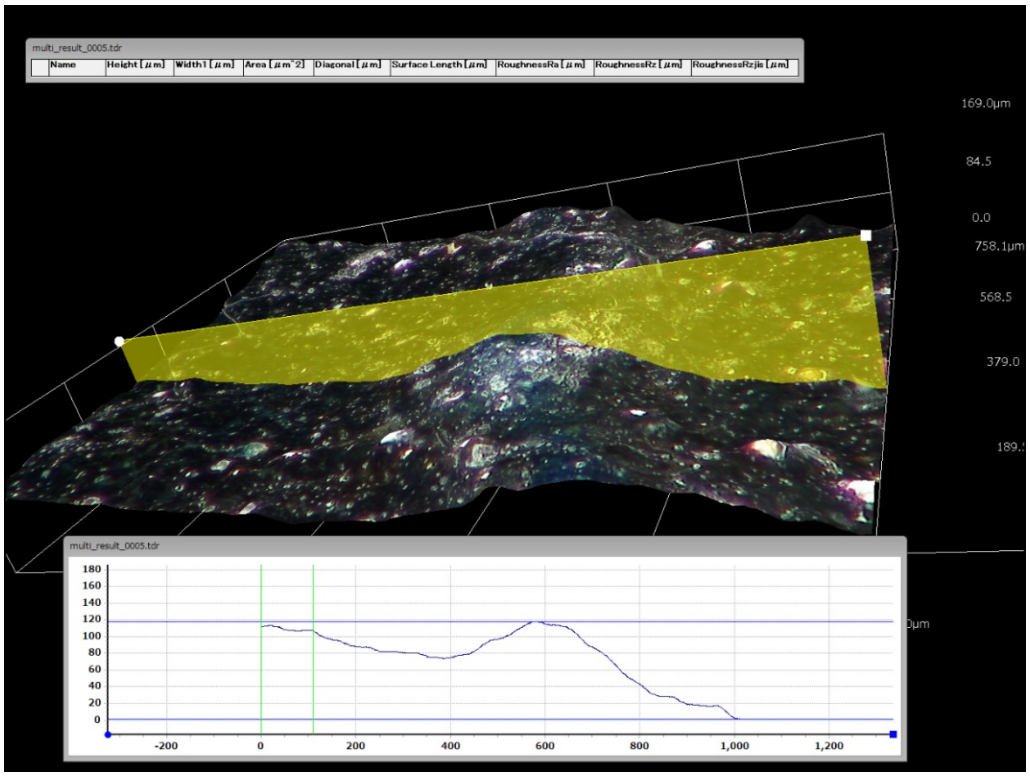

Figure 22(b). HIROX microscopy 3D image showing the thickening in the pictorial surface (thanks to Dr. Marco Brecciaroli of SIMITECNO Srl).

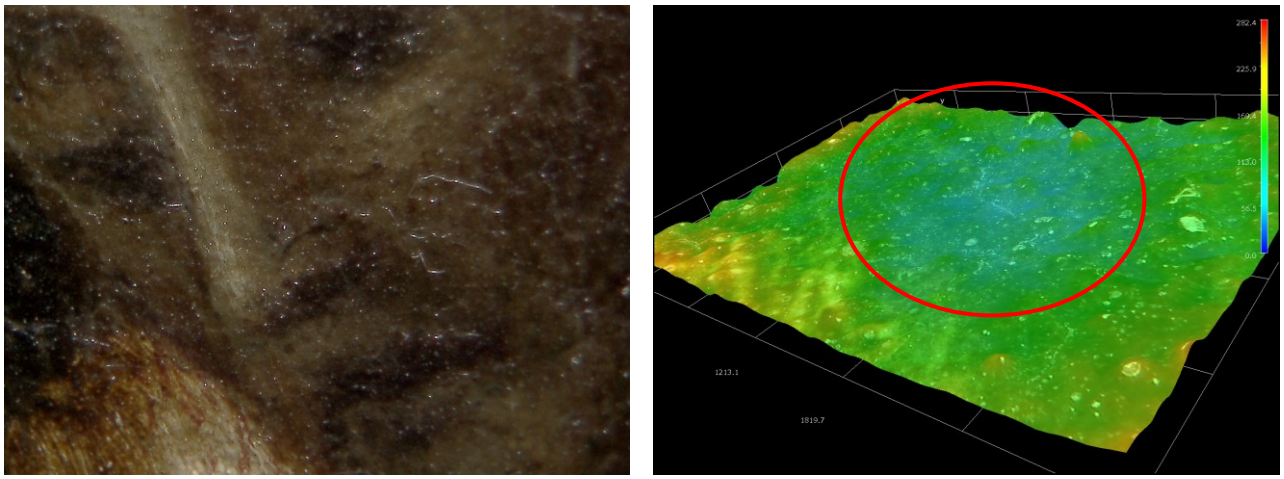
Figure 23. Detail of the altered face of Christ in the *Crucifixion* (left) and HIROX 3D image of the pictorial layer in the corresponding area (pointed out by a red circle) (thanks to Dr. Marco Brecciaroli of SIMITECNO Srl).

In Fig. 20(b) the face of Christ appears as a clearer area respect to the entire figure, showing a difference in terms of surface appearance. In the visible, the face is indeed darker and roughed out with respect to rest of the body (also shown in detail in Fig. 23, left image). In addition, it seems a smoother layer compared with the surrounding background of the painting. HMI investigation confirmed this observation showing that Christ's face has a different spectral response with respect to the rest of the figure, suggesting that this area had been abraded or heavily retouched in previous restorations. It is out of the scope of this paper to explain why the Christ face was abraded and repainted, but art historians could use this datum to make connection with the historical period to which the painting seems to be refereed, i.e., the first half of 16th century.

PCA gave relevant results also in Andrea Mantegna's painting, allowing to appreciate the very good conservation state of the panel, with no discontinuities in the pictorial layer. This result confirms the impression of the restorer after the initial phases of cleaning procedures, when it immediately appeared clear the excellent state of preservation as well as the high quality of the painting technique [93].
Additional digital image processing (DIP) tools such as false-color IR image (Fig. 24) and false-color UV image (Fig. 25) enables to make hypothesis on pigments' typology in the palette of Andrea Mantegna, based on their different spectral reflectance. In IR channels false color, blue areas become vinous red and the red ones appear as intense yellow. The orange zones assume a light-yellow color. The UV images supply other information concerning the painted areas. Specifically, the red and orange parts, which appear yellow in IR false-color, have different color under UV, i.e., the red paint becomes violet whereas the orange one transforms into purple color. The blue paint used for the sky and parts of the clothing becomes green in UV false-color, suggesting that the same blue pigment was used.

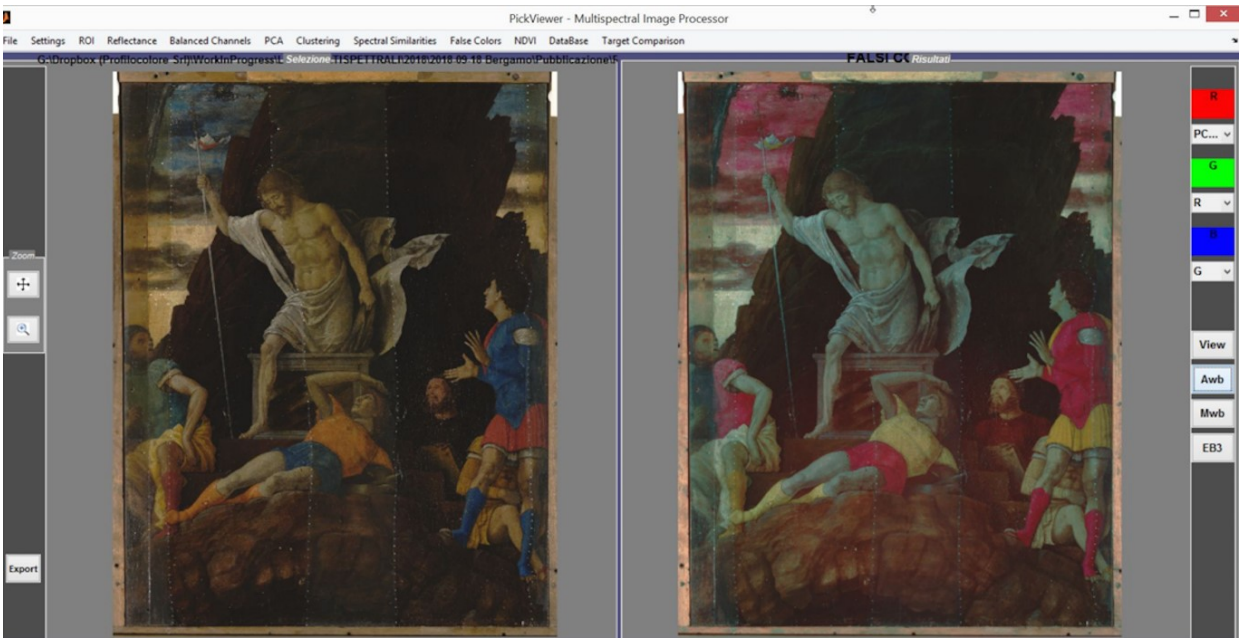

Figure 24. False-color IR image of *The Resurrection of Christ* shown in PickViewer GUI.

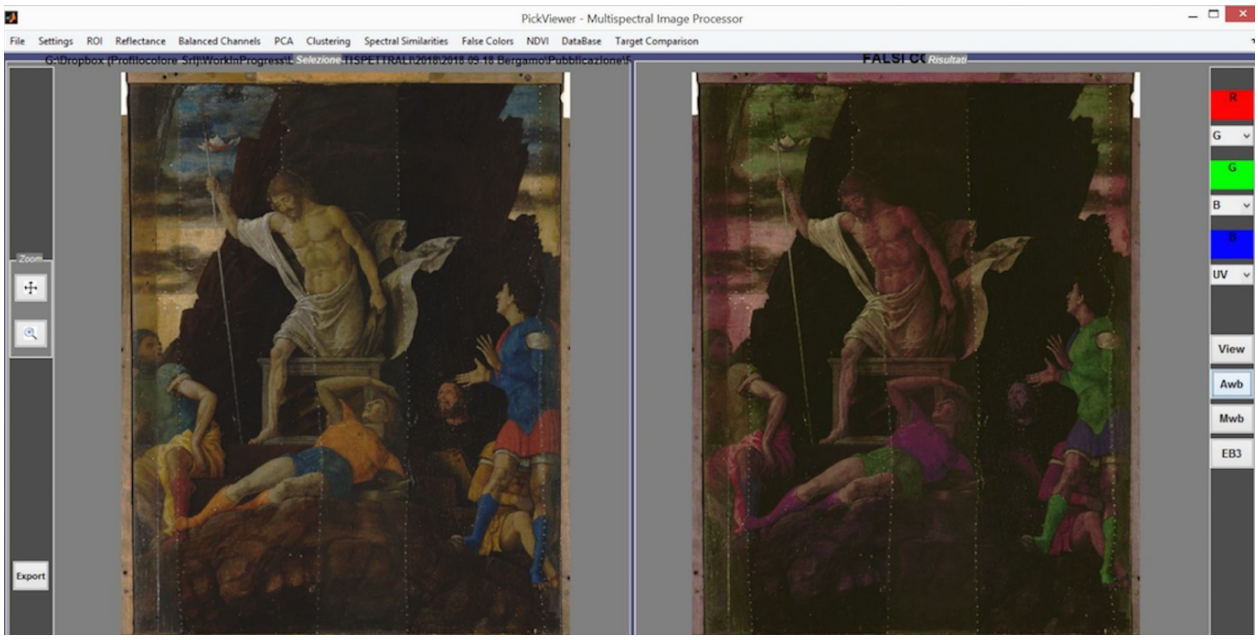

Figure 25. False -color UV image of *The Resurrection of Christ* shown in PickViewer GUI.

By combining these findings, it can be supposed that the artist used ultramarine blue for the blue areas, vermilion/cinnabar for the red ones, and red lead for the orange parts. Furthermore, in the false-color UV image two different spectral responses are observed in the garment of the soldier on the left, suggesting the use of two different yellow pigments, the first one original, while the second used in an ancient restoration.
This datum is in accordance with the addition of the wooden 2-cm board on the left that completed the missing details also with some arbitrary choices, such as the head of the soldier on the left which pertains to another figure in the background. This result is based on the existence of an ancient copy, probably by Girolamo Mocetto (Venetian school, 1458-1531), that showed the original version of Mantegna's Resurrection as it appeared in the Gonzaga inventory of 1627 [92, 95].

Further statistical processing was done through normalized difference of HMI UVF, UV and images in the visible spectrum, which allowed to appreciate details in the rock background whose finest design was not visible before (Fig. 26).

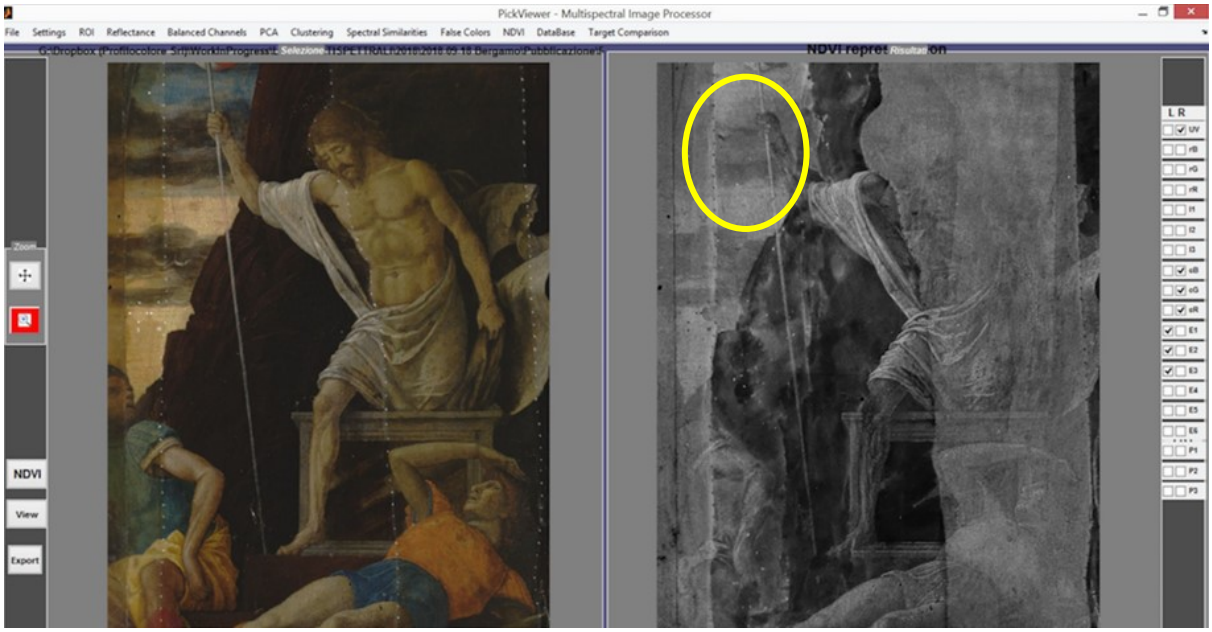

Figure 26. Normalized difference of HMI UVF, UV and VIS images applied in SpectraPick® software GUI.

A clear shift can also be observed in the position of Christ's right arm, probably due to a pentimento of the artist (highlighted in yellow in both Fig. 26 and well visible also in Fig. 27a).
The most interesting results were obtained by combining HMI and PuCT imaging results in Profilocolore PickViewer® software. DIP of multispectral and thermographic data allowed the pictorial surface characteristics and the natural structure of the wooden support to be deeply correlated. This was achieved by applying PCA on HMI UV-induced fluorescence images and on PuCT images at different cooling times.

In *The Resurrection of Christ*, DIP tools as Normalized Difference applied to PuCT and IR images (Fig. 27(a)) stressed the high correlation between the paint layer and the wooden support. In fact, the painting composition seems to follow the wood grain underneath as also shown in the PCA results on PuCT detail of Christ figure (Fig. 27(b)), that is centered in the area of the wood knot. This could probably be due to the very thin gypsum preparation that Mantegna used and which has been esteemed to have a thickness of around 10 μm [96]; such a thin layer allows the natural wood grain of the panel to be seen - Mantegna could have potentially used them as a spatial reference for the realization of the painted scene.

For the *Crucifixion*, the vertical cracks of the panel - restored with stucco during an ancient intervention – running across the right branch of the cross, appear perfectly related and coherent with the underlying wood grain, as shown in the second principal component (Fig. 28(a)). In the second principal component matching HMI UVF and PuCT only at 0.22 s and 0.84 s (deeper layer in the support), a wood knot is clearly visible in correspondence with Christ's right arm (Fig. 28(b)).

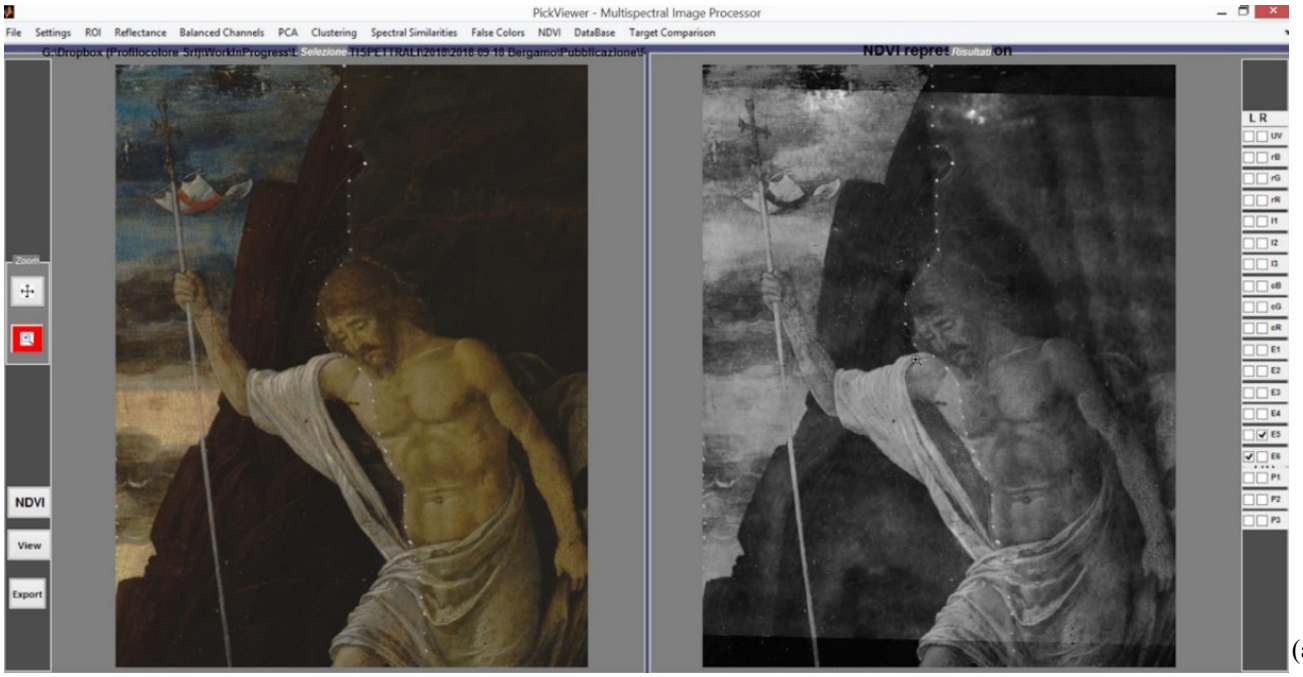

(a)

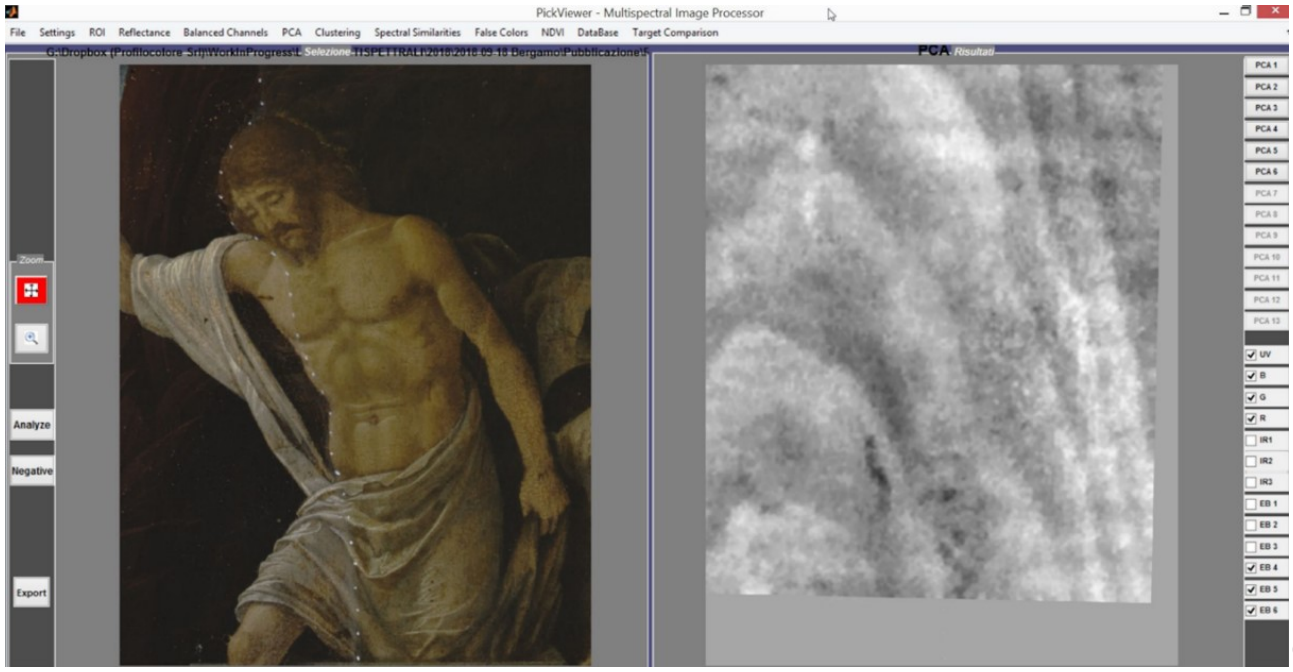

(b)

Figure 27. Details of the output of HMI and PuCT integration. (a) Normalized Difference on PuCT and HMI IR shows how wood grains are visible through the upper pictorial layer. (b) PCA applied over PuCT data shows the panel support in the same investigated area.

The combination of HMI and PuCT imaging results in Profilocolore PickViewer® software allowed to highlight further details in the inspected paintings.
Specifically, for *The Resurrection of Christ*, high correlation between the paint layer and the wooden support was revealed combining only two imaging techniques *in situ* and rapidly in a complete non-invasive way. At the current state of the art, this achievement was not possible before in these conditions, at once and in a reduced time of acquisition without moving the artwork out of its exposition setting.

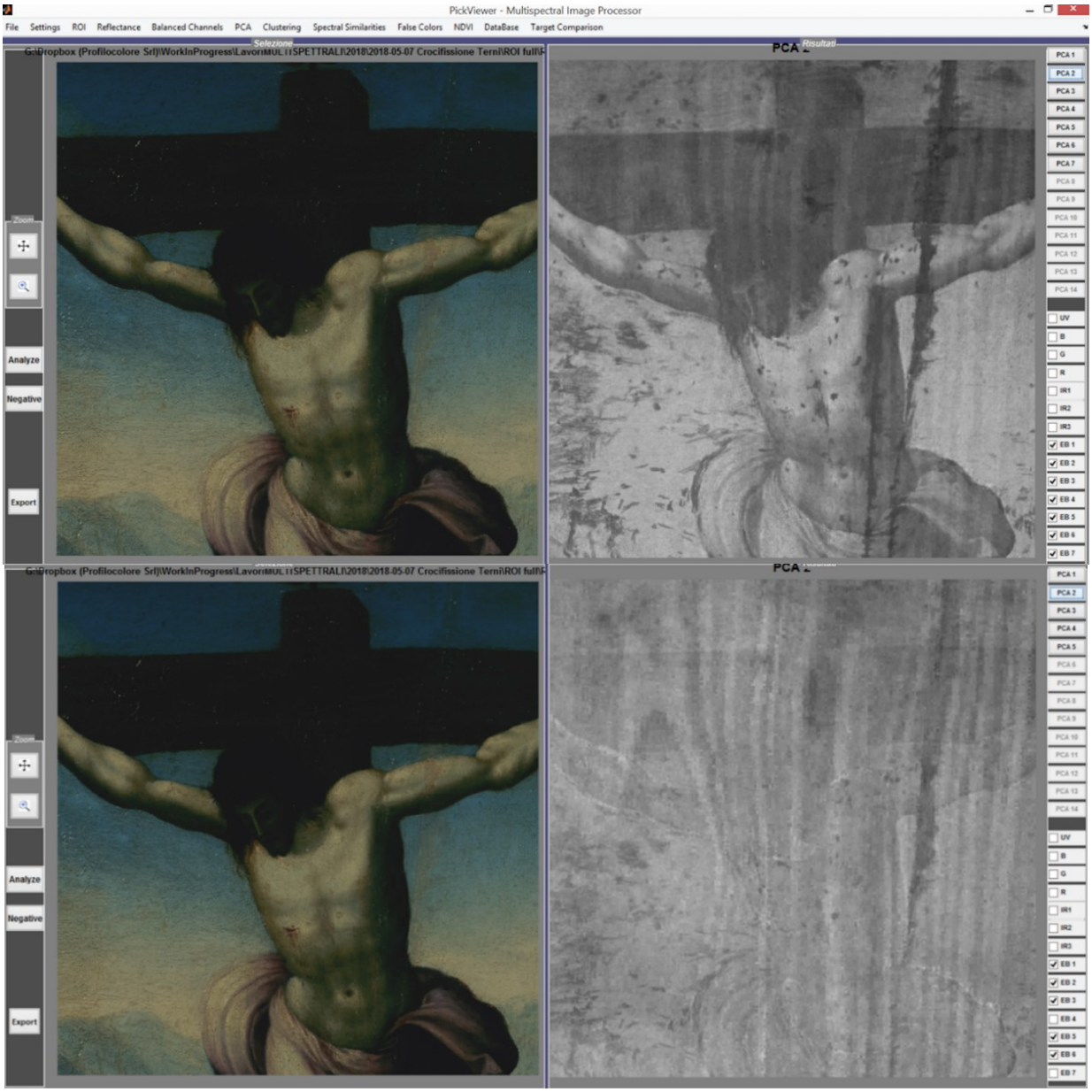

Figure 28. (a) Second principal component from PCA on HMI UVF and PuCT at 0.017 s, 0.22 s, 0.84 s and 1.85s as shown in the PickViewer software interface. (b) Second principal component from PCA on HMI UVF and PuCT at, 0.22 s, and 0.84 s as shown in the PickViewer® software GUI.

Beyond the scientific data on constitutive materials and state of conservation of the artwork, the HMI-PuCT integrated approach allowed to enrich our knowledge on the painting technique of Andrea Mantegna. In fact, the painting composition seems to follow the wood grain underneath as also shown in the PCA results on PuCT detail of Christ figure centered in the area of the wood knot (Fig.29). It is a powerful but not unfounded suggestion that Mantegna could have potentially used the natural lines of the wood panel as a spatial reference grid for the realization of the central body of the scene, centered in the figure of Christ.
Respect to other non-invasive methods for stratigraphic investigation as OCT or CT, which allows to distinguish the upper thin layers of coatings, varnish and painting and to measure their thickness, PuCT allows to study a painting for its entire depth, until the end of the support. Furthermore, compared to X-ray radiography that shows an only

"flattened" imaging output, PuCT gives an imaging datum at different times/depths, so to position a discontinuity or different materials inside the artwork [97].

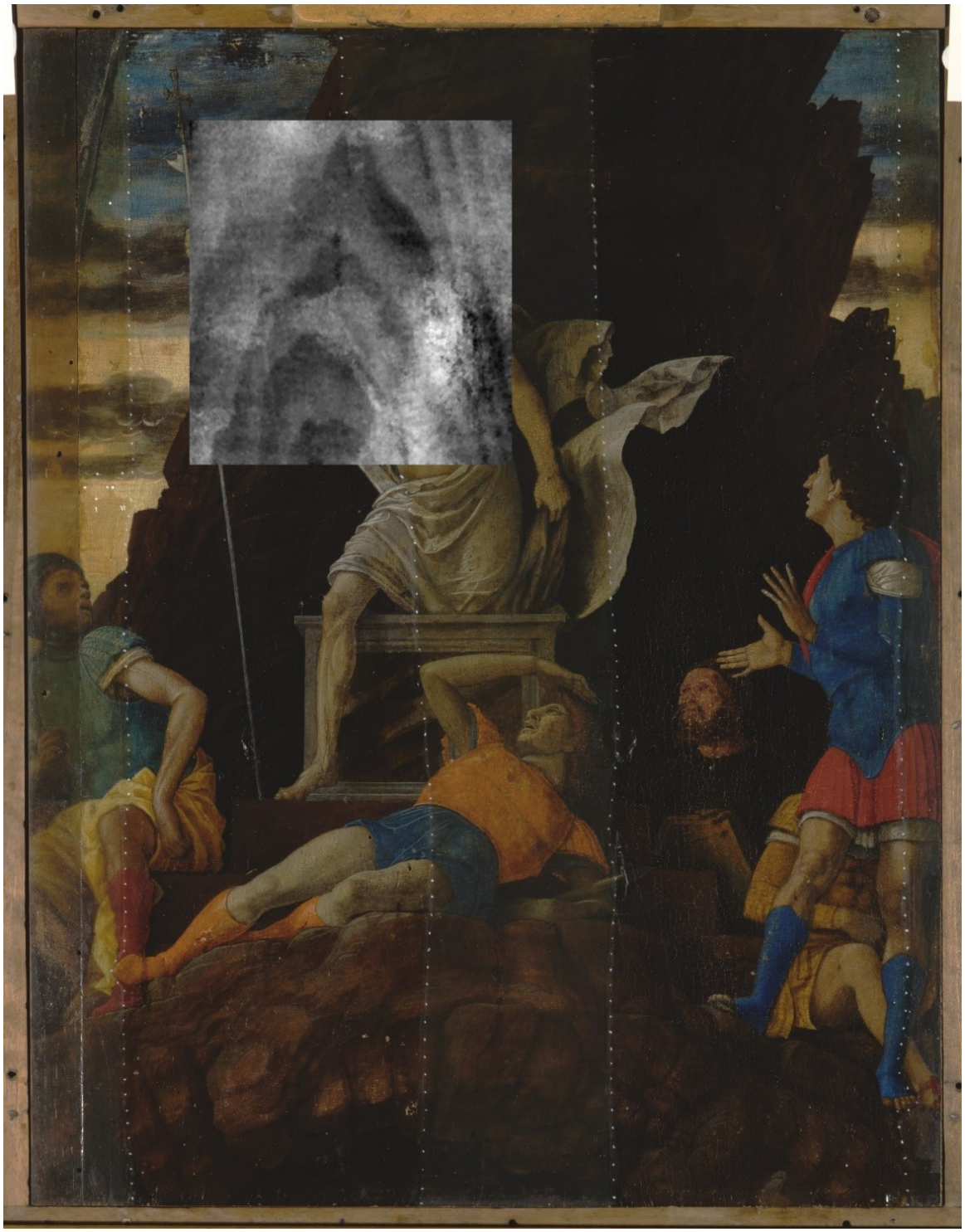

Fig 29. PuCT detail of the wood knot superimposed on VIS HMI image.

Finally, it must be mentioned that, due to its high value and importance, Andrea Mantegna's painting was investigated with traditional diagnostic techniques including X-ray fluorescence spectroscopy (XRF), infrared (IR), infrared (IRFC) and ultraviolet (UVFC) false-color photography, and digital optical imaging used in clinical healthcare

as computed axial tomography (CAT) and Digital Breast Tomosynthesis (DBT). The data from these techniques has not yet been published, but they have been useful during the restoration of the painting. Nonetheless, the integration of HMI and PuCT enabled to obtain all the valuable information achieved through numerous traditional methods, which require normally longer time and higher costs. Furthermore, the combined use of HMI and PuCT allows to gather several further details by applying only two imaging techniques that are rapid, contactless and specifically optimized for painting materials analysis.

PuCT analysis revealed the presence of very regular horizontal lines under the painting layers in The Resurrection that can be related to the application of the gypsum and glue ground layers, as described by the medieval artist Cennino Cennini in his technical essay [51]. PuCT images further highlighted the presence of two nails, the related grouting, and a long crack. An interesting detail revealed by PuCT is that the mountain shape on the background of the Christ figure follows the pattern of the wood grains underneath. In the *Crucifixion* panel painting, PuCT confirmed alterations in Christ's face, since the pictorial layer presents significant differences in the thermographic response in comparison to the body. This result supports the hypothesis of the art historian that the Christ' face was abraded and badly re-painted.

HMI analysis on *The Resurrection of Christ* allowed to appreciate the very good conservation state of the panel, with no discontinuities in the pictorial layer. IRFC and UVFC photographies led to suppose that the artist used ultramarine blue for the blue areas, vermilion/cinnabar for the red ones and red lead for the orange parts. HMI further highlighted the different responses of materials in the original and added parts of the panel painting, particularly evident on the left side.
The main results of HMI on the *Crucifixion* concern the conservation status, affected by several retouches and three main vertical cracks. HMI images also confirmed the singularity of St. John's face that changes its aspect if observed under UV in respect to the visible. Here too, the analysis supported the hypothesis of the art historians who suppose that the painting should be observed through a glass, a mirror and a lamp, according the letter "*del lume*" (of the lamp) that Vittoria Colonna wrote to Michelangelo. Another important result concerns the figure of Magdalene at the foot of the cross that was definitely confirmed to be a later addition, as it overlaps the Virgin's mantle. HMI also highlighted that the face of Christ has a different spectral response with respect to the rest of the figure, suggesting that this area had been abraded or heavily retouched in previous restorations.
In the case of the *The Resurrection of Christ*, HMI allowed the upper varnishing layer over the figure of Christ to be clearly noticed -still not cleaned by the restorer - and to appreciate a vertical discontinuity in the varnish coats on Christ's torso, which could probably be due to different applications of varnishes in different periods.

The combination of HMI and PuCT imaging results in Profilocolore PickViewer® software allowed to highlight further details in the inspected paintings.
Specifically, for *The Resurrection of Christ*, high correlation between the paint layer and the wooden support was revealed. In fact, the painting composition seems to follow the wood grain underneath as also shown in the PCA results on PuCT detail of Christ figure centered in the area of the wood knot. On the one hand, this could probably be due to the very thin gypsum preparation that Mantegna used.

In the case of *Crucifixion*, the combined use of HMI and PuCT showed that the vertical cracks of the panel - restored with stucco during an ancient intervention – running across the right branch of the cross, appear perfectly related and coherent with the underlying wood grain.
In this first applications on ancient wood panel paintings, the combination of HMI and PuCT imaging techniques appears as a convincing and promising non-invasive diagnostic technique to investigate the whole structure of the artwork in-situ, identifying surface degradation, different layers, wood defects and their position in the inner layers of the object. Moreover, the detailed mapping of the conservation state of the painting supported the restoration of this Mantegna's masterpiece.

4.3 "Beyond the visible: The Viterbo Crucifixion panel painting attributed to Michelangelo Buonarroti"

Published in: ***Microchem. J. (2020), 154. DOI 10.1016/j.microc.2020.104636***

The great interest of the scientific results achieved on the *Crucifixion* panel through the new imaging diagnostic campaign shown in chapter 3.2, together with the availability of the painting and the fruitful cooperation with art historians and conservators of the Museo del Colle del Duomo of Viterbo, lead to further study of this artwork.

The peculiarities of the *Crucifixion* painting have been described before in this thesis: the anomalous appearance of Christ's face, very different from the rest of the figures; the plausible later addition of the figure of Magdalene at the foot of the cross; the face of Saint John, that changes when observed under different illuminations.
St. John's face is particularly intriguing since it has a female aspect when observed under visible illumination, but it assumes more masculine traits and a hollowed aspect when observed under UV excitation [82]. This phenomenon, which occurs only in the face of St. John and hence appears intentional, highlights a further link between Michelangelo and Vittoria Colonna.

In fact, art historians relate this effect to a circumstance mentioned by Vittoria Colonna in her letter "del lume" ("about the lamp") to Michelangelo (presumably between 1543 and 1544) [83], where Vittoria Colonna expressed her astonishment regarding a "Crucifixion" sent her by Michelangelo, which she had "well observed with a glass, a lamp and a mirror" (*"Io l'ho ben visto al lume et col vetro et col specchio, et non viddi mai la piu finita cosa"*). Noticeably, in another letter written between 1542 and 1543, Vittoria Colonna requested to Alvise Priuli, the secretary of Cardinal Reginald Pole (leader of Spirituali at Viterbo), some green-colored glass manufactured in Venice ("*quell vetro verde che venne da Venezia*") to donate to Michelangelo who, at that time, was working to the wall paintings of the Cappella Paolina in the Vatican palace [98]. It was beyond the scope of this research to investigate whether and how Michelangelo made use of colored glasses, but the optical properties of glass materials were empirically known since the age of ancient Romans [99], while at the Renaissance time it was common to admire works of art through colored optical glasses, as it is well documented for several artists and patrons [100].

In this debated context, it was decided to run new investigations with other diagnostic methods. Specifically, an innovative protocol of diffuse reflectance hyperspectral imaging (HSI) [101] was applied in combination with punctual X-ray fluorescence spectroscopy (XRF), wood characterization analyses and wiggle matching dating, with the aim of investigating both the paints and the wooden panel of this small, but long-discussed painting. The HSI dataset and the XRF spectra on selected analysis points contribute to the knowledge of paint materials, techniques and pictorial details of the panel, and the related findings are compared with Michelangelo's artistic thought and production.
Wood analysis enables the characterization of the botanical species and the peculiarities of the wooden panel, a further relevant aspect for the analysis and attribution of the painting [102–105,106]. In particular, the identification of the botanical species provides important information to set the wooden artefact in a clear geographical and cultural context. At last, radiocarbon dating, through wiggle matching technique, was performed for establishing a chronological range for the wooden panel [107].

Hyperspectral imaging is a set of methods and devices which enable the acquisition of the continuous light spectrum for each point in the image of a scene [108]. Starting from the spectral information, numerical methods enable extracting quantitative parameters related to chemical and physical properties of the imaged objects [109]. In this work, hyperspectral images of the Crucifixion by an HSI camera were acquired, which is based on Fourier-transform (FT) spectrometry [110] and employs an innovative, highly stable birefringent interferometer [111,112].

The camera combines the advantages of FT spectrometry, such as high signal-to-noise ratio [113], high throughput [114] and flexible spectral resolution, with the excellent compactness, stability and robustness of its interferometer.
Thanks to these properties, the hyperspectral camera can acquire spectral absolute reflectance, transmittance and fluorescence images with spectral coverage ranging from 350 nm to1100 nm and spectral resolution of 3 THz, corresponding to ~4 nm at λ = 635 nm and ~12 nm at λ = 1100 nm. The camera sensitivity enables the acquisition of a hyperspectral imaging dataset in a few minutes, with a spectral background level of only -30dB even with the low-illuminance recommended for the study of works of art [115]. The camera is equipped with an F1.4, 25 mm objective and it employs a 1/ 1.8" format CMOS sensor with 1280 × 1024 pixels and a 10bit dynamic range. The angular FOV is ~ 16 degrees, and the working distance is from 0.2 m to ∞. Spectral calibration of the camera has been performed by imaging the transmission of a set of bandpass interferential filters covering the spectral working range of the camera.
With this hyperspectral camera, we measured two parameters: the absolute reflectivity and the UV-induced fluorescence.

For the absolute reflectivity measurement, the panel painting was illuminated by a broadband 150-W Xenon lamp. The lamp was kept at 2 m distance from the panel and, to reduce the specular reflection, it was placed off-axis with respect to the surface normal, at an angle of about 45°. The resulting illumination irradiance was about 0.1 mW/cm2 in the spectral range between 400 nm and 2 µm, corresponding to illuminance of about 135 lux. The camera was at 2.5 m distance from the panel. The acquisition time of the HSI of the entire painting was 200 s, corresponding to a light dose of 7.5 lux-hour.

Absolute reflectance was calculated after spectral calibration with a white Spectralon with (98.3 ± 1.3)% reflectance in the range from 300 nm to 2.5 µm (Labsphere Inc., North Sutton, USA) and correction for spatial and spectral non-uniformities of the illumination by imaging a white Lambertian surface at the object plane. Once hyperspectral datacube is generated, areas of the painting characterized by similar spectral features (i.e. similar pigment composition) are identified on the basis of a supervised classification algorithm.

For the purpose we considered the spectral angle mapper classification (SAM) method, which calculates the similarity between a reference reflectance spectrum (chosen in correspondence to a certain region of interest – ROI – of the painting) and each reflectance spectrum in the datacube by treating reflectance spectra as vectors in an N-dimensional space (where N is the number of spectral bands in the wavelength dimension, in the present case N = 512) and considering the angle between them as the index of similarity [116]. The lower the angle the closer the spectrum is to the template. The similarity maps were plotted in grayscale form white (perfect match) to black, which corresponds to a full-scale angle of 15 degrees (0.26 radians).
The UV-induced fluorescence was obtained by illuminating the painting with two custom-made UV-A lamps [117] symmetrically placed at the side of the painting at approximately 80 cm from its surface.
The employed UV illumination provided a peak irradiance in the band 340–365 nm of approximately 100 µW/cm^2 on the painting. The weak fluorescence required longer integration, resulting in a total acquisition time of 800 s.

The reconstructed color image of the painting in the RGB color space is displayed in Fig.22. Red-painted areas display close spectral features, as is highlighted by the similarity map constructed by considering as the reference reflectance spectrum the one in a squared area (1 × 1 cm2 in size, equivalent to 10 × 10 pixels) of Saint John's mantle (Fig. 22 (b)). A comparison with the reflectance spectra of red paints typically employed in the 16th century (Fig. 22(c)), available as published database of reflectance spectra [118], shows a strong similarity with both vermillion (HgS) and red ochre- (Fe_2O_3) pigments. In particular, in the Crucifixion red paints it is possible to recognize the typical sigmoidal-shaped spectrum of vermillion, with a transition edge at 600 nm, as well as the spectral features of red ochre with an absorption band around 850–900 nm.

It is noted that these two latter spectral features are more evident in the red paint employed for depicting Saint John mantle, suggesting that - whereas both the paints are composed of a mixture of vermillion and red ochre - Saint John mantle's paint has a higher content of red ochre.
While this issue is not disclosed by the similarity mapping method, this finding is in good agreement with XRF data of the two red paints, where, as already observed, both Hg and Fe have been detected, but with a higher relative content of Fe in Saint John's mantle (relative ratio between the area of the detected Fe_Kα and Hg_Lα emission lines equal to 0.39 and 0.16 in the red mantle of Saint John and the Virgin Mary, respectively).

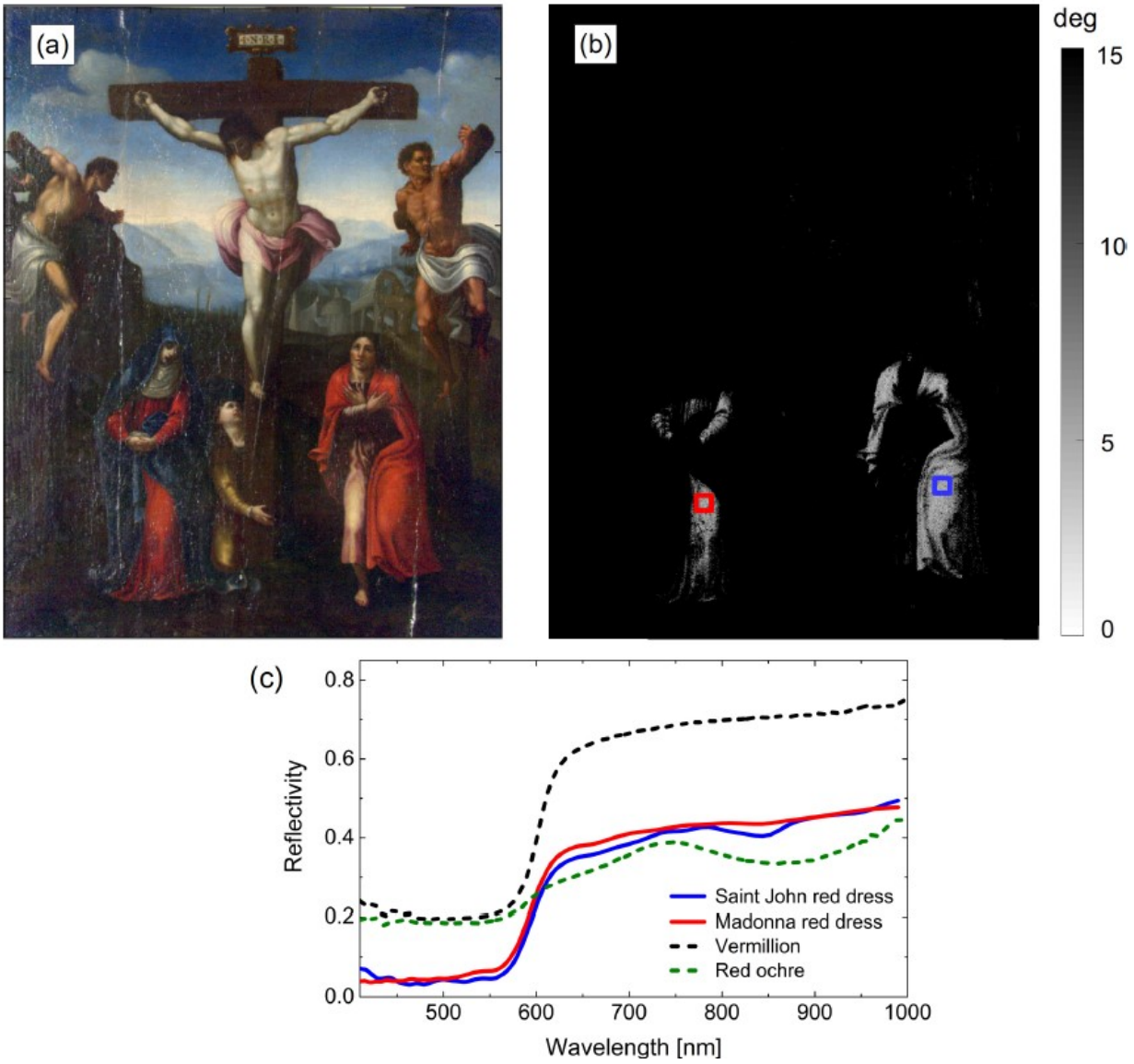

Figure 22. (a) Color image of the painting reconstructed in the RGB color space on the basis of the hyperspectral dataset in the spectral range between 420 and 780 nm. (b) Similarity map achieved by considering as the reference spectrum the one collected on a ROI on the red mantle of Saint John (blue empty square) and the hyperspectral dataset in the spectral range between 420 and 1000 nm. Tolerance angle has been set to 15 degree (0.26 radians). (c) Mean reflectance spectra reconstructed in the red mantle of the Virgin Mary (red continuous line, red square of panel (b)) and in the red mantle of Saint John (blue continuous line, blue square of panel (b)) compared with the reflectance spectra of a vermillion paint (black dashed line) and a red-ochre paint (green dashed line) [120].

Blue-painted areas of the painting show a common feature, i.e. a net increase in reflectance values between 700 and 950 nm, as it is demonstrated by the similarity map constructed considering hyperspectral data in the spectral range between 650 nm and 750 nm taking as the reference reflectance spectrum the one in a squared area (1×1 cm^2 in size, equivalent to 10 × 10 pixels) of the top blue sky (Fig. 23(a)). This feature is indicative of the use of the precious ultramarine pigment in blue-painted areas of the sky and the blue mantle of the Virgin Mary. Indeed, a comparison of the reflectance spectra of these areas with the reflectance spectra of blue pigments typically employed in the Renaissance period (Fig. 23(b)) demonstrates a close similarity with both azurite and ultramarine blue, in agreement with the detection of Si and Cu by XRF spectroscopy in analysis points with a blue color.

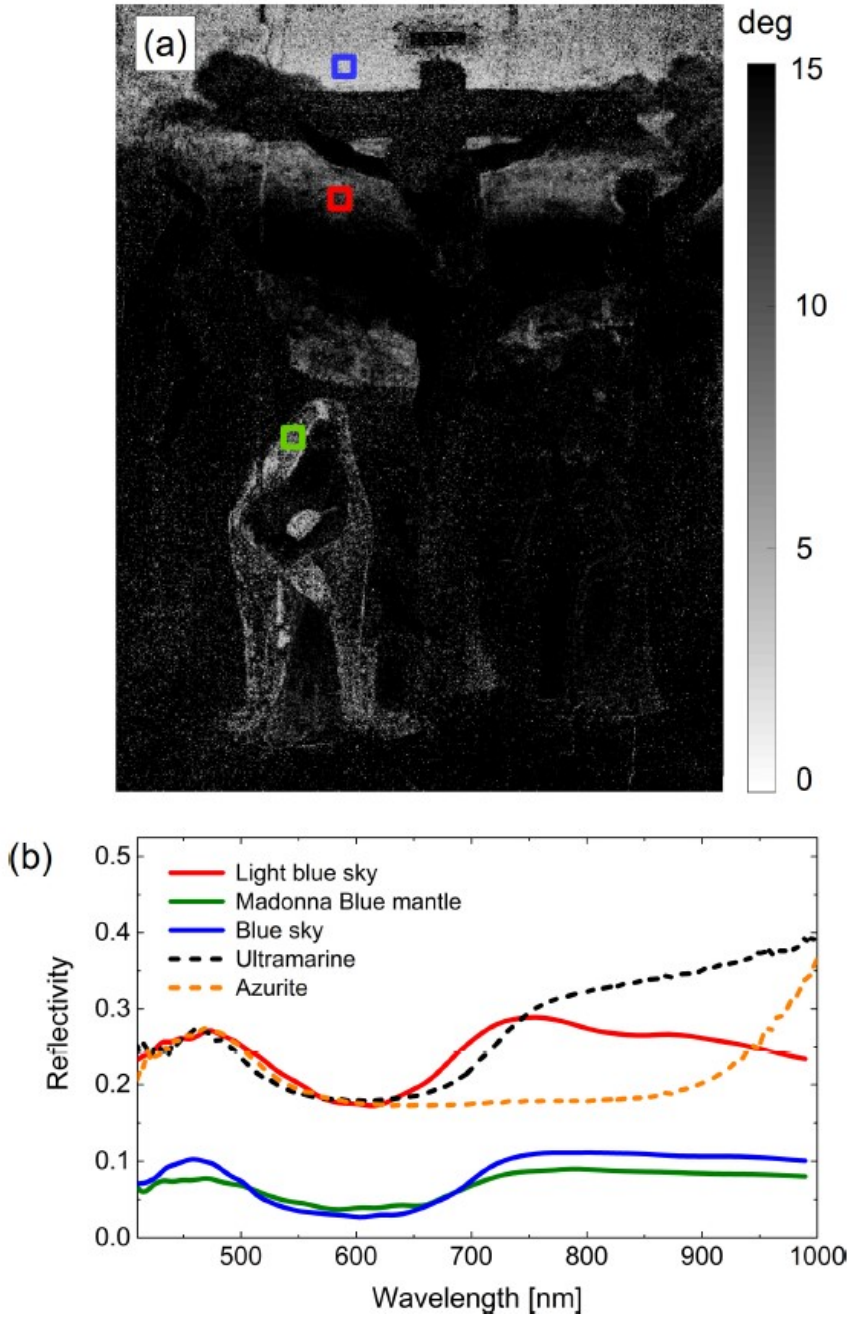

Figure 23. (a) Similarity map achieved by considering as the reference spectrum the one collected on a ROI on blue sky (blue empty square) and the hyperspectral dataset in the spectral range between 650 and 750 nm. Tolerance angle has been set to 15 degree (0.26 radians). (b) Mean reflectance spectra reconstructed in the blue sky (blue continuous line, blue square of panel (a)), in the light blue sky (red continuous line, red square of panel (a)) and in the blue mantle of the Virgin Mary (green continuous line, green square of panel (a)) compared with the reflectance spectra of ultramarine blue (dark dashed line) and azurite (orange dashed line) paints [75].

Hyperspectral imaging was finally focused on the detail of St. John's face. The RGB color image under visible and UV illumination (Fig. 24(a) and (b), respectively) reconstructed on the basis of the corresponding hyperspectral datasets, highlights the change in the face aspect of St. John when observed under different illuminations, as already discussed in chapter 3.2.

This behavior can be further appreciated when observing the reflectivity maps of the painting detail in two different spectral regions (Fig. 24(c) and (d)) in the blue-green and

in the near-infrared, where St. John aspect changes dramatically from a thinner and more masculine character to a feminine one with chubby cheeks. This finding could be related to the use of a red paint for finishing the cheeks of St. John on top the skin tone used to paint his face but, considering the particular spectral behavior in the UVF photography where well-defined shadows become clearly visible on the face as well as hair locks on the shoulders, it could be taken into consideration the hypothesis of the addition of some material that is transparent in the IR and well absorbent in the UV.

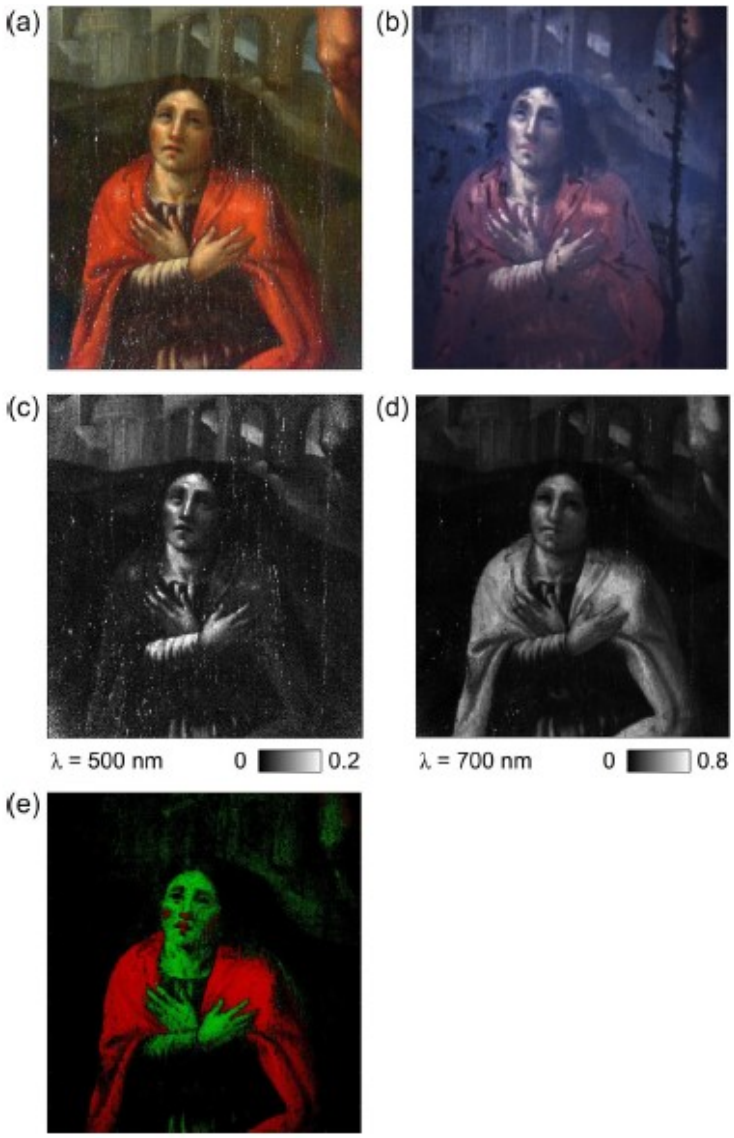

Figure 24. RGB color map of the detail of Saint John face under (a) visible and (b) UV illumination reconstructed on the basis of the collected hyperspectral datasets. Reconstructed images of the reflectivity at (c) 500 nm and (d) 700 nm. (e) Composite image of the similarity maps constructed by considering as the reference spectrum the one in the red mantle (red channel) and the one in the fleshy pink tone of the right hand (green channel). Tolerance value for both similarity maps has been set to 15 degree (0.26 rad).

It is worth nothing that, this specificity is observed in S. John's face only. Indeed, the combination of similarity maps (Fig. 24(e)), constructed by considering as the reference spectrum the one in the red mantle (red channel) and the one in the fleshy pink tone of the right hand (green channel), confirms that the cheeks have a more reddish hue than the rest of the face.

HSI technique is very powerful in charactering painting materials, especially when coupled with X-Ray Fluorescence spectrometry [3, 5]. XRF spectra of selected points of the painting were acquired with a compact, portable and high performances XRF spectrometer (ELIO, XGLab srl/Bruker, Milano, Italy). The instrument is based on a rhodium anode as the excitation source and allows the detection of elements from $_{11}$Na to $_{92}$U with an energy resolution of 130 eV at Mn Kα. The X-ray beam is collimated to a spot diameter of about 1.3 mm in diameter. For all measurements on the painting the following experimental conditions were employed: tube voltage: 40 kV, tube anode current: 100 µA, acquisition time: 60 s. XRF measurements were performed in 14 points, whose positions are marked in Fig. 25.

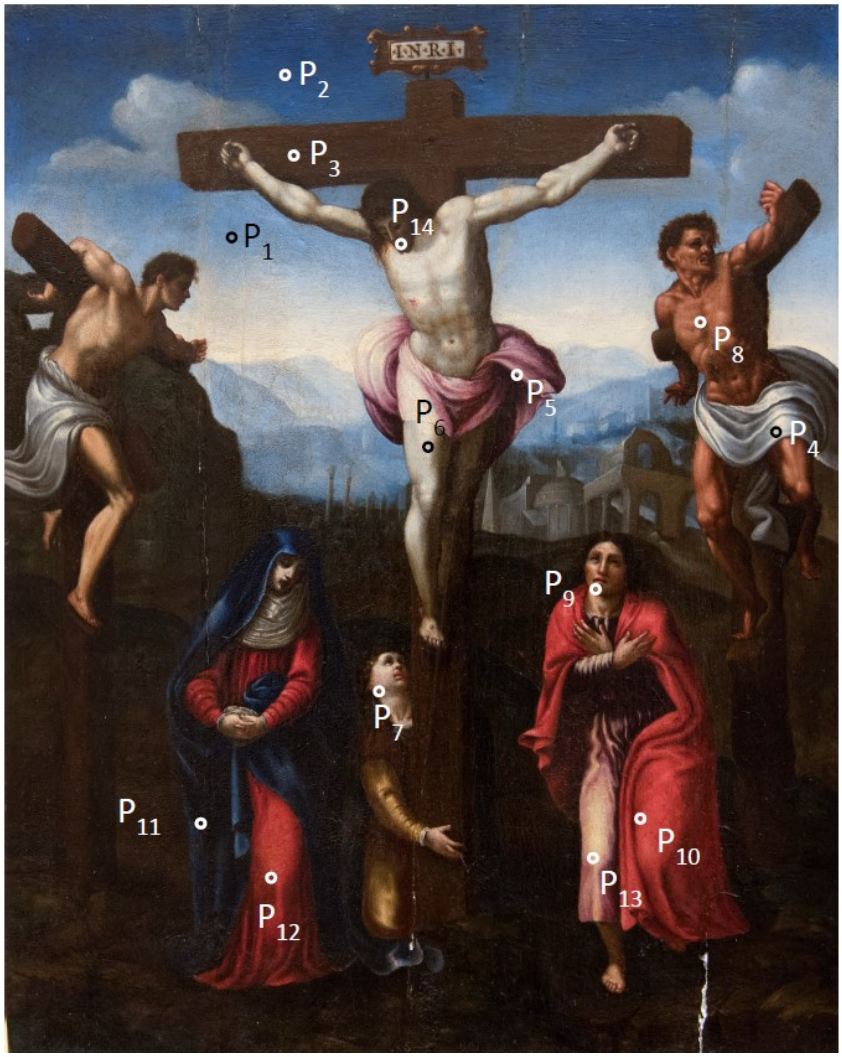

Figure 25. Location of XRF analysis points performed on the Viterbo *Crucifixion*.

Results of XRF spectroscopy on selected analysis points of the painting are provided in Table 2 in terms of the main detected elements and are synthetically resumed in the following. Furthermore, we took advantage of the complementarity of elemental analysis with spectral features of reflectance to strengthen the attribution of pigment composition whenever ambiguous interpretation was possible, as discussed in the Section 3.3.1.

Analysis point	Color	Detected elements	Main pigments on the basis of XRF data
P1 – Light blue sky	BLUE	Pb, Ca, Fe, Cu (minor), Si (minor), K (minor), Ti (minor)	Azurite + Ultramarine blue
P2 - Dark blue sky	BLUE	Pb, Ca, Fe, Cu (minor), Si (minor), K (minor), Ti (minor)	Azurite + Ultramarine blue
P3 - Jesus cross	DARK BROWN	Pb, Fe, Ca, Cu K (minor), Mn (minor), Si(minor)	Umber or Manganese brown
P4 – White drape of the right thief	WHITE	Pb, Ca, Fe (minor)	White lead + red ochre (traces)
p5 – Jesus pink drape	PINK	Pb, Ca, Fe, Cu (minor) K (minor), Mn (minor)	Lead white + red ochre + umber
p6 – Jesus leg skin	FLESHY PINK	Pb, Ti, Fe, Zn, Ca, K (minor), Cu (minor)	Lead white + red ochre
p7 – Maddalena skin	FLESHY PINK	Pb, Hg, Fe, Ca, Ti (minor), Zn (minor), Cu (minor), Mn (minor)	Lead white + vermillion + red ochre + titanium white (traces) + zinc white (traces)
p8 – Right thief skin	FLESHY DARK PINK	Pb, Fe, Hg, Ca, Cu Si (minor), K (minor)	Lead white + red ochre + vermillion
p9 – Saint John skin	FLESHY PINK	Pb, Fe, Hg, Ca, Cu (minor) Si (minor), K (minor)	Lead white + red ochre + vermillion
p10 - Saint John red mantle	RED	Pb, Hg, Fe, Ca Cu (minor), K (minor)	Vermillion + red ochre
p11 – Virgin Mary mantle	BLUE	Pb, Ca, Fe, Cu (minor), Si (minor), K (minor), Ti (minor)	Azurite + Ultramarine blue
p12 - Virgin Mary red dress	RED	Pb, Hg, Fe, Ca Cu (minor), K (minor)	Vermillion + red ochre
p13 - Saint John pink dress	WHITE-PINK	Pb, Ca (minor), Fe (minor), Cu (minor)	Lead white + red ochre (traces)
p14 – Jesus face skin	FLESHY PINK	Pb, Fe, Ca, K (minor), Cu (minor)	Lead white + red ochre

Table 2. Results of XRF spectroscopy analysis in terms of detected elements and proposed pigment identification.

In all analysis points we detected Pb, Ca and Fe, suggesting the presence of ground and preparation layers mainly made of lead white, gypsum and iron-based pigments.
Concerning the coloring agents, the palette appears to be quite simple and most of the identified pigments can be related to the traditional artist materials employed in the Renaissance period:

i. red hues have been achieved by employing vermillion and red ochre;
ii. blue hues have been achieved by employing azurite and ultramarine blue. Minor amounts of Fe (possibly ascribed to the presence of iron ochre) were also detected;
iii. light pink hues and fleshy pink hues have been achieved with a mixture of red ochre and cinnabar. In some points, a Mn-based pigment (umber or Manganese brown) has been also used.

Interestingly, relevant amounts of Cu have been detected also in two non-blue areas: the dark-brown cross of Jesus and the dark skin of the right thief. This occurrence could be related to presence of an underneath painting layer made of azurite, hence suggesting that the sky was painted first and, over it, other details have been added. Some elements, typical of modern pigments, have been further detected and can be ascribed to the use of semiconductor pigments in recent restoration treatments, such as cadmium red, titanium white and zinc white. The presence of titanium could be also associated to the presence of clay minerals in the earth pigments.

By following a well-consolidated approach, the wood of the painting panel was carefully examined in situ before any micro-sampling [119], by measuring the weight and sizes

of the panel. The panel thickness was measured with a gauge at left and right sides, in three positions: top, centre, bottom.
In order to identify the wood species, thin sections (thickness: 15–20 µm) on the transversal, radial and tangential surface of the wooden panel have been observed at the optical and electronic microscope. For optical microscopy, we employed a Zeiss Axioskop, equipped with AxioCam digital camera. The anatomical features were compared with the identification keys of Nardi Berti [120] and Schweingruber [121] and following the IAWA list for softwood identification [122].
Scanning electron microscopy (SEM) was carried out using a Jeol model JSM-5200 scanning electron microscope. The wood samples were sputter-coated with gold in a Balzers MED 010 unit.

The on-site visual examination of the painting panel (Fig. 20) revealed that the painting was made on a single plank with a total mass 4.006 kg and an axial disposition whose dimensions are reported in Table 3.

Panel painting dimensions.

Measurement position	Average	Standard deviation
Width (cm)	46.1	0.212
Length (cm)	58.9	0.009
Thickness (cm)	2.2	0.027

Table 3. Dimensions of *Crucifixion* painting.

The plank was cut radially, as shown by the direction of the growth rings visible on the upper and lower edges. The wood is homoxylous, with irregular shaped rings and growth restarting (false or partial rings), as visible in Fig. 26(c). The pith was also observed (Fig. 26(b)), positioned 29.4 cm from the right longitudinal edge (with respect to the painted surface, Fig. 26(a)). This suggests that the log from which the plank was obtained had a diameter of at least 60 cm.
The wooden panel exhibits a group of knots and traces of processing with manual tools (Fig. 27(a,c)). The knots are the portions of the branches incorporated in the tree stem. They do not show traces of biotic alteration (Fig. 27(b)). Resin canals were not observed. There are axial parenchyma cells scattered in the ring (Fig. 28(a)), sometimes arranged in tangential bands (Fig. 28(b)). Monoseriate rays were detected. In radial section, the tracheids showed bordered pits in a row (Fig. 28(c)). The rays in the cross-fields show from 2 to 3 cupressoid pit.

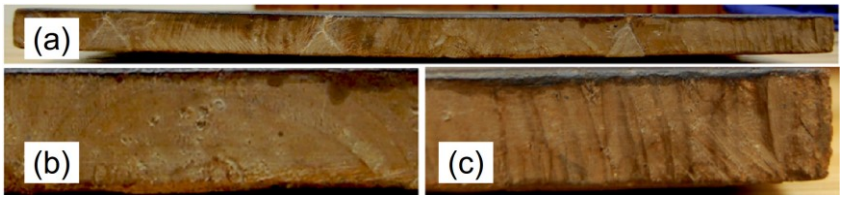

Figure 26. (a) Upper edge of the panel; (b) pith and adjacent rings; (c) false rings, characterized by faded boundaries: they are abnormal rings due to infra-seasonal disturbance of growth.

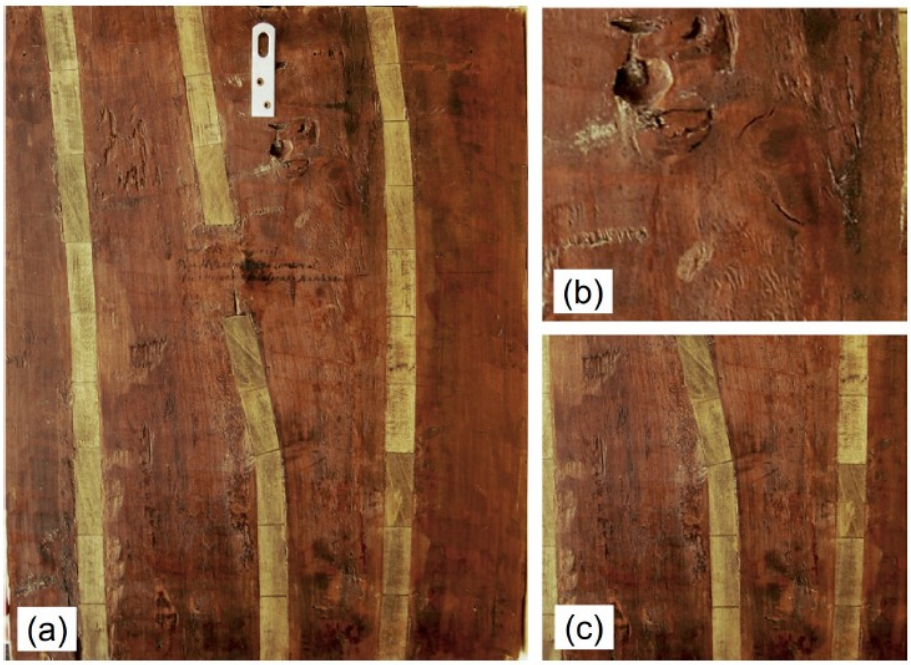

Figure 27. (a) Back of the painting; (b) detail of the knots; (c) traces of processing.

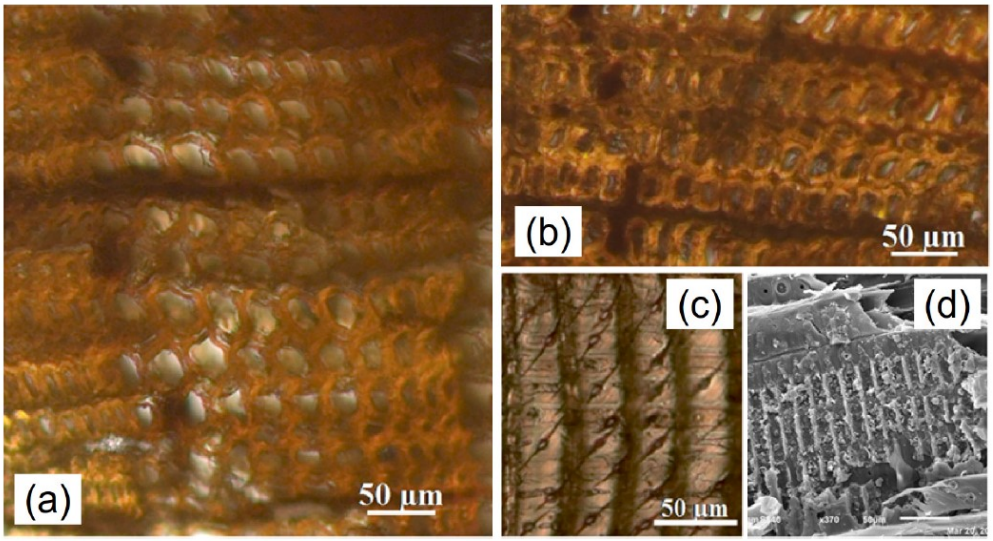

Figure 28. Transmission microscopy images in the visible spectral range: (a) transversal section, magnification 200X, axial parenchymal cells are visible; (b) transversal section, magnification 100X, axial parenchymal cells are arranged tangentially near the ring boundary, recognizable by thickness variation of the cell walls. Moneseriate rays are visible; (c) radial section, magnification 100X, tracheids show bordered pits with small orifice. SEM images: (d) radial section, parenchyma cells.

The anatomical features examined with the optical microscope indicate that the wooden panel was obtained from the stem of Cypress (*Cupressus sempervirens* L.).

Typically, the radial cut is characterized by a lower tendency to dimensional variations and deformation caused by moisture changes and by shrinking and swelling wood. However, the painted surface assumed a convex shape over time, probably due to the different hygroscopic inertia between the painted surface and the back, which is more prone to react to thermo-hygrometric variations of the environment. These undesired deformations required an intervention to restore the flatness of the panel. This intervention led to an excess of reparation that caused an irregular arrangement of the painted surface, which was further enhanced by the lack of a containment system.

Also, the choice of this botanical species deserves a comment: cypress wood is very durable, it has a sacred meaning, it is a symbol of access to eternity. This species was also used for wooden icons, i.e. the icon of the Theotokos housed in the church of Santa Maria in Trastevere [123].

Wiggle matching technique [107] is suited for dating the wood of the painting panel and it is based on the radiocarbon analysis of a sequence at least three samples, selected in order to impose the following conditions to the subsequent statistical analyses [124]:

i. the samples towards the pith are older than the samples towards the bark, due to the centrifugal direction of growth in plants;
ii. the number of years that separates the dating of the samples is equal to the number of rings among them, as a consequence of the annual growth rate of rings.

By applying to the conventional radiocarbon measurements, the principles of Bayesian statistics [125] accounting for the abovementioned conditions, it is possible to improve the dating precision [124, 126-130]. This technique is particularly suited in the case of paintings on tables [129] because the confidence interval of the dating reduces from >±75 years to only±25 years. In order to perform the dating of our panel by wiggle matching technique, we collected three samples (Fig. 29).
From the oldest to the most recent, they are labelled CDD1 (pith side), CDD2 (intermediate) and CDD3 (bark side). The distance between CDD1 and CDD2 samples corresponds to 34 years, while between CDD2 and CDD3 it is 31 years. In addition, the outer edge of the panel is at the bark side and is 23 years younger than CDD3.

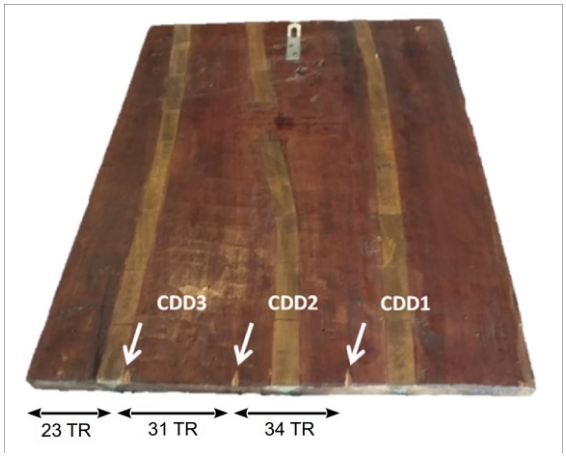

Figure 29. The sampling pattern for the wiggle matching analysis. TR = tree ring.

Radiocarbon dating was performed with the high-resolution mass spectrometry technique (AMS), at the Dating and Diagnostics Center (CEDAD) of the University of Salento [128]. The calibration in calendar years was performed with the OxCal Ver. 3.10 software, based on atmospheric data as reported by Reimer *et al.* [130].
Wood species as Cypress (*Cupressus sempervirens* L.) are not suited for dating techniques based on dendrochronology [131,132] due to their growth peculiarities and to the lack of reference chronologies for the Italian area. For this reason, wiggle matching dating was applied. In Table 4 two results from radiocarbon measurements are shown: the not calibrated one (BP, i.e. Before Present referred to year 1950) and the calibrated one (BC/AD), with the absolute error of the measurement.

Radiocarbon dating, not calibrated and calibrated, with the absolute error.

Sample	*$\delta^{13}C$ (‰)*	*Radiocarbon Age*(BP)	Calibrated 14C-age(2σ, yr cal BC/ cal AD)
CDD1	-31.6 ± 0.6	507 ± 45	1311AD-1458AD (95%) 1386AD (77.7%) 1458AD
CDD2	-27.0 ± 0.4	490 ± 45	1317AD-1477AD (95%) 1390AD (86.5%) 1477AD
CDD3	-30.4 ± 0.6	335 ± 45	1457AD-1645AD (95%)

Table 4. Results of radiocarbon dating on Viterbo *Crucifixion*.

Conventional radiocarbon dating has been corrected for the effects of isotopic fractionation both through the measurement of $\delta^{13}C$ (isotropic fractionation of ^{13}C), and through the calculation of the background values [125,126]. The wiggle matching analysis of the radiocarbon data allowed for refining the dating as shown in Fig. 30 and Table 5.

This technique places the most recent sample (CDD3) in year 1478,5 ± 24,5. By adding 23 years (rings) to this range, we could date the outer edge of the panel. Hence, the dating of the painting panel (*terminus post quem*) is established in year 1500 ± 25.

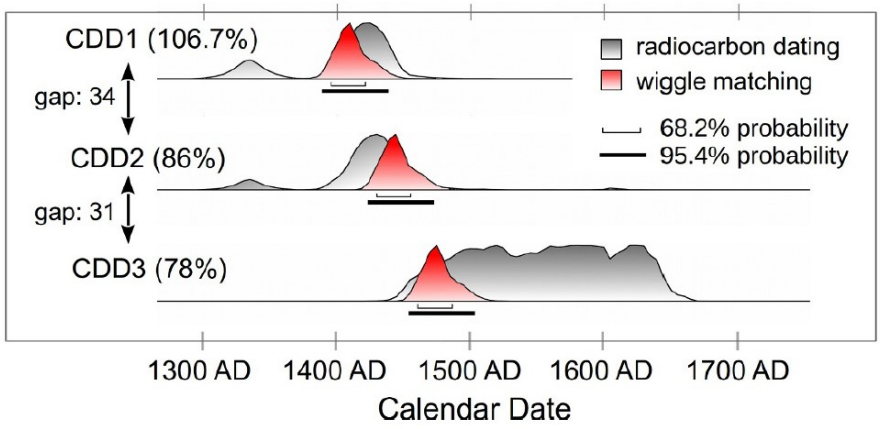

Figure 30. Wiggle matching analysis of the radiocarbon dating. The values in brackets are the agreement indices, conveying the robustness of the wiggle matching technique and the accuracy of the measurement. Atmospheric data from [128]. Data elaborated with OxCal v3.10 Bronk Ramsey (2005); cub r:5 sd:12 prob usp [chron].

Sample	Calibrated 14C-age (2σ, yr cal BC/cal AD)
CDD3	1454AD-1503AD (95.4%)

Table 5. Dating of CDD3 sample obtained through the application of the wiggle matching technique.

The result of the radiocarbon dating refers to the last tree rings visible on the wooden panel, which was generated when the tree was still alive. To identify the date in which the painting has been made, a certain period of time, which is impossible to establish with certainty, must be added to the dating. This period is related to the wood loss due to the trimming of the panel and to its possible seasoning.
Even taking into account these aspects, the dating of the panel definitely places the *Crucifixion* in the first decades of the 16th century, which is compatible with the period of more intense friendship between Michelangelo and the Marquise Vittoria Colonna during her stay in Viterbo (1541–1544) and of their connection with the Spirituali in the town. For art-historians this is a result of paramount importance.
In fact, beyond the attribution of the painting to Michelangelo or other artists of his workshop, the painting represents the only remaining testimony of an important historical moment for the city of Viterbo and for the main European religious debate in the first decades of the 16th century.

4.4 "Hypercolorimetric multispectral Imaging and Pulse Compression thermography as innovative combined techniques for painting investigation: the case of a detached wall painting by Pastura"

In this work, the innovative combination of InfraRed Thermography and Hypercolorimetric Multispectral Imaging was applied to a detached wall-painting, under restoration in the Laboratories of the five-year course in Conservation and Restoration of Cultural Heritage (LMR/02) of University of Tuscia [133].

The wall painting, specifically a lunette, depicts a Madonna and Child enthroned between the angels and the Saints Jerome and Francis (Fig. 31). The painting has been dated back to 1490 and it is attributed to the artist Antonio del Massaro, known as Pastura (1450-1519) [134-135]. Originally it was located in the convent of Santa Maria del Paradiso in Viterbo, a little city in Central Italy [134].

Figure 31. The lunette with Madonna and the Child enthroned between the angels and the Saints Jerome and Francis (AD 1490) attributed to the painter Antonio del Massaro known as Pastura (1450-1519), before the restoration.

After the detachment in 1912, the painting was transferred in the Civic Museum of Viterbo in the occasion of the opening of the new seat in Santa Maria della Verità church [134]. The detachment of the lunette was probably due to its bad state of conservation caused by exposure to weathering and vandalism [135]. In fact, in the photographs of the beginning of 20th century, large grouts were visible confirming the bad state and so the need for interventions [136].

The ancient restoration interventions, made with unsuitable materials and techniques (such as the mimetic reintegration), prevented correct readability of the artwork and of its original painting. So, it was decided, in accordance with the Superintendence and the responsible of the Civic Museum, to perform a restoration with the aim at recovering, as much as possible, the original appearance of the painting [135]. To reach this goal, the lunette was brought in the restoration laboratories of University of Tuscia in 2016 for starting the intervention.

The restoration work was supported by diagnostic investigation aimed at mapping the superimposed materials, the grouts, the lacunae and in general the non-original areas, well-visible under ultraviolet fluorescence photography (Fig. 32). The image under UV radiation showed diffuse blue fluorescence probably due to the presence of glue used for the detachment of the lunette. Grouts and cracks are also well-highlighted by the UV image.

Figure 32. The lunette with Madonna and the Child enthroned between the angels and the Saints Jerome and Francis (AD 1490) attributed to the painter Antonio del Massaro known as Pastura (1450-1519), under UV, before the restoration.

The surface material was sampled in order to perform Fourier transform infrared analysis to characterize its composition. This analysis revealed that the yellowed surface material was made of protein glue (Fig. 33). The main absorptions of glue can be observed in the infrared spectrum at cm-1: 3289, 3064, 2930, 1660, 1542, 1373, 1313, 1246, 1033 [137-138]. The other absorptions in the spectrum of Fig. 33 can be associated to calcium carbonate (1424 and 876 cm^{-1}) and gypsum (1152 cm-1) [135].

This preliminary analysis has been fundamental to address the first cleaning choices of restorers to start the intervention.
After this, further investigation were performed by combining HMI and PuCT, supported by traditional XRF spectroscopy, in order to obtain information about the painting materials and the stratigraphic sequence combining possible original layers and new grounds added during the detachment of the lunette from the church of Santa Maria del Paradiso.

In the present work the two techniques were tested for the first time on a wall painting, which, due to the detachment from the original location, exhibits a peculiar stratigraphy and surface materials deserving investigation.

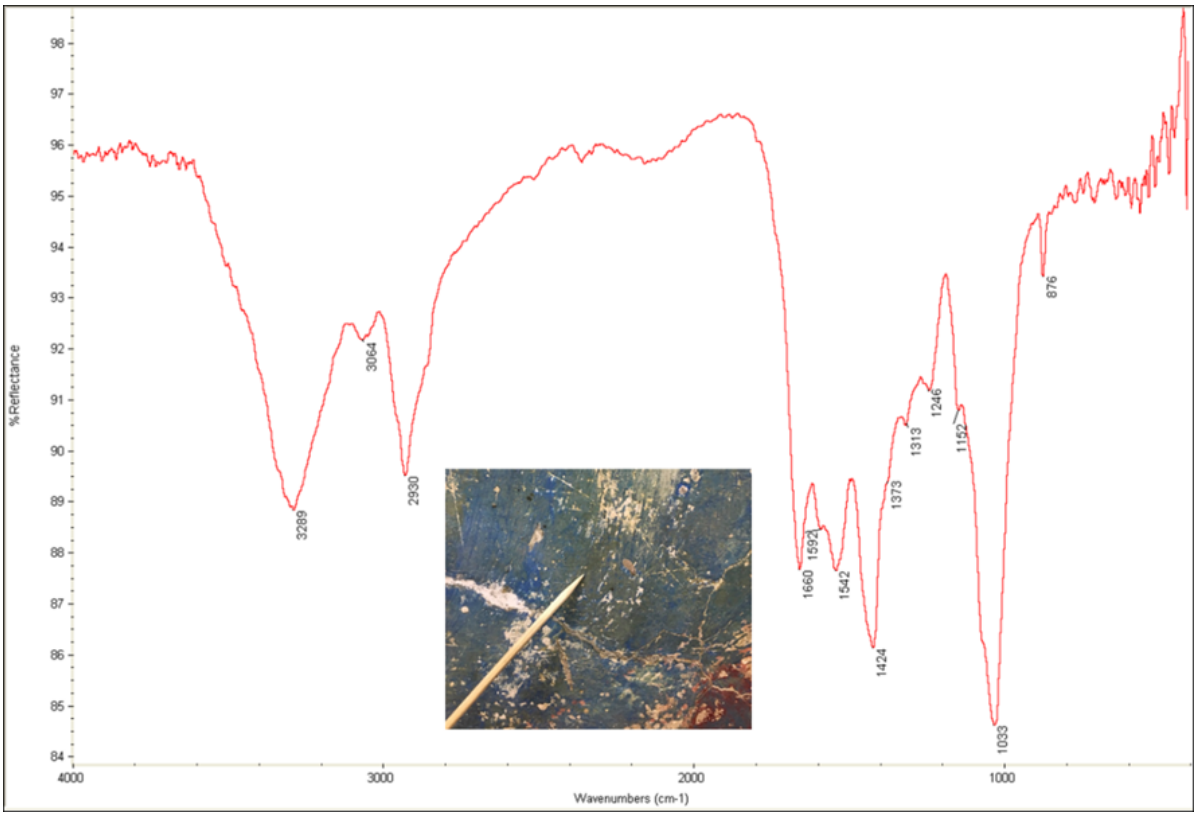

Figure 33. Fourier transform infrared spectrum of the yellowed surface material. The photograph of the sampling point is also shown in the spectrum.

In HMI analysis, the seven calibrated spectral bands were analysed in PickViewer software and some statistical processing tools were applied to the images in order to gain further diagnostic information. The IR2 band (850 nm) gave some details on the preparatory design of the scene (Fig. 34), as in the detail of the pentimento in the foot of Saint Jerome, where other outlines are visible on its left, and in the bottom left part of the Virgin's blue garment, currently covered by restoration. Hidden details of pentimenti and original composition in HMI infrared image at 850 nm are indicated by the red arrows in the Fig. 34.

Infrared and ultraviolet false color analysis (IRFC and UVFC, respectively) were obtained by combining calibrated R, G, B and IR/UV channels in order to hypothesize a non-invasive characterization of pigments based on their characteristic spectral behaviour (Fig. 29).

For the blue pigment of the Virgin's garment, the use of azurite was hypothesized on the base of its characteristic deep blue color in IRFC and opaque light green shade in UVFC.

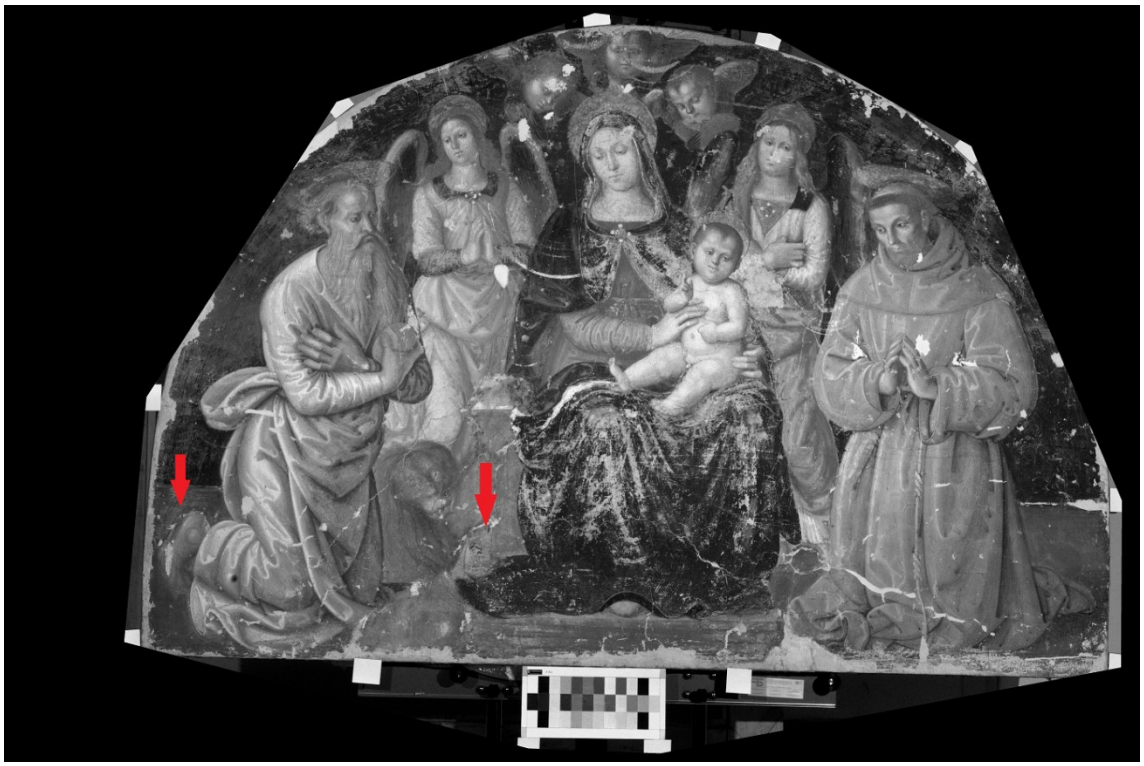

Figure 34. HMI infrared image at 850 nm; hidden details of pentimenti and original composition are indicated by the red arrows.

The sky and parts of the vest of the Virgin have a particular green color in the visible; in IRFC (Fig. 35(a)) they assume a light blue hue and a full brown color in UVFC (Fig. 35(b)), making probable its attribution to malachite.
Considering the bad state of conservation of the artwork after a long exposition to weathering, a preferential degradation caused by humidity with a transformation of azurite into malachite or other green copper-based compounds, seems probable rather than the application of a green pigment in areas meant to be blue-colored. Portion of unaltered azurite are in fact clearly visible in the background sky behind the head of the Virgin as well as traces are appreciable in the lower edge of the sky.

In order to investigate this possibility in a non-invasive way, a map of spectral similarity was built on the base of the 7-bands curve of spectral reflectance measured in a 9×x9 pixels area in the blue Virgin's dress, as shown in PickViewer's graphic user interface (GUI) in Fig. 36. The output, shown on the right of the visible image in the software's GUI, highlights a correspondence between the blue pigment of the vest of the Virgin and the one used to paint the sky, supporting the hypothesis of the use of azurite in all blue areas.
The painting layer of azurite used for the sky is applied over a colored ground layer probably based on red earth (hematite) or charcoal black (*morellone*), usually used for the application of azurite in wall paintings, as described in scientific literature [139].

From the UVFC image it can be seen different responses in the haloes of the characters that deserve a note. In fact, in this analysis, the haloes of Saints Jerome and Francis and of the two angels assume a violet hue, while those of the Virgin and Child turn into a vivid pink color, suggesting the use of different materials. It is possible the presence

of a *missione*, an adhesive oil/resin primer, used to allow the adhesion of gold on haloes and other parts in the wall paintings [140].

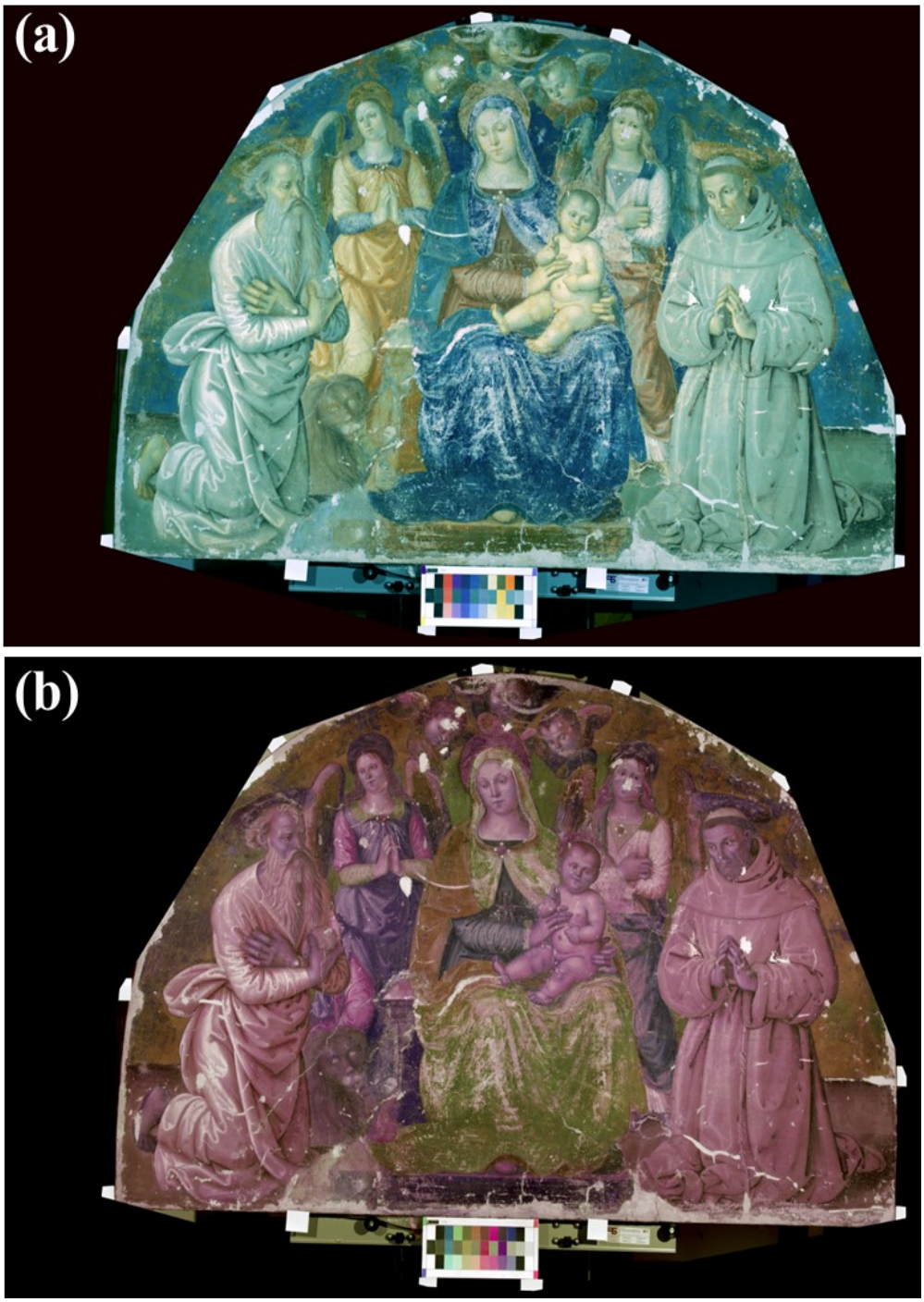

Figure 35. Infrared (a) and ultraviolet (b) false color images obtained through PickViewer®.

Figure 36. PickViewer software's GUI. On the left: visible image and red point highlighting the measurement of multispectral reflectance of possible azurite. On the right: multispectral similarity mapping of azurite.

As regards Pulse Compression Thermography, it was done applying pixelwise the pulse-compression algorithm over the acquired thermograms.

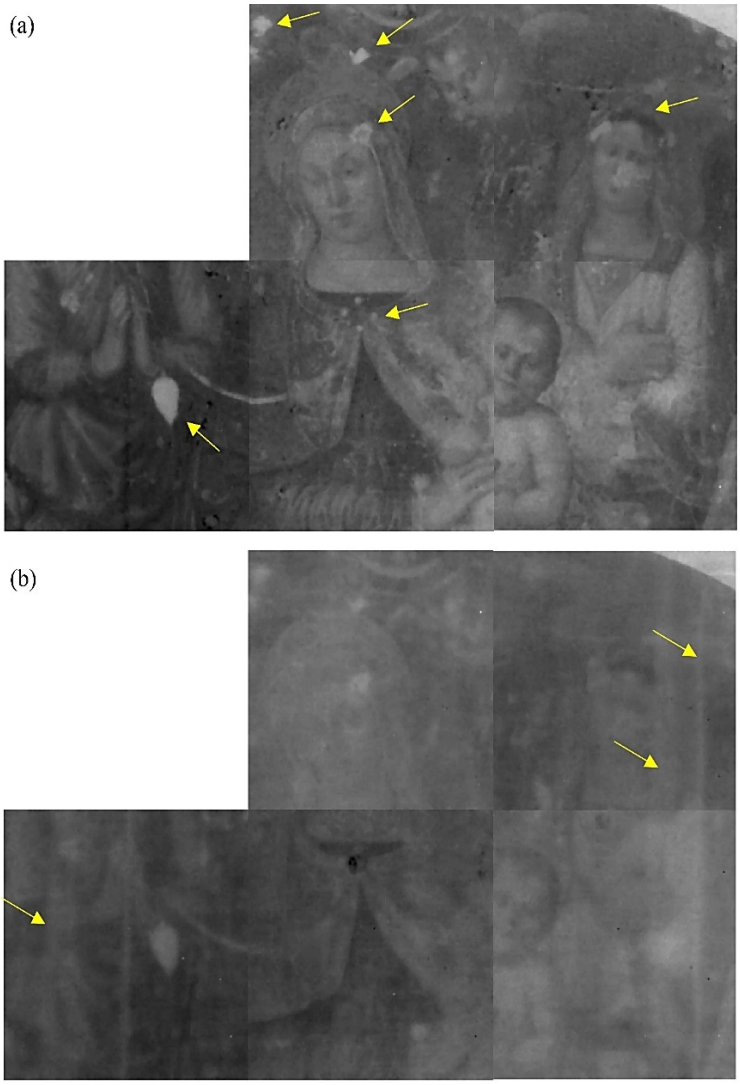

Figure 37. Results of PuCT after 1.5 seconds (a) and 10 seconds (b) from the beginning of the reconstructed thermal pulse.

Note that six thermal acquisitions were needed for testing as much as possible of the painting surface and assuring an enough spatial resolution of the captured thermograms. Those six contributions were then merged during the post-processing, so to obtain a meaningful image of the selected area. However, the top-left acquisition was found to be corrupted, thus is not being shown in the images. Figure 37(a) depicts the results of the PuCT after 1.5 seconds from the beginning of the reconstructed thermal pulse, whilst Figure 37(b) shows the same but after 10 seconds.

It can be noted that detachments, gold coating and different restoration works appear as brighter areas in Fig.37(a) and their signature is still present as time elapses – please compare marked area in Fig. 37(a) to the same in Fig. 37(b). As there is a direct link between the thermal responses of layers at deeper depths within the tested materials and the flow of time, signatures of potential deeper detachments/restorations/gluing are visible as vertical contrasted areas in Fig. 37(b) and located with yellow markers.
The PuCT results are confirming what HMI discovered concerning the presence of gold in some parts of the painting.

4.5 "Integration of optical, spectral and elementary data for non-invasive analysis of 15thcentury Persian illuminated manuscript".

A 15th century illuminated manuscript's page named *Humayun meeting princess Humay* (Fig. 38), belonging to the Musée des Arts Décoratifs and currently on long term deposit in the Department of Islamic Art of the Louvre Museum, was investigated in order to study its state of conservation and manufacturing process.

The page belongs to the Timurid period and, in its current aspect of a detached from its original manuscript, was bought in 1887 from the Union centrale des Arts décoratifs, by a secretary of the French embassy in Istanbul, Alexei Jaroszinski. In 1907, the Louvre conservator for Oriental collections Gaston Migeon, published tha manuscript's page in his "Manual of Muslim Art"' in the chapter dedicated to islamic paintings and illuminated manuscripts. In 1910, the page is sent to Munich, lent for a great exposition called "Masterpieces from Mohammedan art" which gathered for the first time about 3500 Islamic artworks. In the official catalogue of that exposition it is reported that the manuscript's page came from a manuscript that was destroyed at the beginning of the 15th century. French public could admire again the *Humay* page in 1912, when an exposition entirely dedicated to Persian painting was organized by two Paris lovers of Islamic art, engineer Georges Marteau and jeweler Henri Vever. In the catalogue, the scene is described as "the arrival of Humay to the court of the emperor of China". In 1912 Martin published a work in English dedicated to the history of the art of illumination in Persia, India and Turkey, in which he included the *Humay* page identifying its iconography. He considered it as a wonderful example of Timurid dynasty's painting and a charming copy of a Chinese model. The Persian manuscript's page "Humay and Humayun" joined the Department of Islamic Art of the Louvre Museum in October 2011 and it is object of current diagnostic investigations.

Figure 38. *Humayun meeting the princess* Humay (1430-1440), Musée du Louvre, Départment des arts de l'Islam.

First diagnostic analyses were done in the laboratories of Centre de Recherche et Restauration des Musées de France (C2RMF) through scientific imaging with Hasselblad HD4 camera modified in full-range (360-1000 nm) [141], performing UV, visible and near-infrared photography. Infrared false-color imaging was done in order to identify painting materials by comparison with pigments database [142] and macro X-ray fluorescence [143] allowed to obtain complete maps of some diagnostic chemical elements distribution (as Hg, Cu, Fe, As, Pb) to characterize painting materials in the manuscript. Organic colorant, as indigo, and pigments with light elements difficult to detect by XRF, as ultramarine blue, were identified by Raman spectroscopy.
Some parts of the manuscripts were not completely understood, mainly because mixtures and layering of pigments, typical of Persian manuscripts technique, are difficult to investigate without invasive analyses and because Raman spectroscopy was done on limited points.
For this purpose, multispectral imaging analysis through HMI technique was performed.
The 7 monochromatic images that are the output of HMI acquisition on the Persian manuscript (Fig. 39) were analyzed in the Profilocolore® PickViewer Software that allows different statistical tools used in DIP as Principal Component Analysis (PCA) and Normalized Difference Index (NDI) to apply statistical treatment to the imaging data in order to extract further details, not visible in single spectral channels.

Figure 39. The 7 HMI monochromatic images from UV to NIR.

IRFC and UVFC images (Fig. 40) were obtained in the software according to the traditional use of the band's sequence G-R-IR (using the first PC of PCA analysis on the

three IR bands) for IRFC and UV-B-G for UVFC, in order to distinguish different materials that could have the same appearance in the visible, but show different spectral behaviours in UV or IR.
A hypothesis of attribution of pigments and highlighting of restoration materials is also possible in this kind of analysis, especially with the support of specific database [142]. The deep blue pigment used for the sky, the background of the lower frame and the stole of Princess Humay (second figure from left) turning in a vivid red in IRFC and in intense green in UVFC can be identified as ultramarine blue (lapis lazuli, $(Na,Ca)_8[(Al,Si)_{12}O_{14}]Sn$), as hypothesized because of the absence of XRF elemental peaks, as lapis lazuli contains mainly light elements, close to usual XRF limit of detection, and definitively confirmed by Raman spectroscopy.
The same behaviour but with a lower saturation has been observed in the Humayun (last character on the right) figure on the right side of the painting, possibly indicating the use of a mixture of ultramarine blue with a white pigment, probably lead white, according to MA-XRF results (showing the presence of elemental lead, Pb) and literature studies [144].
All MA-XRF data of a chosen set of chemical elements for pigments characterization are shown at the end of this chapter.

Figure 40. IR false-color (left) and UV false-color (right) images generated in the Pickviewer software.

In the same way, the orange pigment used to paint the vest of the princess assumes a light shade of yellow in the IRFC and a vivid pink (cyclamen) color in the UVFC. This characteristic together with the MA-XRF data showing the presence of arsenic (As) in

that area, makes possible to suppose the use of realgar (As_4S_4) rather than orpiment (As_2O_3). The same pigment is used in the group of flowers on the left of the princess and in the panels of the architecture in the upper left of the scene.

Another pigment for which it is possible to make an hypothesis of attribution is the red pigment used in the linear elements the define the above mentioned architecture; assuming a laden yellow color in the IRFC and a deep violet color in the UVFC, it could be probably be identified as cinnabar (HgS). Mixtures of pigments are difficult to recognize in false color analysis, but a probable use of a background layer of ultramarine blue in the blue drapery of the servant holding a flower can be hypothesized in IRFC by the red shade assumed by the contours of the shoulder and red spots between the general false color blue. The coat of ultramarine blue was probably covered with another pigment with a clearer hue, as mixing and layering of pigments was usual in Islamic manuscripts painting technique.

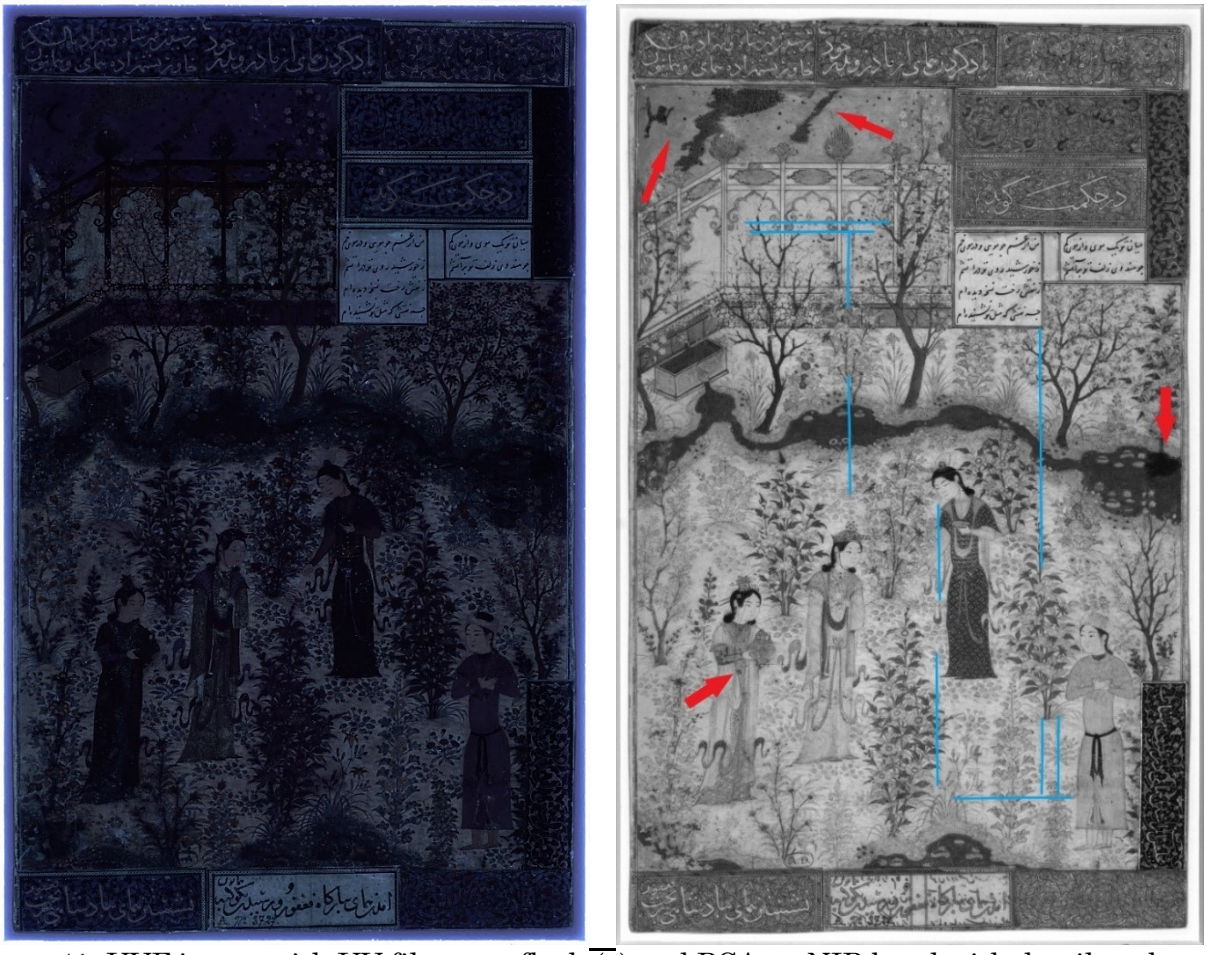

Figure 41. UVF image with UV filters on flash (a) and PCA on NIR band with details enhanced (b).

In the UVF image (Fig. 41(a)) it is possible to recognize restorations in the blue sky (appearing as darker areas) as well as some fluorescent restoration pigment on the right hand and on the front of the princess, in the flower hold by the figure on her right and on the knot of his belt; it is also present in the left written white frame and again in the sky. The restoration in the sky is also visible in PCA image made on the three IR bands (Fig. 41(b)), highlighting also the retouches (enhanced by red arrows) in the river (on

the right edge of the manuscript) and on the dress of the servant bottom left. In this last image also details of the design become visible, like the drapery of the dress of the servant holding a pot and some lines of frames pertaining to the back of the manuscript (retraced with light blue lines in Fig. 41(b)).
More hidden details are noticeable applying NDI statistical tool to UV and IR2 balanced channels (Fig.42); since different materials have different responses in these two diagnostic spectral bands, this kind of analysis helps extracting features from a contrast enhancement. Traces of some restoration products become visible as darker areas (green circles) in the upper frames, on the red dress of the servant bottom left and on the light blue dress of Humayun.

Figure 42. NDI algorithms run with PickViewer software on UV and IR2.

HMI software enables to compare 7-bands spectral reflectance values between different points in the image (minimum area: 3x3 pixels) and to build maps of multispectral similarity to investigate the distribution of painting materials in the artwork.
Multispectral similarity analysis was done to investigate the blue pigment of the upper part of dress of Princess Humayun's vest. Focusing on the black and white output image (Fig.43) (where the measurement point in encircled in red), areas of higher multispectral similarity are enhanced in white, resulting in a mapping distribution of similar painting materials in the manuscript. This data treatment shows a clear affinity of the blue pigment in the vest of Princess with the blue pigment used in the sky, identified as ultramarine blue.

Figure 43. Visible image of the manuscript (left) and mapping of ultramarine blue based on multispectral similarity (right).

The distribution mapping shows its use also in the blue flowers (pointed out with blue arrows in Fig.43 and in the ribbons on the bottom part of the princess's dress, as well as in minor quantity in the light blue vest of Humayun, probably mixed with lead white, according to MA-XRF mapping of lead. The same blue pigment seems present in very few spots in the blue decorated frames, where the spectral similarity shows a correspondence in the restoration of the sky (Fig. 44(b)). This datum could possibly mean the use of two different blue pigments (Fig.44), in particular of two different qualities of lapis lazuli, as both the database of pigments spectral reflectance in the software and Raman spectroscopy confirmed ultramarine blue in the sky and also in the frames. It can be hypothesized the use of a purer lapis lazuli in the sky (as supposed by the Raman

spectrum) and a lower-quality one (or a mixture with other pigments as well as covered by a varnish or a glue) in the background of the other decorated frames that were glued to the page and whose belonging to the same manuscript is uncertain.
According to scientific literature [144-146], the painting technique used to create ancient Islamic manuscripts was based on complex layering and mixtures of pigments; in this case, HMI tools for statistical analysis can be useful to support XRF analysis (which provide only elemental data) in the characterization of painting material and understanding of painting technique. It is important to stress that HMI, as any multispectral imaging techniques, is not an analytic investigation so it should be used in an integrated approach with traditional spectroscopic methods for characterization purposes.

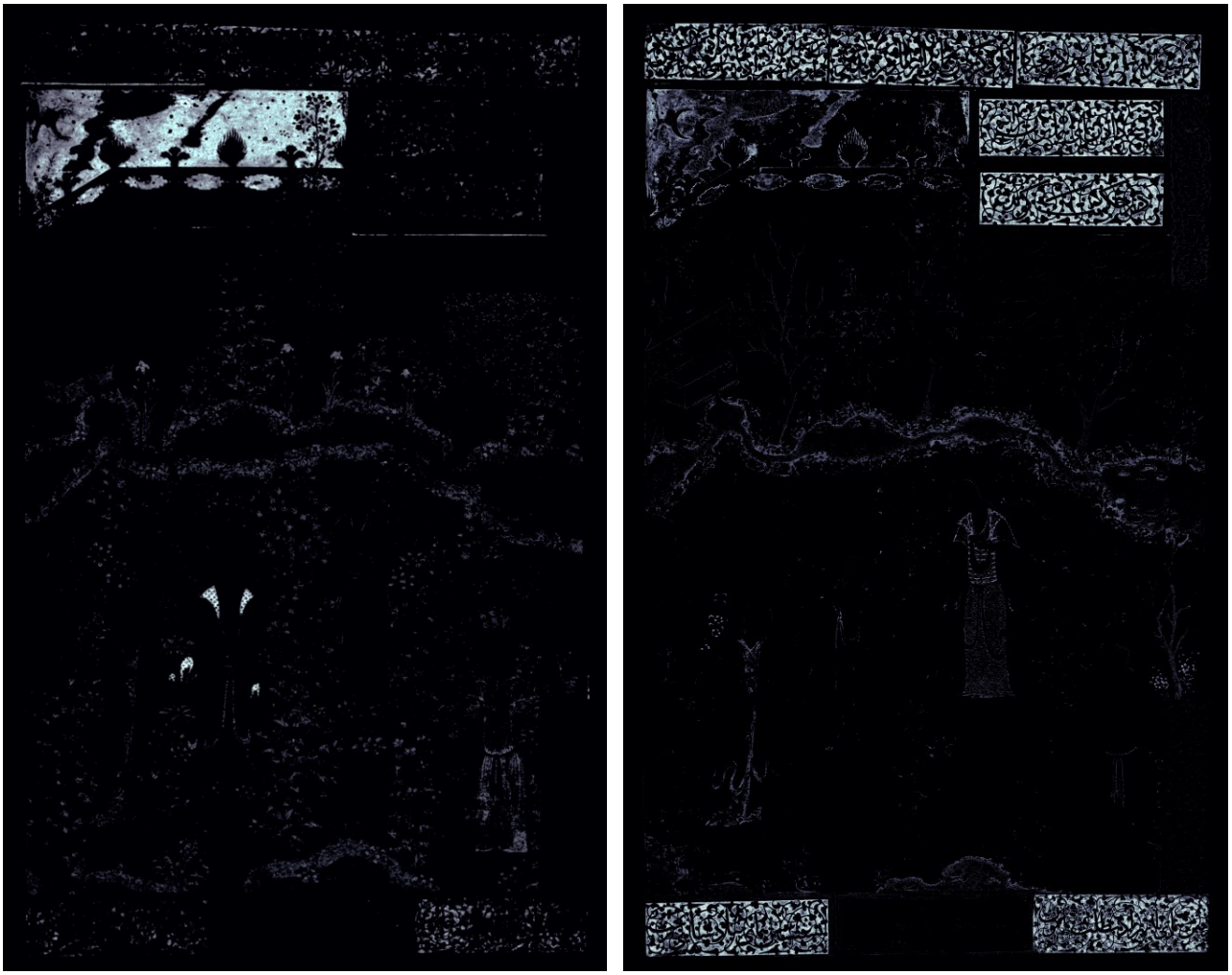

Figure 44. Two different blue pigments used in the sky (a) and in the decorated frames possibly pertaining to a different manuscript (b).

Comparing HMI multispectral similarity data with IRFC and UVFC analysis the use of azurite for the blue background of the frames can be hypothesized. The use of different blue pigments can be also confirmed by another tool in PickViewer software that compares spectral reflectance of any pixel in the image. Focusing the analysis on a region of interest (ROI) and selecting a point in the blue sky and one in the blue decorated frames, it is possible to analyse the values of spectral reflectance (%) in each of the 7 HMI bands; in Fig. 45 it is shown a different spectral response between the two blue pigments in the IR, with a major variance in IR2 (850 nm). Colorimetric coordinates

of the two measurement points are also readable in the bottom of the GUI and shown in CIE 1931 x-y chromaticity diagram.

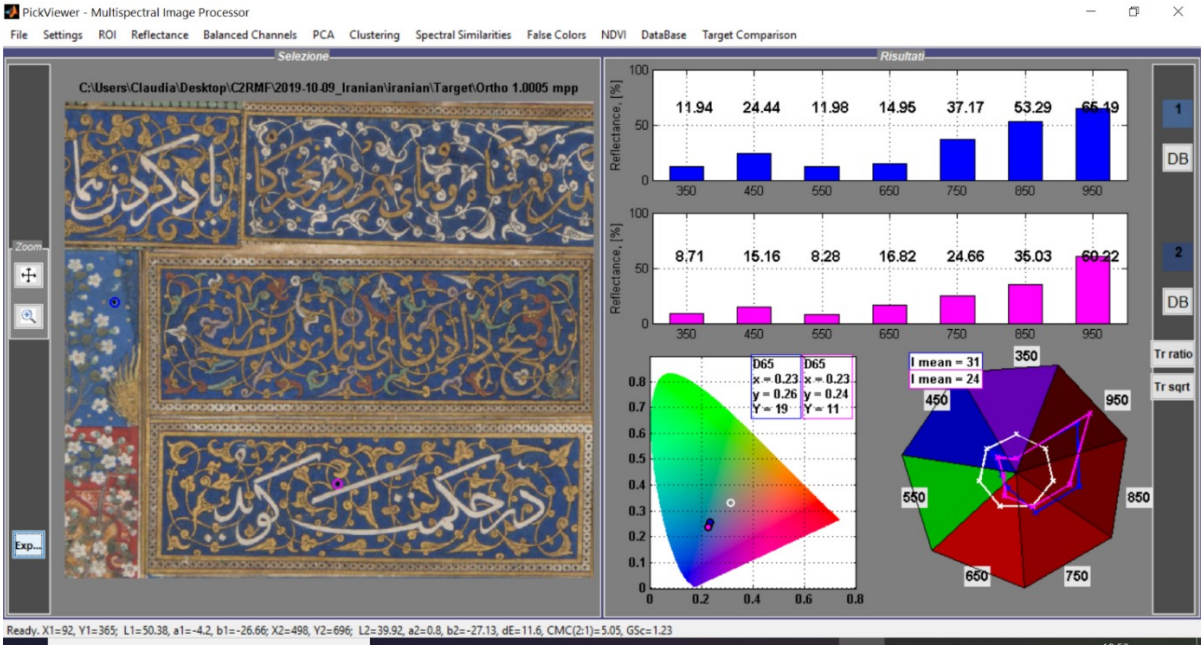

Figure 45. Comparison of spectral reflectance (%) of two different blue pigments in the manuscript.

The same processing was applied on the light blue pigment on the shoulders of the servant holding a flower (Fig.46(a)): it is interesting to notice the correspondence in the MA-XRF distribution of copper in this point and in the light green leaves, but also a clear multispectral similarity with the restorations in the sky also covering some golden stars that now appear dark. A green copper pigment could have been used for the restoration of the sky in mixture with ultramarine blue (Fig. 44(b)), covering also the golden stars above. Since verdigris (copper acetate, $Cu(OH)_2 \cdot (CH_3COO)_2 \cdot 5H_2O$) is known to be aggressive towards paper material [147], considering the good state of conservation of the details painted in green, the use of azurite or malachite (basic copper carbonates) seems more likely.
Raman spectroscopy revealed malachite's characteristic bands (data not shown) in one point of the light green basement of the architecture: considering its spectral behaviour in IRFC and UVFC similar to the green leaves ones and the spectral similarity map (Fig.47), obtained by the spectral reflectance curve extracted for a point in the same area of Raman analysis in the basement, the usage of malachite seems plausible also in the light green leaves and in mixtures with ultramarine blue to paint the light blue parts of the dresses, the groups of small turquoise flowers by the river and in the restoration of the sky.

Focusing the spectral similarity measurement on the dark stars in the sky (Fig. 46(b)), the software revealed a close similarity with the pigment used for the hair of the figures, the trunk of the first tree on the left, portions of the black writings top right, the belt of the prince, the background of the bottom right vertical frame, where Raman spectroscopy detect a carbon-based black pigment s a carbon-based black pigment by the presence of two broad bands at ca 1580 and 1325 cm^{-1} (Fig 48(a)). While the mixtures of carbon-black pigment with some other ink for the text and with cinnabar (revealed

by the presence of mercury in XRF mapping, at the end of this chapter) seems reliable to realize the brown hue of the tree trunk, it is less comprehensible its use to cover the golden stars in the sky.

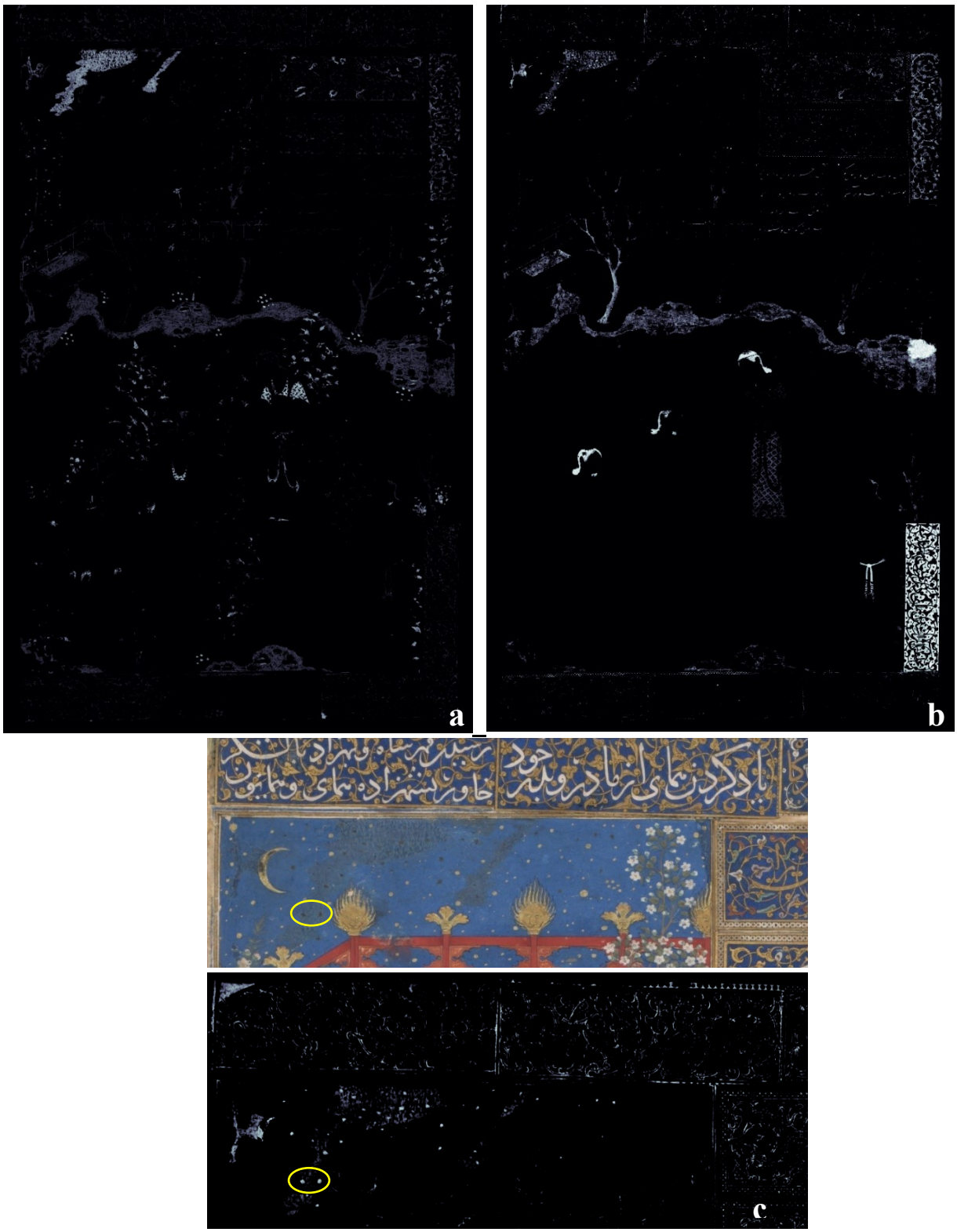

Figure 46. a) HMI mapping of light blue pigment (ultramarine blue + malachite?) based on multispectral similarity; b) same mapping of a painting material covering dark stars (as highlighted in yellow); c) detail of the restoration in the sky: VIS image (top) and similarity map (bottom).

A correspondence is also found in the water fountain and in the tree trunk next to it, as well as in all the river and in the restoration on the left edge of the river. This last data could suggest the use of a mixture of different pigments for the water as carbon black, tin (whose abundance is shown in MA-XRF data) and probably a small quantity of the same light blue color obtained by the mixture of ultramarine blue and malachite.

Figure 47. Visible image of the manuscript (left) and spectral similarity map of the light green pigment used in the basement (right), in the area where Raman spectroscopy identified malachite (green arrow).

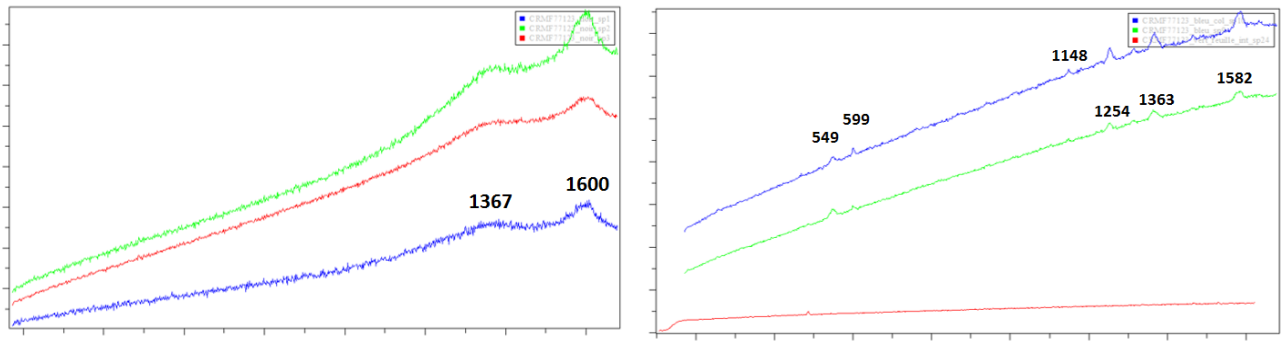

Figure 48. Raman spectra with characteristic vibrational bands of carbon-based black pigment (a) and of indigo (b).

Since HMI Pickviewer software allows to process any imaging data together with multispectral images, MA-XRF images acquired by MA-XRF scanner of C2RMF laboratories have been analysed to extract information on the paint palette used in the investigated manuscript. A selection of MA-XRF images (Table 6) showing the distribution of some diagnostic chemical elements for pigment characterization has been aligned with HMI images and processed through Pickviewer's tools for statistic analysis. In Fig. 49, XRF mapping of elemental distribution of arsenic (As) - transition line K- and of mercury (Hg) - transition line L- are shown.

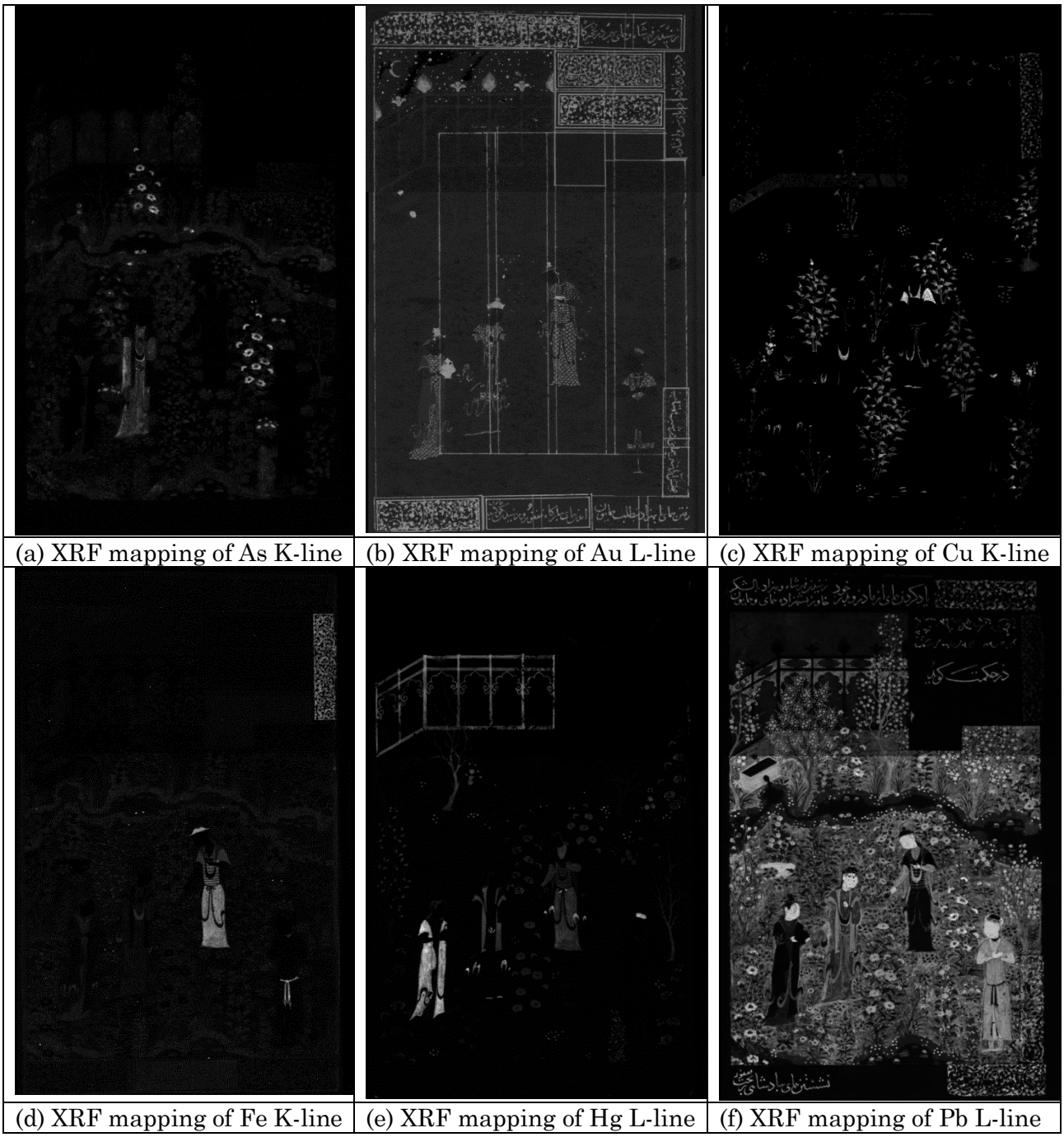

(a) XRF mapping of As K-line | (b) XRF mapping of Au L-line | (c) XRF mapping of Cu K-line

(d) XRF mapping of Fe K-line | (e) XRF mapping of Hg L-line | (f) XRF mapping of Pb L-line

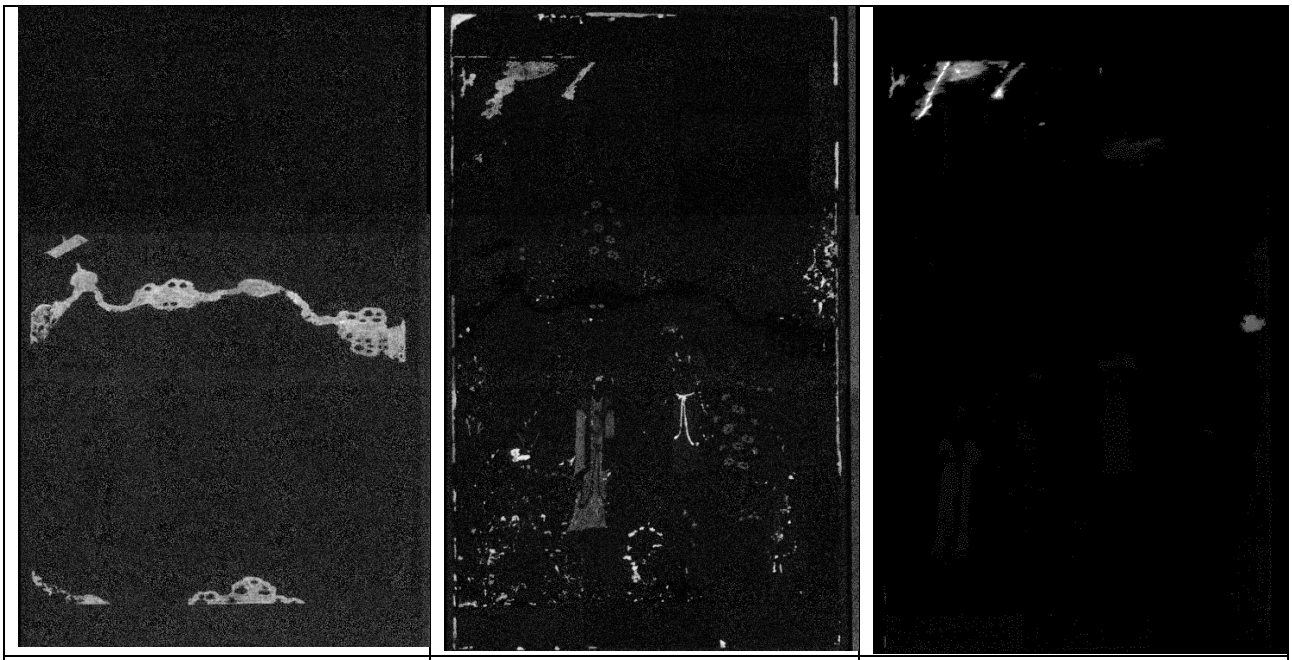

(g) XRF mapping of Sn K-line	(h) XRF mapping of Ba L-line	(i) XRF mapping of Zn L-line

Table 6. MA-XRF images of diagnostic elements for the characterization of main pigments used in Persian manuscripts palette (courtesy of C2RMF).

Arsenic and mercury MA-XRF images have been loaded as extra-bands in the HMI software and aligned to the multispectral images. A useful DIP tool to understand pigment distribution in the painting is cluster analysis. Selecting as input bands colorimetric L, a, b values and MA-XRF extra-band for As and Hg, cluster analysis is able to differentiate groups of data on the base of spectral similarity correlating them with the colorimetric (L, a, b) information.
Clustering the spectra of the data set according to their HMI multispectral similarity allows to map of similar painting materials and associating the calibrated colorimetric data is possible to visualize the distribution of pigments with their real appearance in the visible light (Fig. 49).

This data processing allowed to easily visualize the distribution of cinnabar in the artwork and to better understand when it was used alone (deep red in Fig. 49(b)) and when in mixtures with other pigments, as in the trees and in the red and orange flowers. Multispectral similarity maps supported with XRF data give a clearer view of the distribution of pigments compared to MA-XRF alone, whose black and white imaging output can be difficult to read, especially in areas of lower elemental abundance.
In the same way, in Fig. 49(a) it is possible to clearly distinguish the presence of arsenic as orange pigment orpiment used for some group of flowers (where only some portions are enhanced as it was used –as XRF data suggest- in mixture with cinnabar and maybe white lead), and as *vergaut* – a mixture of orpiment and indigo used to paint all the deep green leaves and the grass around the river, extensively found in the study of Islamic ancient manuscripts [135]. Indigo, a blue organic colorant of vegetal origin, was indeed supposed by the light red shade shown by deep green leaves in IRFC and analytically identified by punctual Raman spectroscopy in the painted foliage (Fig.48(b)).

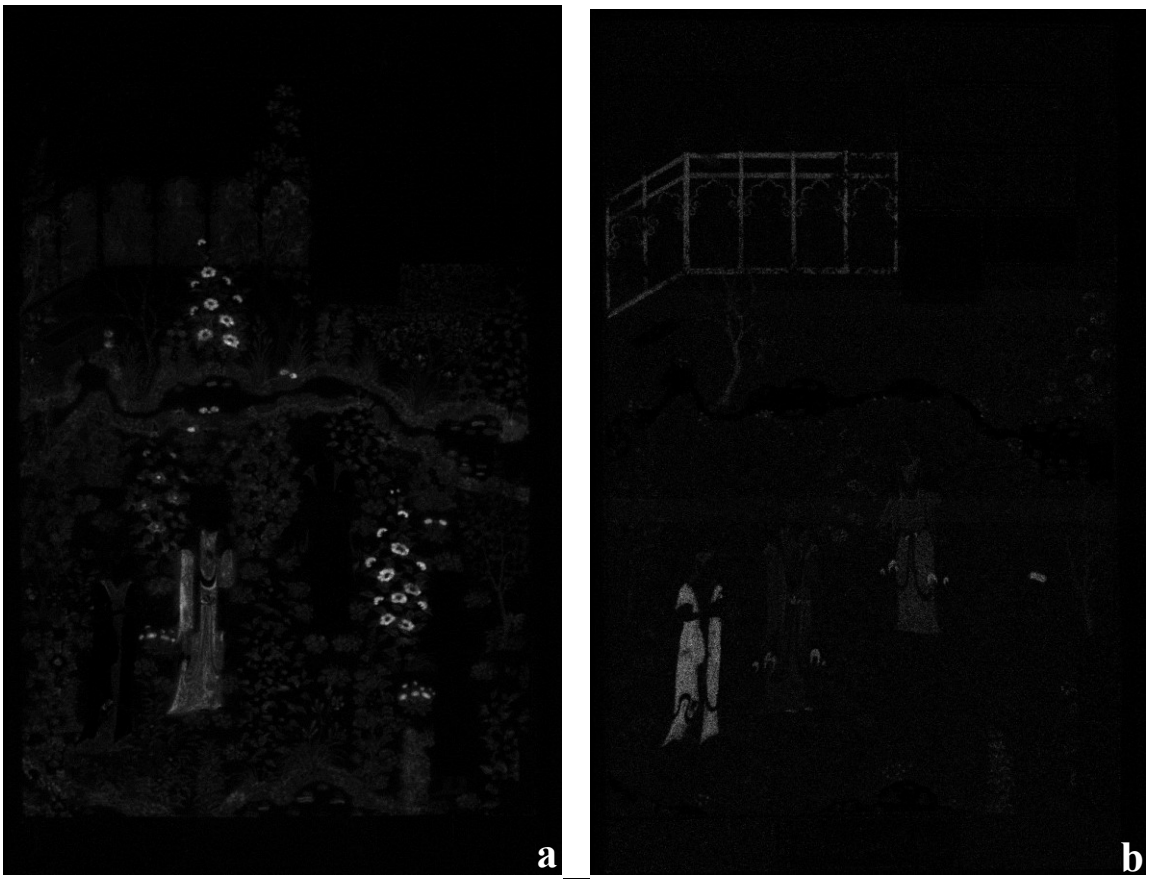

Figure 49. MA-XRF mapping: (a) elemental arsenic (As); (b) elemental mercury (Hg).

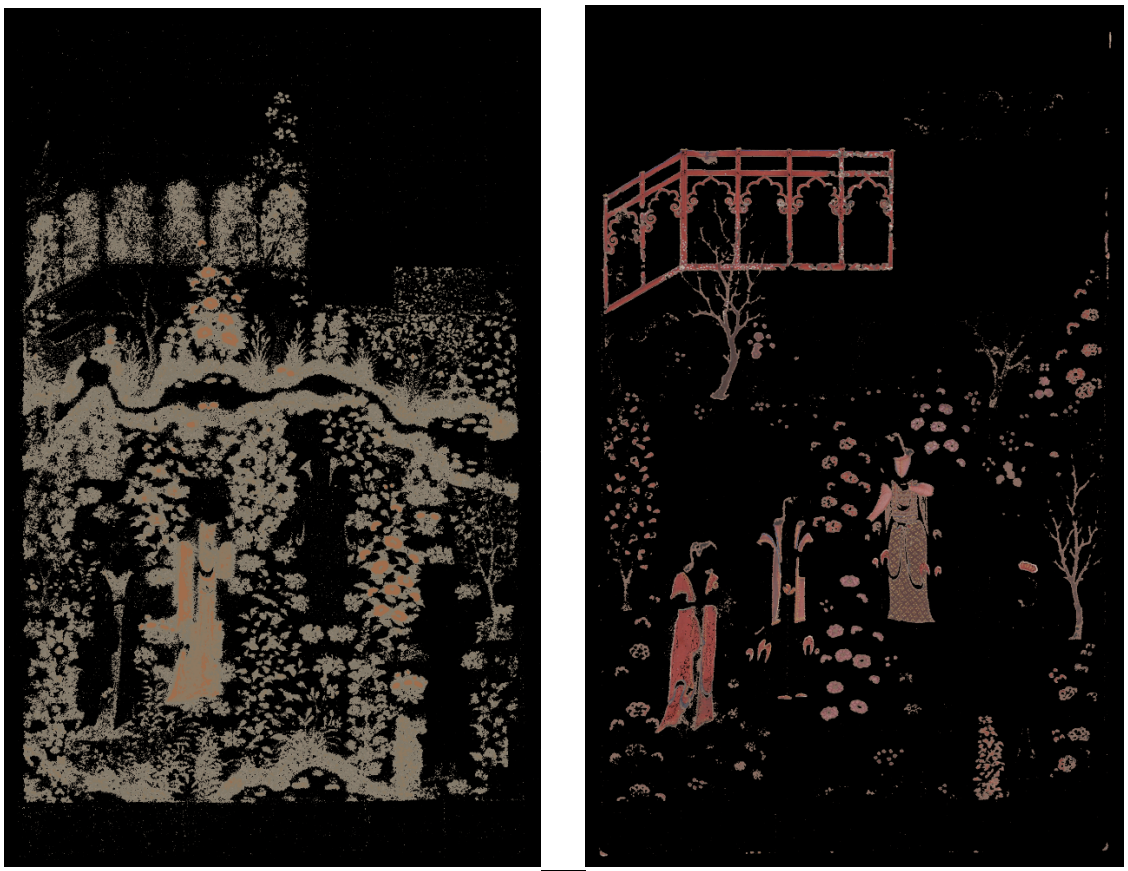
Figure 50. Distribution of orpiment and *vergaut* (a) and of cinnabar and its mixtures on the base of MA-XRF and HMI data.

4.6 Building of a spectral signatures database for pigments characterization.

During a four-months period of research at the Imaging laboratory of Centre de Recherche et Restauration des Musées de France (C2RMF) in Paris, HMI images of more than 300 pigments on paper (listed in Table 7) were analysed in order to build a database of calibrated spectral reflectance curves for multispectral characterization of pigments.

All the pigments (property of C2RMF) are produced by Kremer Pigmente GmbH & Co. KG [148], a leading company in artist's materials specialized in production and distribution of rare and historical pigments.
The Kremer charts of pigments are realized applying the original pigment by screen-printing on acid-free paper 180 g sheets in A4 format. All colors are applied in one layer. A part of the paper is previously printed with a gray scale, which should clarify the opacity of the pigments. The gray strips have ink coverage of 25%, 50% and 75%. With more opaque pigments the grayscale is less visible (Fig. 51).

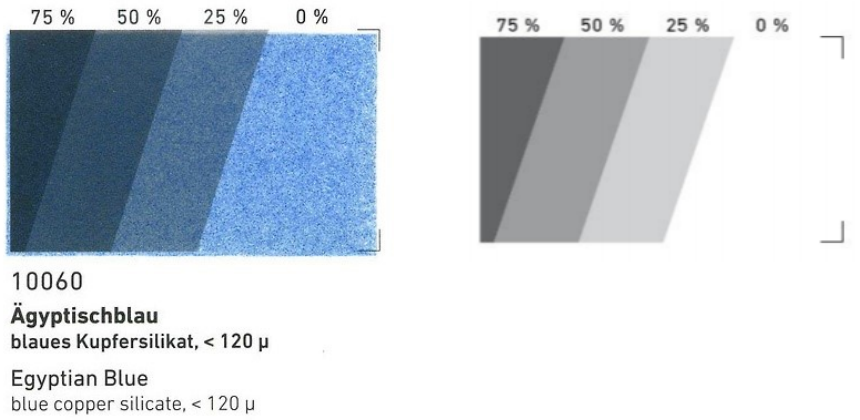

Figure 51. Sample of Kremer pigment (left) on a printed opacity gray scale (right).

Except for some exclusions, the pigments are being bound in an aqueous binder, based on gum Arabic (natural untreated gum arabic #63300, CAS No. 9000-01-5). As a result, the coloring of the pigment barely changes. Exceptions are pigments, that cannot be used in this binder, such as Dragon Blood or Copper resinate. Every color chart is generally composed by 12 samples of pigments, each measuring 3 x 5 cm.
The Kremer color charts acquired by HMI system are: Blue Pigments (#990001), Cadmium Pigments (#990002), Kremer-made and historic Pigments (#990004), Iron Oxides (#990005), (#990006) Earth Pigments, Yellow Pigments (#990008), Green Pigments (#990010), Organic Pigments (#990012), Red Pigments (#990015). All the pigments, organized by color, are listed in Table 5, reporting Kremer catalogue number, commercial names and a brief description.
The collected mineral and organic pigments, of natural and synthetic origin, extensively represent artists palette in ancient, modern and contemporary art [149, 150].

All the Kremer charts were acquired with HMI system of two filters and calibration was performed by white reference polymers on the edge of the chart and by the NCS color checker (as shown in Fig. 52). Furthermore, a second set of Kremer pigments in oil

binder applied on a plexiglass support was also acquired (Fig.53, Fig. 54). Each of these pigments was applied in a single and a double layer, with and without varnish on top.

These acquisitions allowed to register all the pigments spectral reflectance's curve in just two photographic shots and to collect them in a database of spectral signatures, in order to enables analyses of pigment characterization on the base of spectral similarity. In addition, an imaging database of ultraviolet false-color (Fig.55(a)) and infrared false-color (Fig.55(b)) images of pigments was also collected.

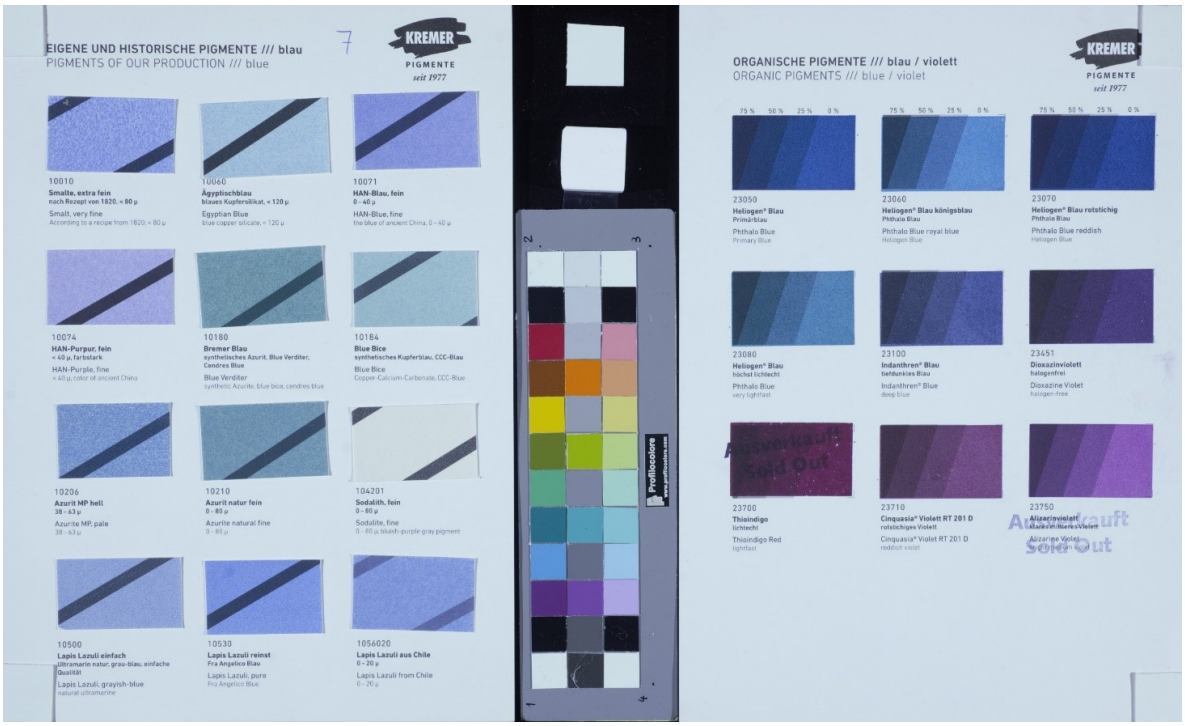

Figure 52. HMI acquisition of pigments on paper with white reference and color checker for calibration.

Blue/violet pigments		
Id catalogo	**Nome**	**Descrizione**
10010	Smalt, very fine	according to a recipe from 1820, < 80 µ
10060	Egyptian Blue	blue copper silicate, < 120 µ
10071	HAN-Blue, fine	the blue of ancient China, 0 - 40 µ
10074	HAN-Purple, fine	< 40 µ, high tinting strength
10180	Blue Verditer	synthetic Azurite, blue bice, cendres blue
10184	Blue Bice	Copper-Calcium-Carbonate, CCC-Blue
10206	Azurite MP light	38 - 63 µ
10210	Azurite natural fine	very fine grind, 0 - 80 µ
104201	Sodalite, fine	0 - 80 µ, bluish-purple gray pigment
10500	Lapis Lazuli, grayish-blue	natural ultramarine
10530	Lapis Lazuli, pure	Fra Angelico Blue
1056020	Lapis Lazuli from Chile	0 - 20 µ, washed and separated by flotation
Organic Pigments, synth.		
23050	Phthalo Blue	Primary Blue
23060	Phthalo Blue Royal Blue	Heliogen Blue

23070	Phthalo Blue reddish	Heliogen Blue
23080	Phthalo Blue	very lightfast
23100	Indanthren® Blue	deep blue
23451	Dioxazine Violet	halogen-free
23700	Thioindigo Red	lightfast
23710	Cinquasia® Violet RT 201 D	reddish violet
23750*	Alizarin Violet	bright medium violet
Indigo		
36000	Indigo, genuine	Indian, powder, Indigofera tinctoria
36006*	Indigo red-violet	natural blue pigment
36007*	Maya blue	genuine, indigo, in a silicic crystal matrix
Ultramarine Pigments		
45000	Ultramarine Blue, very dark	synthetic mineral pigment
45010	Ultramarine Blue, dark	synthetic mineral pigment
45020	Ultramarine Blue, reddish	synthetic mineral pigment
45030	Ultramarine Blue, greenish extra	synthetic mineral pigment
45040	Ultramarine Blue, greenish light	synthetic mineral pigment
45080	Ultramarine Blue, light	synthetic mineral pigment
45100	Ultramarine Violet, medium	bluish, mixture
45110	Ultramarine Violet,	reddish, dark
45120	Ultramarine Violet, light reddish	synthetic mineral pigment
45202	Prussian Blue LUX	also Milori Blue, Berlin Blue
45350	Manganese Violet,	synthetic mineral pigment
45364	Copper blue	Very light turquoise blue
45400	Zirconium Cerulean Blue	semi-opaque, light blue
Cobalt pigments		
45700	Cobalt Blue Dark	synthetic mineral pigment
45701	Cobalt Blue Dark, greenish,	slightly lighter and more greenish than 45700
45702	Cobalt Blue, Sapporo	
45710	Cobalt Blue Medium	opaque
457141	Cobalt Blue Pale	synthetic mineral pigment
45720	Cobalt Blue Light	synthetic mineral pigment
45730	Cobalt Cerulean Blue	
45740	Cobalt Blue, greenish	
45750	Cobalt Blue Turquoise Light	
45760	Cobalt Blue Turquoise Dark	
45800	Cobalt Violet, dark	semi-opaque
45810	Cobalt Violet Brilliant, dark	< 75 µ
45820	Cobalt Violet Brilliant, light	brilliant
Studio pigments		
55500	Studio Pigment Sky Blue,	synthetic organic pigment and filler
55600	Studio Pigment Dark Blue	synthetic organic pigment and filler
55900	Studio Pigment Violet	synthetic organic pigment and filler

Red Kremer-made pigments		
10150	Pinkcolor,	lightfast, < 38 µ
10154	Pinkcolor Deep	very lightfast, < 38 µ

10620	Natural Cinnabar	mineral pigment, from China
10625	Cinnabar, fine	chu piao, 20 - 50 µ
11300	Red Jasper	semi-transparent, 0 - 120 µ
11350*	Cote d'Azur Violet	Light caput mortuum
Red earths		
11360	Brown-Red Slate	from Austria
11574	Burgundy Red Ochre, fine	from France, 0 - 80 µ
11576	Burgundy Red Ochre Deep, fine	from France, 0 - 80 µ
11585	Spanish Red Ochre, extra fine	Bauxite, 0 - 63 µ
11530	Gold Ochre	from Saxony, Germany, deep brown-gold, very fine grind
11620	Brown Earth from Otranto	Italy, pea-ore, sanguine-rust brown, standard grind

Orange/red organic pigments, synthetic		
23178	Irgazine® Orange DPP RA	transparent
23179	Irgazine® Scarlet DPP EK	opaque
23180	Irgazine® Red DPP BO	opaque
23181	DPP - Red	transparent
23182	Irgazine® Ruby DPP-TR	opaque
23200	Scarlet Red	most brilliant scarlet
23202	CPT - Scarlet Red	warm orange
23230	Permanent Red A	deep clear red, anthraquinone pigment
23250*	Permanent Red Dark	GOLO limited availability
23290	Permanent Red	neutral red B
23291	Permanent Red FRLL	neutral red C
23293	CPT - Red	Medici-Red
23402	Quindo® Pink D	organic pigment
23490*	Purple-Red	Brownish Urbino red, very lightfast
23493	Gubbio Red	transparent brownish-red
23540	Paliotol® Orange	bright orange
23570	Pyranthrone Orange	reddish orange
23585	Cinquasia® Gold, red-gold	glazing, reddish
23600	Alizarine Crimson Light	bright red
23610	Alizarine Crimson Dark	bluish red
23720	Hostaperm® Red	light reddish violet
23800	Isoindolol Orange	warm dark orange

Yellow pigments		
43010	Massicot, Litharge	yellow lead oxide, litharge, pieces, contains lead, toxic
43101	Bristol Yellow, pale	naples yellow imitation, lead-free
43111	Bristol Yellow, medium	naples yellow imitation, lead-free
43131	Bristol Yellow, reddish	naples yellow reddish imitation, lead-free
43121*	Naples Yellow, lemon	genuine, contains lead, toxic
43125	Naples Yellow, dark	genuine, contains lead, toxic
43130	Naples Yellow, reddish	contains lead, toxic
43200	Nickel-Titanium Yellow	artificial mineral pigment

43210	Nickel-Titanium Yellow, greenish	artificial mineral pigment
43230	Praseodym Yellow	pale
43300	Titanium Orange	golden-orange
43600	Antimony Red	golden antimony sulphide
43870	Yellow Zircon	Zircon-Praseodymium-Silicicate
43880	Intensive Yellow	transparent
43910	Bismuth-Vanadate Yellow, lemon	very lightfast
55100	Studio Pigment Yellow	synthetic organic pigment and filler
55125	Studio Pigment Egg Yolk Yellow	synthetic organic pigment and filler
55140	Studio Pigment Yellow Sun Gold	synthetic organic pigment and filler
Kremer-made Pigments		
10100	Lead Tin Yellow Light	< 38 µ, contains lead, toxic
10110	Lead Tin Yellow Deep	changed hue, < 38 µ, contains lead, toxic
10120	Lead Tin Yellow II	yellow lead glass, 0 - 63 µ, contains lead, toxic
10130	Naples Yellow from Paris	< 50 µ, contains lead, toxic
10700	Orpiment, genuine	King´s Yellow, coarse, 175 µ, contains arsenic, toxic
10800	Realgar, genuine	red orpiment, 175 µ, contains arsenic, toxic
17000	Jarosite, from Cyprus	genuine, pale yellow ochre
17050	Natural Sienna, Monte Amiata	Italian, washed, brilliant, very light
40010	French Ochre JTCLES	clear yellow earth pigment, washed
40012	French Ochre, very light	yellow
40013	French Ochre, extra light	yellow
40030	French Ochre JOLES	yellow earth pigment, washed
40040	French Ochre JCLES	yellow earth pigment, washed
40050	French Ochre JFLES	yellow earth pigment, washed
40060	French Ochre JALS	warm yellow earth pigment, washed
40195	Gold Ochre, from Poland	Carpathia
40070	French Ochre SOFODOR	golden earth pigment
40130	French Ochre SAHARA	French yellow ochre
40200	Ochre Avana, greenish-yellow	Italian
40214	Gold Ochre DD	very fine, clear golden yellow, German
40220	Italian Gold Ochre Light	Sienna de Verona
40241	Fawn Ochre	German, very light umber, greenish
40260	Satin Ochre	Monte Amiata, gold-orange, from Tuscany, Italy
40280	Amberg Yellow	deep, German
40301	Iron Oxide Yellow	deep yellow
40310	Dark Ochre, German	
40320	Dark Ochre, Italian	light ochre
40392	Raw Sienna, French	natural yellow earth
40400	Raw Sienna, Italian	natural yellow earth
40404	Raw Sienna Badia, Italian	natural earth pigment
40410	Raw Sienna brownish, Italian	natural earth pigment
11520	Jarosite	clear yellow ochre, < 100 µ

11540	Taunus Ochre	light, German
11572	Burgundy Yellow Ochre, fine	from France, 0 - 80 µ
116421	Yellow Moroccan Ochre, fine	< 80 µ
11650	Elba Brown Ochre deep	dark brown, fine grind, from Tuscany
Iron Oxides		
48000	Iron Oxide Yellow 920, medium	synthetic iron oxide
48020	Iron Oxide Yellow 415, greenish	synthetic iron oxide
48040	Iron Oxide Yellow 940, dar	synthetic iron oxide
48050	Iron Oxide Yellow-Orange, Gamma	synthetic iron oxide, acicular particles
48060	Iron Oxide Orange 960, light	synthetic iron oxide
48100	Iron Oxide Red 110 M, light	synthetic iron oxide
48120	Iron Oxide Red 120 M	synthetic iron oxide
48150	Iron Oxide Red 130 B, medium	synthetic iron oxide
48200	Iron Oxide Red 130 M, medium	synthetic iron oxide
8220	Caput Mortuum Synthetic 180 M	bluish dark iron oxide red, Persian red
48250	Iron Oxide Red 222, dark	synthetic iron oxide, rust protection
48289	Iron Oxide Red, micronized	very pure, strong tinting strength
48600	Iron Oxide Red, natural	haematite, medium grind
48651	Haematite, intense tinting	powder
48700	Caput Mortuum reddish	natural, very opaque
Organic pigments, synth.		
23300	Permanent Yellow light	organic pigment
23310	Permanent Yellow medium	organic pigment
23330	Irgazine® Yellow, greenish	transparent
23340	Isoindole Yellow	organic pigment
23350	Indian Yellow Imitation	contains nickel
23370	Pyramid-Yellow medium	clear warm yellow
23650	Brilliant Yellow	Hansa yellow
23660	Isoindolinon Yellow	greenish
23670	Irgazine® Yellow	light orange
23850	Studio Yellow	Hansa yellow
24000	Paliotol® Yellow-Orange	brilliant orange

Cadmium yellow/red pigments		
21010	Cadmium Yellow No. 1, lemon	very lightfast, opaque
21020	Cadmium Yellow No. 2, very light	very lightfast, opaque
21030	Cadmium Yellow No. 4, light	very lightfast, opaque
21040	Cadmium Yellow No. 6, medium	very lightfast, opaque
21060	Cadmium Yellow No. 9, dark	very lightfast, opaque
21080	Cadmium Orange No. 0, very light	very lightfast, opaque
21090	Cadmium Orange No. 0.5, light,	very lightfast, opaque

21100	Cadmium Orange No. 1, medium	very lightfast, opaque
21110	Cadmium Orange No. 2, vermilion	very lightfast, opaque
21120	Cadmium Red No. 1, light	very lightfast, opaque
21130	Cadmium Red No. 2, medium	very lightfast, opaque

Red Earth colors		
40020	French Ochre RTFLES	red earth pigment, washed
40080	French Ochre HAVANE	orange earth pigment
40090	French Ochre SOFOROUGE	red earth pigment
40430	Dark Burnt Sienna	Italian, No. 3
40440	Pompeii Red	burnt natural sienna, Tuscan earth
40470	Burnt Sienna, from France	natural earth
40490	Rosso Sartorius	natural red earth from Sardinia, Italy
40503	Red Bole	natural red earth from Germany
40510	Venetian Red	Italian red earth
English Red		
40542	English Red Light	mixed red earth, orange, burnt
40545	English Red Deep	German, mixed red earth, burnt, cool red
41550	Terra Pozzuoli	mixed red earths
40231	Brown Ochre light	German

Earth Colors, Umbers		
40610	Raw Umber	from Cyprus
40611	Raw Umber, light	from Cyprus
40612	Raw Umber, greenish	from Italy
40623	Manganese Brown Intense	from Morocco, Caledonian brown, Cappagh brown, contains manganese
40630	Raw Umber, greenish dark	German
40650	Chromite	iron chromium oxide mineral, similar to a dark green umber
40660	Raw Umber, dark	brown slightly greenish, from Cyprus
40700	Burnt Umber, reddish	Italian
40710	Burnt Umber, brownish	from Cyprus
40720	Burnt Umber, dark brown	from Cyprus
40723	Burnt Umber, type B	from Cyprus
40730	Burnt Umber Light, reddish-brown	from Cyprus

Green colors		
10064	Egyptian Green	copper glass, 40 - 120 µ
10170*	Ploss blue	Sky-blue crystals of very brilliant luminosity
10310	Malachite natural, extra fine	0 - 80 µ, intense color
10345	Malachite MP extra fine	0 - 63 µ, intense color
10350	Chrysocolla	bluish green, copper silicate, 0 - 120 µ
103601	Fibrous Malachite, fine	0 - 80 µ
103701	Malachite Arabian, fine	0 - 80 µ

103801*	Turquoise, sky-blue, fine	0 - 80 µ
103901	Atacamite, fine	0 - 80 µ
104602*	Cavansite, extra fine	0 - 40 µ
11181	Andeer Green, fine	0 - 200 µ, Green Gneiss from Andeer, Switzerland
11140	Aegirine fine	0 - 63 µ, dark green earth
11200	Green Jasper	crystalline bluish green, 0 - 120 µ
11250	Celadonite	green earth, from the Côte d'Azur, France
12200	Copper Resinate	transparent copper green
44100	Cobalt Green	contains cobalt
44110	Cobalt Oxide Green Blue	deep turquoise, contains cobalt
44130	Cobalt Bottle Green	dark green, contains cobalt
44151	Cobalt Green bluish A	Rinmann Green, contains cobalt
44190	Pastel Green, Victoria Green	bright, very lightfast, transparent
44200	Chrome Oxide Green	cool green, opaque
44204	Chrome Oxide Green DD	pure, intensive color, very fine
44250	Viridian Green	hydrated chrome oxide, bright, transparent
44280	Permanent Green	mixture, lightfast
44400	Malachite, synthetic	contains copper
44450	Verdigris, synthetic	coarse bluish green powder, contains copper
44700*	Ultramarine Green, genuine	historic pigment
55700	Studio Pigment Light Green	synthetic organic pigment and filler
55800	Studio Pigment Dark Green	synthetic organic pigment and filler
Cadmium pigments		
44500	Cadmium Green, light	mixture of cadmium yellow and phthalocyanine blue
44510	Cadmium Green, dark	mixture of cadmium yellow and phthalocyanine blue
Green Earths		
11000	Verona Green Earth	0 - 120 µ, genuine earth pigment
11100	Bavarian Green Earth	0 - 120 µ, similar to Bohemian Green Earth
11111	Russian Green Earth, extra fine	0 - 63 µ, natural earth pigment
11152	Florentine Green	60 - 120 µ, washed
40800	Green Earth light	yellowish, German
40810	Bohemian Green Earth	genuine, brilliant hue, extra fine grinding
40821	Green Earth from Verona	genuine, pure
40830	Green Earth from France	light
40850	Burnt Green Earth	reddish, coarser grind
41700	Verona Green Earth	
41750	Vagone Green Earth	mixture of different pigments
41770	Nicosia Green	mixed green earths with cobalt blue, enhanced
41800	Bohemian Green Earth, imitation	enhanced earth color, yellowish green light

41820	Verona Green Earth, imitation	mixed green earths
11150	Epidote	yellow-green earth
17400	Green Earth, from Cyprus	genuine, standard
17410	Bluish Green Earth, from Cyprus	genuine, brilliant
Organic Pigments, synth		
23000	Phthalo Green Dark	bluish
23010	Phthalo Green, yellowish	lightfast

Black and brown Kremer-made pigments

10900	Galena	gray-black lustrous powder, contains lead, toxic
10930	Pyrite Powder fine	0 - 80 µ
10940	Antimony	stibium, gray metallic, baroque, 0 - 200 µ
11282	Nero Bernino	gray-green slate from Bernina, Switzerland, 0 - 120 µ
11356	Gray from Mels,	Switzerland
11670	Onyx Black	0 - 120 µ
12400	Sepia	from adriatic cuttlefish, raw, dry, 0 - 120 µ
Carbonic black		
12000	Ivory Black, genuine	own production
12010	Peach Black	genuine, matt black
12015	Grape Black	genuine, bluish-black
12020	Cherry Black	genuine, brownish-black
12030	Atramentum	ink stone, black
12100	Bistre	genuine beechwood soot
Iron Oxides		
48710	Caput Mortuum dark	Haematite
48750	Caput Mortuum violet	Haematite, brownish
52300*	Translucent Orange	iron oxide
52350	Translucent Orange-Red	iron oxide
52400	Translucent Red medium	iron oxide
48300	Iron Oxide Brown 610, light	synthetic iron oxide
48320	Iron Oxide Brown 640, medium	synthetic iron oxide
48340	Iron Oxide Brown 655 reddish	beautiful, rich shade of brown
48350	Iron Oxide Brown 660, dark	synthetic iron oxide
48400	Iron Oxide Brown 318, high tinting	Mars Black, synthetic iron oxide, opaque
48420	Iron Oxide Black 306, bluish	synthetic iron oxide
48440	Iron Oxide Black 320, brownish	synthetic iron oxide
48800	Magnetite, very fine	10 µ, deep dark gray powder, almost transparent
48804*	Magnetite, fine	natural iron oxide black, approx. 63 µ
48806	Magnetite, coarse	deep dark gray, approx. 100 µ
48910	Natural Iron Glimmer	< 63 µ, gray
48930	Iron Glimmer Violet	flakes, red and glossy, transparent

White pigments		
11283	Alba Albula	buff white colored chalk, from Albula, Switzerland
11290	Sugar Dolomite	0 - 120 µ
11320	Rhodochrosite	pale-coral pink, 0 - 120 µ
11354*	Slate Green from Mels	Switzerland
11390*	Jade, very fine	Russian, < 63 µ
11401	Rock Crystal, fine	powder, 0 - 63 µ
11410	Eggshell White, fine	white powder
11420*	Fuchsite, extra fine	0 - 100 µ
11810	Selenite, Marienglas, fine	0 - 80 µ, gypseous spar, from Cyprus
11830	Aragonite	extra white, fine grind, 0 - 63 µ
Slate and Clay, powder		
40900	Slate Gray, extra light	stone chalk, semi opaque
40911	Slate Gray, light, greenish	stone chalk
40920	Slate Gray, gray-green	stone chalk
40930	Slate Gray, dark	stone chalk, neutral gray
40960	Pencil Clay, powder	light warm gray, 0 - 0.5 mm
41000	Van Dyck Brown	Cassel earth, dark
41050	Cassel Brown, wood stain	water-soluble, Van Dyck Brown, oak stain, walnut stain

Table 7. List of 310 Kremer pigments used to build HMI database. Pigments signed with a (*) are out of production in last Kremer catalogue 2019.

The HMI pigment database was built in Spectrapick software measuring the spectral reflectance in a 9x9 pixel area and exporting the reflectance curve in a database file.bin (Fig.56), that can be loaded in the software in the analysis of painted surface of real artworks for future diagnostic campaigns.

Figure 53. Pigments in oil binder on plexiglass.

Pigments in oil, with and without varnish

Malachite	Chrysocolla	Green earth	Lead tin yellow I	Lead tin yellow II	Vermillion HgS China	Smalt
Verdigris synth.	Green earth	Calcium carbonate	Massicot	Naples yellow	Cinnabar natur.	varnish alone
Azurite natur.	Smalt	Calcium sulfate	Sienna earth	Lead tin antimony yellow	Madder lake	Carbon black
Indigo genuine	Lapis lazuli good quality	Egg yolk	Iron oxide yellow	Lead carbonate	Red ochre	Ivory black
Azurite synth. MP	Azurite synth.	Copper calcium acetate	Yellow ochre	Minium	Hematite synth.	Umber earth

Figure 54. Identification of the pigments in Fig. 53.

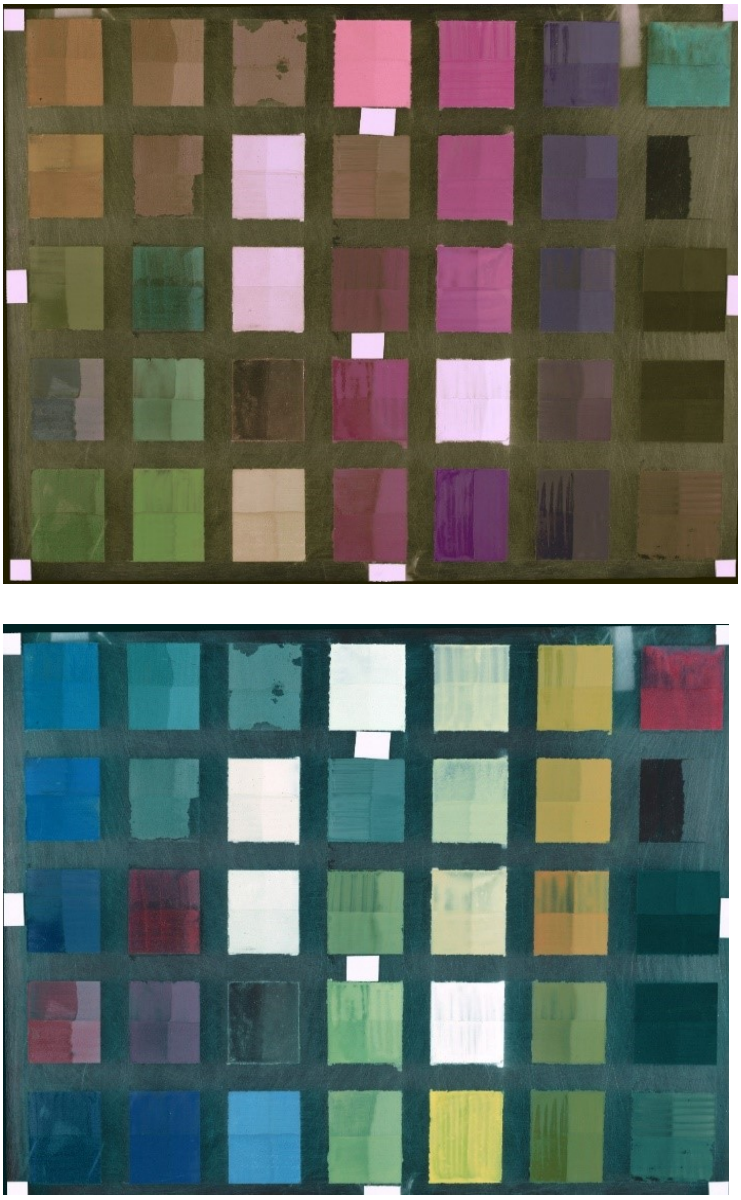

Figure 55. IRFC (a) and UVFC (b) images of the pigments on plexiglass.

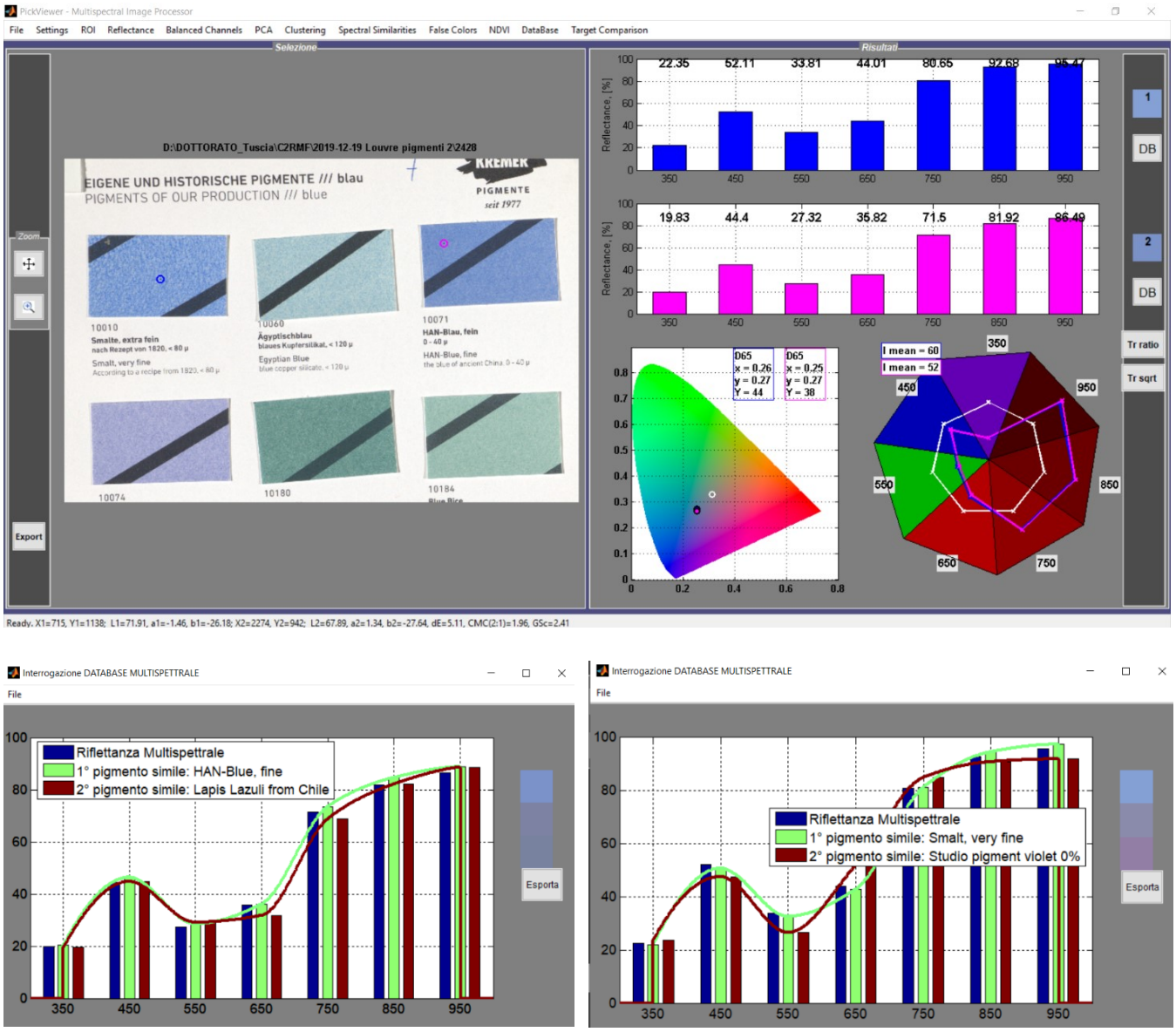

Figure 56. Pickviewer GUI with a comparison of spectral reflectance (%) of two blue pigments and their spectral curves registered in the database.

5. CONCLUSIONS

In this doctoral thesis new non-invasive methods for painting diagnostics were tested on several artworks and for the first time used in an integrated approach as a valid investigation method to support the process of identification and classification of heritage materials as well as artwork authentication. The application of non-invasive imaging led to outstanding results in the investigation of different kind of materials, some of them very ancient and fragile where other traditional investigations were not possible. The innovative imaging techniques, Hypercolorimetric multispectral Imaging (HMI) and Pulse Compression Thermography (PuCT), tested for the first time in a combined approach proved to be non-invasive, portable, contactless, rapid and reproducible methods to investigate art materials and to support the conservation process. Such characteristics are extremely important in restoration campaigns dealing with fragile and valuable objects and can be successfully used in scientific investigations to run (exactly as it happens in medical diagnostics) an early screening process to later eventually address a reasonable number of micro-invasive sampling points for confirming material characterization with traditional analytical techniques.

In different applications done in the last three years of doctoral research, HMI was used in combination with another innovative non-destructive technique, Pulse Compression Thermography (PuCT), for the first time applied on real artworks. Results of the combined use of HMI and PuCT demonstrated how new non-invasive imaging techniques and their integration can supply accurate and valuable information on ancient paintings, especially to map the conservation condition and to reveal invisible details useful for possible restoration works and for painting attributions, respectively. In these diagnostic campaigns, HMI acquisitions and digital image processing tools allowed to investigate the upper painting layer, while PuCT imaging data gave relevant information on the structure of the wooden support proving to be an innovative stratigraphic investigation method. In both investigated artworks, the combined use of HMI and PuCT gave interesting results, highlighting aspects concerning both state of conservation of the artworks and art materials and painting technique. The most interesting aspect of the combined used of the two techniques is the output of the integration of their native imaging data.
In the investigated Renaissance panel paintings- the Viterbo *Crucifixion* attributed to Michelangelo and *The Resurrection of Christ* by Mantegna- and in the detached wall painting by Pastura, a significant correlation between the pictorial layer and the support was revealed, both in terms of state of conservation and of executive technique. At the current state of the art, this achievement was not possible before in these conditions, combining only two imaging techniques *in situ* at once and in a reduced time of acquisition, without moving the artwork out of its exposition setting, nonetheless obtaining all the valuable information commonly achievable through multiple traditional methods, which normally require longer time and higher costs.

The use of HMI and PuCT cannot replace analytic characterization methods as XRF, μ-Raman or FTIR spectroscopies, but certainly is a high performance and smarter alternative to traditional scientific photography, realized through several devices giving separated imaging results. HMI, in fact, can register UV, visible and IR calibrated high resolution images with a single acquisition system, in a rapid and reproducible way and

its main advantage is the capability to apply statistical processing to enhance hidden information in the multispectral dataset and integrate multisource imaging data in the multispectral processing software. PuCT can perform a non-invasive stratigraphic investigation of the painting to reveal defects, discontinuities, alterations, cracks, inclusions of foreign materials, and so on, through a rapid contactless and portable apparatus. PuCT imaging data, get at different cooling times, allow to observe layer by layer the inner structure of the painting.
A combined use of HMI and PuCT supported the restoration of *The Resurrection of Christ*, also contributing to enrich our knowledge on the painting technique of Andrea Mantegna, while they will help the conservators in the case of *Crucifixion* whose restoration is hopefully going to start in the near future.
Considering once again the comparison with traditional diagnostic methods, imaging non-invasive technique can successfully be used as a first and complete diagnostic survey of an artwork to later address a reasoned number of other specific micro-invasive or destructive investigations. But the real frontier to deeply explore is correlation between imaging data coming from different physical sources (multi- and hyperspectral, thermography, TeraHertz, X-ray) and representing different materials responses that could be interdependent in the whole conservation frame. A further level of integrated diagnostic approach is the association between spectral imaging and chemical data from punctual analysis [161] correlating them with spectral reflectance measurement in the same micro-area, as done in the case of the ancient Persian illuminated manuscript from the Louvre Museum.

Multispectral system offers a limited set of spectral bands compared to HSI techniques, but one of the downfalls of HSI is that it adds a level of complexity connected to the necessity to reduce redundancy between to hundreds of narrow spectral bands, which implies complex post-processing. Supporting multispectral acquisition with powerful but user-friendly DIP software tool for statistical treatment of multispectral data, as in HMI applied in this research, can provide a wider and more complete information on investigated surfaces and a robust diagnostic datum, easy to access also for restorers and conservators.

In the last years, non-invasive diagnostics of artworks is assuming a key role not only in the restoration and conservation of cultural heritage, but also in difficult authentication issues. In both cases, it implies activities and markets with high added value, that moves human and economic capitals.
In this perspective, restoration hold a position of outstanding importance, recovering not only the history and the aesthetic of an art piece, but also returning an assertion of identity to a social community, increasing its cultural and economic strength.
Nevertheless, not all museums and restoration centres have got the necessary skills and resources to deal with advanced non-invasive diagnostics, usually renouncing to preventive scientific analyses and to a planned monitoring of their art collections.
As regards authentication issues, recent studies demonstrated how multispectral imaging and hypercolorimetric analysis can successfully support and trail traditional diagnostics commonly used by conservation scientists that cooperate with art historians, restorers and conservators for an optimal interpretation of scientific data.
Non-scientific art expertise – known in the art world as connoisseurship – is a common practice to assess the authenticity. Nevertheless, an experienced specialist can only

evaluate a limited amount of the artwork and when not supported by additional scientific tests, that evaluation is subjective and as such it is not infallible.
New non-invasive portable diagnostics as HMI and PuCT can become increasingly fundamental considering that the art selling market has reached the world value of about $67.4 billion, according to economist Clare McAndrew's report "The Art Market 2019" and counts millions of transactions every year which are not so slowly moving outside popular international auction houses, passing through the intermediation of gallery owner, private dealer and antiquarians in a proportion of more than 60% of the global art market [162].
It is indeed clear the importance to divulge the fundamental role of non-invasive investigation of artworks through scientific publications and to engage in scientific research projects that can develop new affordable and user-friendly diagnostics for a safe conservation of museum collections, provide new tools for the restoration market and also support authentication issues in debated case of attribution.
As a curiosity on this point, it must be considered that younger people are joining the art market in the last few years, a target that is considerably used to the influential contribution of technology in the fields of art, society, communication, before considered exclusive of human sciences. In fact , in previous surveys of US collectors, the majority of respondents were aged 50years and over, however, in the newer markets in Asia, a very different age profile emerged in 2018: in Singapore, 46% of collectors were millennials, and 39% were millennials in Hong Kong.

Considering this purpose, this doctoral research focused on the testing and development of new non-invasive diagnostic solution through national and international cooperation agreements to work on shared research project that could suggest new diagnostic solutions and methodological approach. In the doctoral triennium 2016-2019 some research projects were successfully funded:

- SteadyPick, a national research project (ID A0199-2018-17547, funded by Regione Lazio, POR FESR Lazio 2014-2020, "Cultural Heritage and Tourism" - Integrated Projects - decision no. G11238 of 27/08/2019) dedicated to the development a multi-sensor system for multispectral and thermographic imaging and photogrammetric survey of 3D surfaces, with main contribution of Tuscia University in the testing of the prototype on mock ups made of different artists materials and restoration products and in the monitoring of artificially induced alterations. SteadyPick non-invasive diagnostics will be developed to provide a rapid and complete survey of the structure for material characterization and surface mapping to address -when necessary- a limited and conscious number of analytic investigations (micro-samplings) and best plan any restoration interventions.

- EHEM project (ID JPICH-0127, funded European Union's Horizon2020, JPI Cultural Heritage "Conservation, Protection and Use Call 2019") by will integrate innovative non-invasive and traditional diagnostic in virtual 3D models to rebuild the original aspect of Middle Age decorated architectures and monitor their current state of conservation. Main expected output of the project is the development of a powerful platform thought to enable a most complete storing, documenting, sharing and semantic enrichment of cultural heritage to support conservation experts, as well as to pursue dissemination purposes, exploiting the

virtual and augmented reality both *in situ* and *ex situ* to enhance the experience of the visitors, integrate the models in haptic devices to facilitate the access to the monument to people with disabilities, create games and entertainment applications for a younger audience.

These future projects as the whole doctoral research reached another advantageous achievement which is worthy of mention is the productive collaboration realized between public research and private business. This aspect can encourage private investments devoted to Heritage Conservation, which unfortunately does not beneficiate of the same economic engagement given to engineering applications for industrial productions, but is nonetheless a major priority for European Union's cultural policies which in the 2014-2020 programming made undeniable efforts in this sense. The development of best practices for a shared management of Cultural Heritage which involve private and public subjects, giving them mutual benefits and a wider positive return for the knowledge and conservation of collective Heritage, is without a doubt a direction we should pursue.

A new shared discussion also on the generation, storage, function and usability of scientific digital images is by now necessary and a near branch of conservation policies having its own right. Standard protocols are desirable to ensure data interoperability and long-term usability in a world coping with an increasing amount of digital data and ever-changing technologies. Differently from many point-analysis techniques, portable investigative techniques, increasingly affordable and easy to use imaging methods have seen an early democratization for the analysis of large and immovable art objects, for the identification of representative sampling areas, the production of technical mapping and documentation purposes. Imaging is an invaluable tool for the study and communication of world cultural, historical and architectural heritage which assumes a further humanitarian value considering recent intentional destruction in war zones or severe losses due to natural catastrophic events. Experienced and shared by millions, the world's heritage lives on in those images, with the added value of a deeper understanding of artworks offered by scientific imaging and the benefit of digital information in terms of easily accessible open source, increasing awareness of the importance of documentation devoted to appropriate conservation strategies. An increasing public interest in imaging techniques and their capacity to visually communicate Heritage to experts and the public alike, could convey the demand for more sophisticated and accessible imaging techniques inspiring technological progress, which in turn could enhance the heritage professional's toolbox (including the currently less accessible chemical and physical imaging) [163].

Finally, an aspect of the research to deepen in the next future should be focused on a stronger integration between the multi-source imaging techniques, exploring higher possibility of data correlation through multisource signal processing, computational imaging and machine learning. This approach reduces the ambiguities of information coming from a single diagnostic method and could enable the creation of dedicated diagnostic protocols for different kind of artworks and specific database of artists materials to be shared and participated by the whole scientific community. Significant advances in integrated imaging analysis will hopefully encourage the development of new dedicated classification techniques to distinguish and map original materials,

restorations, defects and degradation evidences to support conservators as well as museums and organizations in charge of Heritage safeguard.

In such a rich scenario of high standing technologies, it must be taken into consideration not only the multidisciplinary cooperation between scientific experts and technicians, but also the fundamental role of the collaboration between art historians, archaeologists, restorers and conservation scientists in order to make a real advancement in the diagnostic approach, restoration protocols and in the full-fledged study of artworks to address the complexity of heritage protection.

ACKNOWLEDGEMENTS

The last three years have been an intense, sometimes difficult, but always fascinating challenge to me.
My thanks full of gratitude and admiration are due to my PhD supervisor, Professor Giuseppe Calabrò, that decided to invest his time in a research far from his fields of interest of industrial engineering and thermonuclear fusion in order to discover that conservation science can produce great results in terms of scientific achievements with an unexpected energy, even if not nuclear.

A heartfelt thanks is due to Professor Claudia Pelosi, that supported me in every research activity, led me to improve my scientific reasoning and approach and taught me the meaning of the true dedication to scientific Research.

The greatest Thanks is for my parents, Carlo and Antonella, who believed in me even when I didn't. They never had a doubt and let me free to make my choices and my mistakes, going on my own way. Thanks to my brother Fabio for sharing debates, passions and respect in a way that no one else could understand.

A sincere thanks to Andrea, that arrived in my life without any invitation or excuse, in his limpid and honest way to live. Your love is a harbour in the tempest.

Thanks to my soccer team mates, because in that green pitch with them I forget the world to find the simplest and purest joy a person could feel.

Thanks to my friends of Radio Libera Tutti, a dream we built for ourselves in our twenties and that keeps united the ones of us that stay dreamers. Thank You Radio, "my only friend in teenage nights."

Finally, a thanks to all those records who have been a constant inspiration in all my days as a student since I was fifteen years old, from David Bowie to Pink Floyd, Billie Holiday and Freddie Mercury, Lucio Dalla, Joplin, U2, Lennon, Dylan, Battiato, The Smiths, The Cure, Vedder, and all the others companions who showed me the way.

Rock 'n' roll.

BIBLIOGRAPHY

[1] Ricciardi P., Delaney J., Glinsman L., Thoury M., Facini M., De La Rie R. (2009). "Use of visible and infrared reflectance and luminescence imaging spectroscopy to study illuminated manuscripts: Pigment identification and visualization of underdrawings", Proceedings of SPIE - The International Society for Optical Engineering. 7391. DOI:10.1117/12.827415.

[2] Mulholland T., Howell R., Beeby, A., Nicholson C. E., Domoney K. (2017). "Identifying eighteenth century watercolor pigments using in situ Raman spectroscopy, XRF and hyperspectral imaging", Heritage Science, 5 (43).

[3] Mounier A., Le Bourdon G., Aupetit C., Belin C., Servant L., Lazare S., Lefrais Y., Daniel F. (2018). "Hyperspectral imaging, spectrofluorimetry, FORS and XRF for the non-invasive study of medieval miniatures materials", Heritage Science, 2 (24).

[4] Amato S.R., Burnstock A., Cross M., Koen J., Rosi F., Cartechini L., Fontana R., Dal Fovo A., Paolantoni M., Grazia C., Romani A., Michelin A., Andraud C. Tounié A., Dik J. (2018). "Interpreting technical evidence from spectral imaging of paintings by Édouard Manet in the Courtauld Gallery", X-Ray Spectrometry, pp. 1–11.

[5] Delaney J., Dooley K., Radpour R., Kakoulli I. (2017). "Macroscale multimodal imaging reveals ancient painting production technology and the vogue in Greco-Roman Egypt", Scientific Reports, 7.

[6] Catelli E., Sciutto G., Prati S., Mazzeo R. (2019). "Mid-infrared macroscopic mapping and hyperspectral imaging: state-of-the-art and new perspectives for non-invasive in-situ investigation of artworks", Proc. SPIE 11058, Optics for Arts, Architecture, and Archaeology VII, 110580R (23 July 2019).

[7] Landgrebe D. (1999). "Information extraction principles and methods for multispectral and hyperspectral image data", Inf. Process. Remote Sens., vol. 82, pp. 3-37.

[8] Khan M.J., Khan H.S., Yousaf A., Khurshid K., Abbas A. (2018). "Modern Trends in Hyperspectral Image Analysis: A Review," in IEEE Access, vol. 6, pp. 14118-14129.

[9] A. Cosentino (2015). "Panoramic, Macro and Micro Multispectral Imaging: An Affordable System for Mapping Pigments on Artworks", J. Conserv. Museum Stud. 13(1), pp. 1–17.

[10] Daffara C., Fontana R. (2011). "Multispectral Infrared Reflectography to differentiate features in paintings", Microscopy and microanalysis, 17, pp. 691-695.

[11] Pelagotti A., Del Mastio A., De Rosa A., Piva A. (2008). "Multispectral imaging of paintings: a way to material identification", IEEE Signal Proc. Mag. 25 (4), pp. 27–36.

[12] Casini A., Lotti F., Picollo M., Stefani L., Buzzegoli E. (1999). "Image spectroscopy mapping technique for non-invasive analysis of paintings", Stud. Conserv. 44 (1), pp. 39–48.

[13] Polak A., Kelman T., Murray P., Marshall S., Stothard D.J.M., Eastaugh N., Eastaugh F. (2017). "Hyperspectral imaging combined with data classification techniques as an aid for artwork authentication", J. Cult. Herit. 26, pp. 1–11.

[14] Cornelis B., Dooms A., Leen F., Munteanu A., Schelkens P. (2010). "Multispectral imaging for digital painting analysis: A Gauguin case study", Proceedings SPIE 7798, Applications of Digital Image Processing XXXIII.

[15] Samadelli M., Melis M., Miccoli M., Egarter-Vigl E., Zink A., (2015). "Complete mapping of the tattoos of the 5300-year-old Tyrolean Iceman", Journal of Cultural Heritage, 16(5), pp. 753-758.

[16] Huang X., Uffelman E., Cossairt O., Walton M., Katsaggelos A.K., 2016. "Computational Imaging for Cultural Heritage Recent developments in spectral imaging, 3-D surface measurement, image relighting and X-ray mapping", Signal Processing for Computational Photography and Displays, pp. 130-138.

[17] Sayre V., Lechtman H.N., 1968. "Neutron Activation Autoradiography Of Oil Paintings", Studies in Conservation, 13(4), pp. 161-185.

[18] Legrand S., Vanmeert F., Snickt G. V. D., Alfeld M., Nolf W. D., Dik J., Janssens K., 2014. "Examination of historical paintings by state-of-the-art hyperspectral imaging methods: from scanning infra-red spectroscopy to computed X-ray laminography," Heritage Science, 2(13), pp. 2-13.

[19] Targowski P., Iwanicka M., 2012. "Optical Coherence Tomography: its role in the non-invasive structural examination and conservation of cultural heritage objects - a review", Appl. Phys. A 106, pp. 265–277.

[20] Guillet J.P., Recur B., Frédérique L., Bousquet B., 2014. "Review of Terahertz Tomography Techniques", Journal of infrared, millimeter and terahertz waves, 35(4), pp. 382-411.

[21] Rodríguez-Gonzálvez P., Jiménez Fernández-Palacios B., Muñoz-Nieto Á.L., Arias-Sanchez P., Gonzalez-Aguilera D., 2017. "Mobile LiDAR System: New Possibilities for the Documentation and Dissemination of Large Cultural Heritage Sites", Remote Sensing, 9(3), pp. 189.

[22] Green S., Bevan A., Shapland M, 2014. "A comparative assessment of structure from motion methods for archaeological research", Journal of Archaeological, 46, pp. 173-181.

[23] Huang X., Uffelman E., Cossairt O., Walton M., Katsaggelos A.K., 2016. "Computational Imaging for Cultural Heritage. Recent developments in spectral imaging, 3-D surface measurement, image relighting, and X-ray mapping", IEEE Signal Processing Magazine, 33(5), pp. 130-138.

[24] Melis M., Miccoli M. (2013). "Trasformazione evoluzionistica di una fotocamera reflex digitale in un sofisticato strumento per misure fotometriche e colorimetriche", Atti della IX Conferenza del Colore, Università degli Studi di Firenze, 19-20 settembre 2013.

[25] Melis M., Miccoli M., Quarta D. (2013). "Multispectral hypercolorimetry and automatic guided pigment identification: some masterpieces case studies", in: Pezzati L., Targowski P. (Eds.), Proceedings of SPIE 8790, Optics for Arts, Architecture and Archaeology IV, Vol. 8790, 33, SPIE, Washington, pp. 1–14.

[26] De la Rie R. (1982). "Fluorescence of paint and varnish layers (part I- II- III)", Studies in Conservation 27, pp. 1-7, 65-69, 102-108.

[27] Pronti L., Felici A.C., Menager M., Vieillescazes C., Piacentini M. (2017). "Spectral Behavior of White Pigment Mixtures Using Reflectance, Ultraviolet-Fluorescence Spectroscopy and Multispectral Imaging", Applied Spectroscopy, Society for Applied Spectroscopy, 71 (12), pp. 2616-2625.

[28] Maldague X. (2001). "Theory and practice of infrared thermography for nondestructive testing". Wiley series in microwave and optical engineering, Wiley, Hoboken, New Jersey, USA, pp. 684.

[29] Trimm M.V. (2001). "Introduction to infrared and thermal testing: Part 1 Nondestructive Testing", in "Nondestructive Handbook, Infrared and Thermal Testing", in: Maldague X., Moore P.O. (Eds.), The American Society for Nondestructive Testing, 3rd ed., ASNT Press, Columbus, OH, 3 , pp. 2–11.

[30] Ibarra-Castanedo C., Sfarra S., Klein M., Maldague X. (2017). "Solar loading thermography: time-lapsed thermographic survey and advanced thermographic signal processing for the inspection of civil engineering and cultural heritage structures", Infrared Phys. Techn. 82, pp. 56–74.

[31] Maldague X. (1993). "Nondestructive evaluation of materials by infrared thermography", Springer-Verlag, pp. 207.

[32] Bulgholzer P. (2015). "Thermodynamic limits of spatial resolution in active thermography", Int. J. Thermophys. 36, pp. 2328–2341.

[33] H.S. Carslaw, J.C. Jaeger, Conduction of heat in solids, 2nd ed., Claredon Press, Oxford, 1959, pp. 510.

[34] Thomachot-Schneider C., Gommeaux M., Lelarge N., Conreux A., Mouhoubi K., Bodnar J.L., Vàzquez P. (2016). "Relationship between Na2SO4concentration and thermal response of reconstituted stone in the laboratory and on site, Environ. Earth Sci. 75(762).

[35] Sfarra S., Ibarra-Castanedo C., Paoletti D., Maldague X. (2013). "Infrared vision inspection of cultural heritage objects from the city of L'Aquila, Italy and its surroundings", Mater. Eval. 71(5), pp. 561–570.

[36] Pucci M., Cicero C., Orazi N., Mercuri F., Zammit U., Paoloni S., Marinelli M. (2015). "Active infrared thermography applied to the study of a painting on paper representing the Chigi's family tree", Stud. Conserv. 60(2), pp. 88–96.

[37] Seeboth A., Lötzsch D. (2013). "Thermochromic and Thermotropic Materials", Pan Stanford Publishing Pte. Ltd, pp. 228.

[38] Mulaveesala R., Venkata Ghali S. (2011). "Coded excitation for infrared non-destructive testing of carbon fiber reinforced plastics", Rev. Sci. Instrum. 82(5), 054902.

[39] Silipigni G., Burrascano P., Hutchins D.A, Laureti S., Petrucci R., Senni L., Torre L., Ricci M. (2017). "Optimization of the pulse-compression technique applied to the infrared thermography nondestructive evaluation", NDT&E Int. 87, pp- 100-110.

[40] Laureti S., Sfarra S., Malekmohammadi H., Burrascano P., Hutchins D.A., Senni L., Silipigni G., Maldague X., Ricci M. (2018). "The use of pulse-compression thermography for detecting defects in paintings", NDT&E Int. 98, pp. 147–154.

[41] Tabatabaei N., Mandelis A. (2009). “Thermal-wave radar: a novel subsurface imaging modality with extended depth-resolution dynamic range”, Rev. Sci. Instrum. 80, pp. 1–11.

[42] Mulaveesala R., Tuli S. (2006). “Theory of frequency modulated thermal wave imaging for nondestructive subsurface defect detection”, Appl. Phys. Lett. 89 (19), 191913.

[43] Laureti S., Silipigni G., Senni L., Tomasello R., Burrascano P., Ricci M. (2018). “Comparative study between linear and non-linear frequency-modulated pulse-compression thermography”, Appl. Optics 57 (18), D32–D39.

[44] Chatterjee K., Tuli S., Pickering S.G., Almond D.P. (2011). A comparison of the pulsed, lock-in and frequency modulated thermography nondestructive evaluation techniques, NDT&E Int. 44, pp. 655–667.

[45] Misaridis T., Jensen J.A. (2005). “Use of modulated excitation signals in medical ultra-sound. Part III: high frame rate imaging”, IEEE Trans. Ultrason. Ferroelectr. Freq.Control. 52, pp. 208–218.

[46] Zhang G., Zhou Q. (2002). “Pseudonoise codes constructed by Legendre sequence”, Electr.Lett. 38(8), pp. 376–377.

[47] Ricci M., Senni L., Burrascano P. (2012). “Exploiting pseudorandom sequences to enhance noise immunity for air-coupled ultrasonic nondestructive testing”, IEEETrans. Instrum. Meas. 61(11), pp. 2905–2915.

[48] Hutchins D., Burrascano P., Lee D., Laureti S., Ricci M. (2014). “Coded waveforms for optimised air-coupled ultrasonic nondestructive evaluation”, Ultrasonics 54(7), pp. 1745–1759.

[49] Barker R.H. (1953). “Group synchronizing of binary digital systems”, Commun. Theory, pp. 273–287.

[50] Vasari G., “Le vite de' più eccellenti pittori, scultori e architettori”, 1st ed. of 1568, Giunti (Firenze), Capitolo XXI.

[51] Cennini C. (1982). “Il libro dell’arte”, a cura di F. Brunello, Neri Pozza Editore, Vicenza, pp. 120-121.

[52] Coccato A., Moens L., Vandenabeele P. (2017). “On the stability of mediaeval inorganic pigments: a literature review of the effect of climate, material selection, biological activity, analysis and conservation treatments”, Herit. Sci. 5(12), pp. 1-25.

[53] Pelosi C., Agresti G., Coralli D., Santamaria U. (2013). “Applicazione della spettrocolorimetria e della spettroscopia di fluorescenza dei raggi X per la caratterizzazione di pigmenti in miscela”, Colore e Colorimetria – Contributi multidisciplinari, vol. IX, M. Rossi and A. Siniscalco (Eds.), Maggioli Editore, Rimini, pp. 334-340.

[54] Oleari C. (2002), “Misurare il Colore”, Ulrico Hoepli.

[55] CIE Publication No 15.3 (2004). “Colorimetry” (3rd edition), Bureau Central de la Commission Internationale de l'Éclairage, Vienna.

[56] Horovitz I. (1986). “The Conservator” 10 (44).

[57] Scott D.A. (2002). “Copper and Bronze in Art: Corrosion, Colorants, and Conservation”, J. Paul Getty Museum Pubs, Los Angeles.

[58] Oliveira M.L. (2015). “A technical investigation of an oil painting on copper support, including a story on consolidants for treatment”, Master Thesis, Faculdade de Ciências e Tecnologia, Universidade Nova de Lisboa.

[59] Vega D., Cardoso I.P., Carlyle L. (2018). Conserv. Patrim. 27(23).

[60] Bowron E.P. (1999). “A brief history of European oil paintings on copper, 1560–1775”, in “Copper as Canvas: Two Centuries of Masterpiece Paintings on Copper, 1575-1775”, edited by M. Komanecky (Oxford University Press, Phoenix Art Museum, New York) pp. 9–30.

[61] Palopoulou L.C., Watkinson D. (2006). Rev. Conserv. 7(65).

[62] Martinez K., Cupitt J., Saunders D., Pillay R. (2002). Proc. IEEE 90(28).

[63] Polak A., Kelmana T., Murray P., Marshall S., Stothard D.J.M., Eastaugh N., Eastaugh F. (2017). J. Cult. Herit. 26(1).

[64] Casini A., Bacci M., Cucci C., Lotti F., Porcinai S., Picollo M., Radicati B., Poggesi M., Stefani L. (2005). “Fiber optic reflectance spectroscopy and hyper-spectral image spectroscopy: two integrated techniques for the study of the Madonna dei Fusi”, in Proceedings of SPIE 5857, Optical Methods for Arts and Archaeology, Munich, edited by R. Salimbeni, L. Pezzati, Vol. 585 (SPIE, Washington).

[65] Daniel F., Mounier A., Pérez-Arantegui J., Pardos C., Prieto-Taboada N., Vallejuelo S.F.-O.d., Castro K. (2016). Microchem. J. 126(113).

[66] Dyer J., Verri G., Cupitt J. (2013). “Multispectral Imaging in Reflectance and Photo-induced Luminescence modes: A User Manual”, The British Museum, London.
[59] Cosentino A. (2015). Archeomatica 2(12).

[67] Cosentino A. (2015). e-Preserv. Sci. 12(1).

[68] Cosentino A. (2015). J. Conserv. Museum Stud. 13(1).

[69] Liang H., Saunders D., Cupitt J., Imag J. (2005). Sci. Technol. 49(551).

[70] Pelagotti A., Del Mastio A., De Rosa A., Piva A. (2008). IEEE Signal Process. Mag. 25(27).

[71] Sitnik R., Krzeslowski J.F., M¸aczkowski G. (2012). Opt. Eng. 51(021115).

[72] Fischer C., Kakoulli I. (2006). Stud. Conserv. 51(3).

[73] D. Lau, C. Villis, S. Furmanc, M. Livetta, Anal. Chim. Acta 610, 15 (2008).

[74] A. Stock, Preparing a copper panel for painting: a late sixteenth-century reconstruction, in Artists’ Footsteps - The Reconstruction of Pigments and Paintings, edited by L. Wrapson, J. Rose, R. Miller, B. Bucklow (Archetype Publications, London, 2012) pp. 197–202.

[75] Gonzalez R.C., Woods R.E. (2008). Digital Image Processing, 3rd edition (Prentice Hall, Upper Saddle River, N.J.).

[76] Capobianco G., Calienno L., Pelosi C., Scacchi M., Bonifazi G., Agresti G., Picchio R., Santamaria U., Serranti S., Lo Monaco A. (2017). Spectrochim. Acta A 172(34).

[77] Pelosi C., Capobianco G., Agresti G., Bonifazi G., Morresi F., Rossi S., Santamaria U., Serranti S. (2018). Spectrochim. Acta A 198(92).

[78] Fragrasso L., Masini N., 2011. "Postprocessing of Infrared Reflectography to Support the Study of a Painting: The Case of Vivarini's Polyptych", International Journal of Geophysics, Volume 2011, Article ID 738279, pp. 1-8.

[79] Barni M., Pelagotti A., Piva A. (2005). IEEE Sign. Proc. Mag. 22(141).

[80] Abry P., Klein A.G., Sethares W.A., Johnson Jr. C.R. (2015). IEEE Signal Process Mag. 16(14).

[81] Agresti G., Gnignera E., Pelosi C., Rocca A., Serone G., Santamaria U. (2016). "The Crucifixion: a panel painting in the museum of Colle del Duomo in Viterbo (Italy)", in: Pelosi C., Agresti G., Lanteri L., Parisi C. (Eds.), "New insights in the light of a first analytical campaign", Proceedings of the 8th European Symposium on Religious Art, Restoration and Conservation, Nardini Editore, Firenze, pp.21–24.

[82] ARCHEOARES (2015). Crocifissione Michelangiolesca: Digital Edition, Gennaio 2015. http://www.archeoares.it/storico-artistica/crocifissione-di-michelangelo-2/.

[83] Firpo M., (2016). "Juan de Valdés e la Riforma nell'Italia del Cinquecento", Eds. Laterza, Roma.

[84] Calì M. (1980). "Da Michelangelo all'Escorial. Momenti del dibattito religioso nell'arte del Cinquecento", Eds. Einaudi, Torino.

[85] E. Campi, Michelangelo e Vittoria Colonna. Un dialogo artistico-teologico ispirato da Bernardino Ochino e altri saggi di storia della Riforma, Claudiana, Torino, 1994.

[86] Nagel A. (1997). "Gifts for Michelangelo and Vittoria Colonna", Art Bull. 79 (4), pp. 647.

[87] Nagel A. (2000). "Michelangelo and the Reform of Art", Cambridge University Press, Cambridge.

[88] Brundin A.S. (2008). "Vittoria Colonna and the Spiritual Poetics of the Italian Reformation", Ashgate Publishing, Farnham.

[89] ARCHEOARES (2016). "La Crocifissione di Viterbo. Esiti delle indagini", digital edition, Gennaio 2016. http://www.archeoares.it/blog/la-crocifissione-diviterbo-esiti-delle-indagini.

[90] Benedetto da Mantova, Marcantonio Flaminio, "Trattato utilissimo del beneficio di Gesù Cristo crocifisso verso i cristiani", tipografia Bernardo de' Bindoni, Venezia, 1543.

[91] Rocca A., (2016). "Savonarola e Michelangelo Tra forma e Riforma", Edizioni Archeoares, Viterbo.

[92] Valagussa G. (2018). “Dipinti italiani del Trecento e del Quattrocento”, Accademia Carrara Bergamo, Catalogo completo, Officina Libraria, Milano, pp.356–361.

[93] UNESCO (1974). “An illustrated inventory of famous dismembered works of art: European painting”, Unipub.

[94] Forcellino M. (2009). “Michelangelo, Vittoria Colonna e gli “spirituali””, Viella, Roma.

[95] D’Arco C., Delle arti e degli artefici di Mantova. Notizie raccolte ed illustrate con disegni e con monumenti, II, Tipografia Ditta G. Agazzi, Mantova, 1857.

[96] Poldi G., Bonizzoni L., Galli A. (2006). In: Andrea Mantegna, la Madonna dei Cherubini, Eds. M. Olivari, Electa Milano, pp. 44–56.

[97] Targowski P., Iwanicka M., Sylwestrzak M., Frosinini C., Striova J., Fontana R. (2018). “Using Optical Coherence Tomography to Reveal the Hidden History of The Landsdowne Virgin of the Yarnwinder by Leonardo da Vinci and Studio”, Angewandte Chemie, International Edition, Vol. 57(25), pp. 7396-7400.

[98] Mayer T., Walters C. (eds.) (2002-2008), “The Correspondence of Reginald Pole, Aldershot and Burlington”, Ashgate, Vol. I, 311, cat. 407.

[99] Freestone I., Meeks N., Sax M., Higgitt C. (2007). “The Lycurgus Cup - A Roman nanotechnology”, Gold Bull. 40(4), pp. 270–277.

[100] Ilardi V., (2007). “Renaissance Vision from Spectacles to Telescopes”, American Philosophical Society, Philadelphia, pp. 167–168 and 193.

[101] Perri A., Nogueira de Faria B.E, Teles Ferreira D.C., Comelli D., Valentini G., Preda F., Polli D., De Paula A.M., Cerullo G., Manzoni C. (2019). "Hyperspectral imaging with a TWINS birefringent interferometer”, Optics Express 27(11), pp. 15956–15967.

[102] UNI 11118 (2004). Cultural heritage. Wooden Artefacts. Criteria for the Identification of the Wood Species.

[103] Lo Monaco A., Giagnacovo C., Falcucci C., Pelosi C. (2015). “The triptych of the Holy Saviour in the Tivoli Cathedral: diagnosis, conservation and religious requirements”, Eur. J. Sci. Theol. 11(2), pp. 241–252.

[104] Baraldi P., Lo Monaco A., Ortenzi F., Pelosi C., Quarato F., Rossi L. (2014). “Study of the technique and of the materials of a 19th c. polychrome wood mask from Papua New Guinea”, Archaeometry 56, pp. 313–330.

[105] Lo Monaco A., Marabelli M., Pelosi C., Salvo M. (2012). “The altar machine in the Church Mother of Gangi (Palermo, Italy). Interpretation of the past uses, scientific investigation and preservation challenge”, Chem. Central J. 6, pp. 1–11.

[106] Agresti G., Genco G., Giagnacovo C., Pelosi C., Lo Monaco A., Castorina R. (2010). “Wood of chestnut in cultural heritage, Acta Horticolturae 866, pp. 51–57.

[107] Bronk Ramsey C., van der Plicht J., Weninger B. (2001). “Wiggle-matching radiocarbon dates”, Radiocarbon 43(2A), pp. 381–389.

[108] Wolfe W.L. (1997). “Introduction to Imaging Spectrometers”, SPIE.

[109] Amigo J.M., Babamoradi H., Elcoroaristizabal S. (2015). “Hyperspectral image analysis. A tutorial”, Anal. Chim. Acta 896, pp. 34–51.

[110] Davis S.P., Abrams M.C., Brault J.W. (2001). “Fourier Transform Spectrometry”, Elsevier.

[111] Brida D., Manzoni C., Cerullo G. (2012). “Phase-locked pulses for two-dimensional spectroscopy by a birefringent delay line”, Opt. Lett. 37(15), pp. 3027–3029.

[112] Manzoni C.A., Brida D., Cerullo G.N.F., (2015). US Patent: 9182284.

[113] Fellgett P.B. (1949). “On the ultimate sensitivity and practical performance of radiation detectors”, J. Opt. Soc. Am. 39(11), pp. 970–976.

[114] Jacquinot P. (1960). “New developments in interference spectroscopy”, Rep. Prog. Phys. 23(1), pp. 267–312.

[115] Sharif-Askari H., Abu-Hijleh B. (2018). “Review of museums' indoor environment conditions studies and guidelines and their impact on the museums' artifacts and energy consumption”, Building and Environment 143, pp. 186–195.

[116] Kruse F.A, Lefkoff A.B., Boardman W., Heidebrecht K.B., Shapiro A.T., Barloon P.J., Goetz A.F.H. (1993. “The spectral image processing system (SIPS)—interactive visualization and analysis of imaging spectrometer data”, Remote Sens. Environ. 44 (2-3), pp. 145–163.

[117] Comelli D., Valentini G., Nevin A., Farina A., Toniolo L., Cubeddu R. (2008). “A portable UV fluorescence multispectral imaging system for the analysis of painted surfaces”, Rev. Sci. Instrum. 79 (086112).

[118] http://e-conservation.org/issue-2/36-FORS-spectral-database.

[119] Lo Monaco A., Balletti F., Pelosi C. (2018). “Wood in cultural Heritage. Properties and conservation of historical wooden artefacts”, Eur J. Sci. Theol. 14 (2), pp. 161–171.

[120] Nardi Berti R. (2006). “La struttura anatomica del legno ed il riconoscimento dei legnami italiani di più corrente impiego”, CNR-IVALSA, Sesto Fiorentino, p. 155.

[121] Schweingruber F.H. (1990). “Anatomy of European Woods: An Atlas for the Identification of European Trees”, WSL/FNP Paul Haupt, Berne, pp. 98–99.

[122] IAWA list of microscopic features for softwood identification (2004), in: Richter H.G., Grosser D., Heinz I., Gasson P.E. (Eds.), IAWA Journal, 25, pp. 1–70.

[123] Corona E. (1972). “Note dendrocronologiche sul quadro di S. Maria della Clemenza di Roma”, St. Trentini Sc. Nat. 2, pp. 133–140 XLVII.

[124] Galimberti M., Ramsey C.B., Manning S.W. (2004). “Wiggle-match dating of tree-ring sequences”, Radiocarbon 46(2), pp. 917–924.

[125] Steier P., Rom W. (2000). “The use of Bayesian statistics for 14C dates of chronologically ordered samples: a critical analysis”, Radiocarbon 42(2), pp. 183–198.

[126] Calcagnile L., Quarta G., D'Elia M. (2005). "High resolution accelerator-based mass spectrometry: precision accuracy and background", Appl. Radiat. Isot. 62, pp. 623–629.

[127] Calcagnile L., Quarta G., D'Elia M., Gottdang A., Klein M., Mous D.J.W., 2004. "Radiocarbon precision tests at the Lecce AMS facility using a sequential injection system", Nuclear Instruments and Methods in Physics Research B. Beam Interactions with Materials and Atoms, 215(3-4), pp.561-564.

[128] Calcagnile L., Maruccio L., Scrimieri L., delle Side D., D'Elia M., Braione E., Quarta G. (2019). "Development and application of facilities at the Centre for Applied Physics, Dating and Diagnostics (CEDAD) at the University of Salento during the last 15 years", Nuclear Instrum. Methods Phys. Res. B 456, pp. 252–256.

[129] Bernabei M., Quarta G., Calcagnile L., Macchioni N. (2007). "Dating and technological features of wooden panel painting attributed to Cesare da Sesto", J. Cult. Herit. 8, pp. 202–208.

[130] Reimer P.J., Bard E., Bayliss A., Beck J.W., Blackwell P.G., Bronk Ramsey C., Buck C.E., Cheng H., Edwards R.L., Friedrich M., Grootes P.M., Guilderson T.P., Haflidason H., Hajdas I., Hatté C., Heaton T.J., Hoffmann D.L., Hogg A.G., Hughen K.A., Kaiser K.F., B. Kromer, S.W. Manning, M. Niu, R.W. Reimer, D.A. Richards, E.M. Scott, J.R. Southon, Staff R.A., Turney C.S.M., van der Plicht J. (2013). "Int-Cal13 and Marine13 radiocarbon age calibration curves 0–50,000 years cal BP", Radiocarbon 55(4), pp. 1869–1887.

[131] Schweingruber F.H. (1993). "Tree Species in Eurasia and Japan", Trees and Wood in Dendrochronology, Springer Series in Wood Science, Springer, Berlin, Heidelberg.

[132] Corona E. 1970). "Valore dendrocronologico del cipresso sempreverde", Monti E Boschi 19(5), pp. 21-25.

[133] Gittins M., Agresti G., Catalano M.I., Pelosi C., Pogliani P. (2017). "La lunetta raffigurante Madonna con Bambino in trono tra gli angeli e i Santi Francesco e Girolamo staccato dal convento di Santa Maria del Paradiso per il Museo Civico di Viterbo: fortuna dell'opera e storia conservativa alla luce dell'ultimo restauro (2016-2017)", Proc. XV Congresso Nazionale IGIIC Lo Stato dell'Arte (Bari), Nardini Editore, Firenze, pp. 461-468.

[134] Ricci C. (1912). "Antonio da Viterbo detto il Pastura e l'Appartamento Borgia", Per l'inaugurazione del Museo Civico di Viterbo (Viterbo: Agnesotti), pp. 23-27.

[135] Rinaldi S. (2004). "I dipinti del Museo Civico di Viterbo. Censimento conservativo in omaggio a Michele Cordaro", Ediart, Todi, p. 75.

[136] Zuccari A. (1983). "L'attività viterbese di Antonio del Massaro detto il Pastura" in Cannatà R, Strinati C., Calvesi M. (eds.), "Il Quattrocento a Viterbo", De Luca, Milano, pp 222-239.

[137] Derrick M.R., Stulik D., Landry J.M. (1999). Infrared Spectroscopy in Conservation Science (Los Angeles: The Getty Conservation Institute), p. 235.

[138] Meilunas R.J., Brentsen J.G., Steinberg A. (1990). Analysis of Aged Paint Binders by FTIR Spectroscopy, Stud. Conserv. (35), pp. 33-51.

[139] Cavallo G. (2009). "Alteration of azurite into paratacamite at the St. Alessandro Church (Lasnigo, Italy)", Conservar Património 9, pp. 5-11.

[140] Sandu I.C.A., Afonso L.U., Murta E., De Sa M.H. (2010). "Gilding Techniques in Religious Art between East and West, 14th–18th Centuries", Int. J. Conserv. Sci., 1(1), pp. 47-62.

[141] Boust C., Mélard N., Lambert E., Clivet L., Maigret A. (2006). "Imagerie scientifique pour la conservation et la restauration du patrimoine", in Actes des journées d'étude sur les préalables à la restauration, C2RMF, Nancy.

[142] Boust C., (2017). "Pigments image database, in Scientific imaging for cultural heritage", http://copa.hypotheses.org/category/database.

[143] Ravaud E., Pichon L., Laval E., Gonzalez V., Eveno M., Calligaro T. (2016). "Development of a versatile XRF scanner for the elemental imaging of paintworks", Applied Physics A. 122.

[144] Knipe P., Eremin K., Walton M., Babini A., Rayner G. (2018). Materials and techniques of Islamic manuscripts, Heritage Science, 6 (55).

[145] Burgio L., Clark R.J.H., Muralha V.S.F., Stanley T. (2008). "Pigment analysis by Raman spectroscopy of the non-figurative illumination in 16th - to 18th century Islamic manuscripts.

[146] Purinton N., Watters M. (1991). "A study of the materials used by medieval Persian painters", Journal of American Institute for Conservation, 30(2), pp. 125-144.

[147] Barkeshli M. (1999). "The presence of saffron in Persian miniature paintings and its use as an inhibitor for the destructive effects of Verdigris". In: ICOM committee for conservation: 12th triennial meeting, Lyon. 29th August-3rd September 1999, vol II, pp. 494-494.

[148] https://shop.kremerpigments.com/media/pdf/krp_katalog_US_140806_web.pdf

[149] Berrie B. (2007). "Artists' Pigments: A Handbook of Their History and Characteristics", 1, 2, 3, 4.

[150] Keijzer M. (2001). "The history of modern synthetic inorganic and organic artist's pigments." In Mosk J.A., Tennant N.H. eds., "Contribution to Conservation: research in conservation at the Netherlands Institute for Cultural Heritage (ICN)", pp. 42-54.

[151] Boardman C., Bryan P. (2018). "3D Laser Scanning for Heritage: Advice and guidance on the use of laser scanning in archaeology and architecture", 3rd ed. Historic England, Swindon.

[152] Bedford J. (2017). "Photogrammetric applications for Cultural Heritage. Guidance for good practice", Historic England Eds., Swindon.

[153] Remondino F., El-Hakim S. (2006). "Image-based 3D modelling: a review." The photogrammetric record 21.115, pp. 269-291.

[154] Vandermeulen B., Hameeuw H., Watteeuw L., Van-Gool L., Proesmans M. (2018). "Bridging Multilight & Multi-Spectral images to study, preserve and disseminate archival documents", Society for Imaging Science and Technology, Archiving Conference, 1, pp.64-69.

[155] Cerezo E., Pérez F., Pueyo X., Seron F.J., Sillion F.X. (2005). "A Survey on Participating Media Rendering Techniques", The Visual Computer, 21(5), pp.303-328.

[156] Happa J., Mudge M., Debattista K., Artusi A., Gonçalves A., Chalmers A. (2009). "Illuminating the Past - State of the Art". 10th International Symposium on VR, Archaeology and CH VAST – State-of-the-Art Reports, Eds. M.Ashley and F.Liarokapis.

[157] Lamorlette A., Foster N. (2002). "Structural Modeling of Flames for a Production Environment". ACM ToG. 21(3), pp.729-735.

[158] Windhager F., Federico P., Schreder G., Glinka K., Dörk M., Miksch S., Mayr E. (2019). "Visualization of cultural heritage collection data: State of the art and future challenges", IEEE TVCG, 25(6), pp. 2311-2330.

[159] Virtual Angkor, https://www.virtualangkor.com.

[160] Exploring the historical recreation of an ancient metropolis through virtual simulations, https://sensilab.monash.edu/research/visualising-angkor.

[161] Dooley K. A., Conover D. M., Glinsman L. D., Delaney J. K. (2014). "Complementary standoff chemical imaging to map and identify artist materials in an early Italian Renaissance panel painting", Angewandte Chemie, International Edition, 53 (50), pp.13775-13779.

[162] https://www.artbasel.com/news/art-market-report

[163] Verri G., 2017. "Imaging In Conservation "It's All Imaging To Me": Documentation, Investigation, Visualization, and Communication", Conservation Perspectives Spring, Getty Eds.